

---

# Information Processing at the Calyx of Held Synapse Under Natural Conditions

Joachim Hermann

---

Zur Erlangung des akademischen Grades eines  
Doktors der Naturwissenschaften (Dr. rer. nat.)  
vorgelegte Dissertation der Fakultät für Biologie  
der Ludwig–Maximilians–Universität München von

Joachim Hermann  
aus Münster / Westfalen

München, 17.01.2008

Erstgutachter: ..... Univ.-Prof. Dr. Benedikt Grothe  
Zweitgutachter: ..... Univ.-Prof. Dr. Christian Leibold  
Tag der mündlichen Prüfung: ..... 11.03.2008

“No job too dirty for a fucking scientist”  
– *William S. Burroughs*



# Contents

|   |           |
|---|-----------|
| <b>List of Figures</b>  | <b>9</b>  |
| <b>Abbreviations</b>  | <b>11</b> |
| <b>Summary</b>  | <b>13</b> |
| <b>Zusammenfassung</b>  | <b>15</b> |
| <b>1 Introduction</b>   | <b>19</b> |
| 1.1 The auditory brainstem . . . . .                          | 20        |
| 1.2 The calyx of Held . . . . .                               | 23        |
| 1.3 Short-term plasticity . . . . .                           | 24        |
| 1.4 Objective of this work . . . . .                          | 26        |
| <b>2 Materials and Methods</b>                                | <b>29</b> |
| 2.1 In vivo recordings . . . . .                              | 29        |
| 2.1.1 Surgical procedures . . . . .                           | 29        |
| 2.1.2 Recordings of neural activity . . . . .                 | 30        |
| 2.1.3 Stimulus presentation and recording protocols . . . . . | 32        |
| 2.2 In vitro recordings . . . . .                             | 32        |
| 2.2.1 Slice preparation . . . . .                             | 33        |
| 2.2.2 Whole-cell recordings . . . . .                         | 33        |
| 2.2.3 Stimulation of synaptic inputs . . . . .                | 34        |
| 2.2.4 Conductance clamp experiments . . . . .                 | 34        |
| 2.2.5 Miniature EPSC analysis . . . . .                       | 35        |
| 2.3 Vesicle release model . . . . .                           | 35        |
| 2.3.1 Model variants . . . . .                                | 36        |
| 2.3.2 Model predictions . . . . .                             | 37        |
| 2.4 Statistical analysis . . . . .                            | 38        |

|          |  |           |
|----------|--|-----------|
| <b>3</b> | <b>Synaptic Transmission at the Calyx of Held</b>                          | <b>39</b> |
| 3.1      | Introduction . . . . .   | 39        |
| 3.2      | Results . . . . .  | 40        |
| 3.2.1    | Spontaneous firing rates . . . . .   | 40        |
| 3.2.2    | Introducing spontaneous rates . . . . .                                    | 42        |
| 3.2.3    | Effects of ‘spontaneous’ firing . . . . .                                  | 43        |
| 3.2.4    | Effects of simulated tone-bursts . . . . .                                 | 45        |
| 3.2.5    | Recovery of firing . . . . .   | 48        |
| 3.2.6    | Recovery from depression . . . . .   | 50        |
| 3.2.7    | Reduced synaptic reliability . . . . .                                     | 53        |
| 3.3      | Discussion . . . . .   | 59        |
| 3.3.1    | Background firing in MNTB neurons . . . . .                                | 59        |
| 3.3.2    | Prolonged spontaneous spiking . . . . .                                    | 61        |
| 3.3.3    | Reliability of synaptic transmission . . . . .                             | 62        |
| <b>4</b> | <b>Modeling Short-Term Synaptic Plasticity</b>                             | <b>65</b> |
| 4.1      | Introduction . . . . .   | 65        |
| 4.2      | Results . . . . .  | 66        |
| 4.2.1    | Poisson distributed test trains . . . . .                                  | 67        |
| 4.2.2    | Model variants . . . . .   | 71        |
| 4.2.3    | Stimulation with trains consisting of regularly spaced intervals . . . . . | 74        |
| 4.2.4    | Natural stimuli . . . . .  | 78        |
| 4.3      | Discussion . . . . .   | 80        |
| <b>5</b> | <b>Transition Between Unconditioned and Conditioned State</b>              | <b>83</b> |
| 5.1      | Introduction . . . . .   | 83        |
| 5.2      | Results . . . . .  | 84        |
| 5.2.1    | Beginning of conditioning period . . . . .                                 | 84        |
| 5.2.2    | Vesicle pool recovery . . . . .  | 87        |
| 5.2.3    | Miniature EPSCs . . . . .  | 92        |
| 5.3      | Discussion . . . . .   | 94        |
| <b>6</b> | <b>General Discussion</b>  | <b>97</b> |
| 6.1      | The functional role of the MNTB . . . . .                                  | 97        |
| 6.2      | Additional input to the MNTB . . . . .                                     | 100       |

|   |            |
|---|------------|
| 6.3 Implications for other nuclei . . . . . | 101        |
| <b>Bibliography</b>                         | <b>105</b> |
| <b>Contributions to the Manuscript</b>      | <b>117</b> |
| <b>Curriculum Vitæ</b>                      | <b>119</b> |
| <b>Danksagung</b>                           | <b>121</b> |
| <b>Ehrenwörtliche Versicherung</b>          | <b>123</b> |





# List of Figures

|     |  |    |
|-----|--|----|
| 1.1 | A schematic drawing of the auditory brainstem. . . . .   | 21 |
| 1.2 | An artist's rendering of a MNTB neuron. . . . .  | 24 |
| 2.1 | Spike waveforms and raster displays of two single MNTB neurons . . .                               | 31 |
| 3.1 | Illustration of <i>in vivo</i> activity in the MNTB . . . . .                                      | 41 |
| 3.2 | Spontaneous firing rates . . . . .   | 42 |
| 3.3 | EPSC amplitudes in response to different conditioning pulse trains . . .                           | 44 |
| 3.4 | Response of neurons to high frequency stimulation . . . . .  | 47 |
| 3.5 | PSTHs of a single MNTB neuron's <i>in vivo</i> response . . . . .                                  | 49 |
| 3.6 | Recovery from depression . . . . .   | 51 |
| 3.7 | Reliability of synaptic transmission in spontaneously active synapses . .                          | 55 |
| 4.1 | Poisson distributed test trains . . . . .  | 69 |
| 4.2 | Model variants . . . . .   | 72 |
| 4.3 | Stimulation with trains consisting of regularly spaced intervals . . . . .                         | 75 |
| 4.4 | Summary graphs showing the differences between experimental data<br>and model prediction . . . . . | 77 |
| 4.5 | Natural stimuli . . . . .  | 79 |
| 5.1 | Development of EPSC amplitudes during conditioning . . . . .                                       | 85 |
| 5.2 | Development of model parameters over time . . . . .  | 86 |
| 5.3 | Vesicle pool recovery . . . . .  | 88 |
| 5.4 | Comparison of recovery between unconditioned and conditioned state .                               | 91 |
| 5.5 | Development of miniature EPSCs . . . . .   | 93 |



# Abbreviations

|              |  |
|--------------|--|
| <b>AMPA</b>  | $\alpha$ -Amino-3-hydroxy-5-methyl-4-isoxazolepropionic acid |
| <b>BF</b>    | best frequency   |
| <b>CV</b>    | coefficient of variation                                     |
| <b>CN</b>    | cochlear nucleus   |
| <b>ECS</b>   | extracellular solution                                       |
| <b>EPSC</b>  | excitatory postsynaptic current                              |
| <b>EPSCG</b> | excitatory postsynaptic conductance                          |
| <b>EPSP</b>  | excitatory postsynaptic potential                            |
| <b>IID</b>   | interaural intensity difference                              |
| <b>IPSP</b>  | inhibitory postsynaptic potential                            |
| <b>ISI</b>   | inter spike interval   |
| <b>ITD</b>   | interaural time difference                                   |
| <b>LSO</b>   | lateral superior olive                                       |
| <b>LTD</b>   | long term depression   |
| <b>LTP</b>   | long term potentiation                                       |
| <b>MNTB</b>  | medial nucleus of the trapezoid body                         |
| <b>MSO</b>   | medial superior olive  |
| <b>NMDA</b>  | N-methyl-D-aspartate   |
| <b>PSTH</b>  | peri stimulus time histogram                                 |
| <b>PTP</b>   | post tetanic potentiation                                    |



# Summary

This study investigates the role of the medial nucleus of the trapezoid body (MNTB) in sound processing. The experimental part focuses on *in vitro* experiments in acute brain slices of Mongolian gerbils, in parallel a theoretical approach explains the experimental results in the context of a mathematical vesicle-release model.

One of the hallmarks of auditory neurons *in vivo* is spontaneous activity that occurs even in the absence of any sensory stimuli. Sound evoked bursts of discharges are thus embedded within this background of random firing. The calyx of Held synapse has been characterized *in vitro* as a fast relay that reliably fires at high stimulus frequencies (up to 800 Hz). However, inherently due to the preparation method, spontaneous activity is absent in studies using brain slices. This study deals with the question how this ongoing activity is influencing synaptic transmission. The answer is divided into three parts.

In the first part a phenomenological description of the effects of spontaneous activity on synaptic transmission is given. Therefore *in vivo* spontaneous firing rates were determined and then reintroduced as random firing patterns to *in vitro* brain stem synapses. After conditioning synapses for two minutes at Poisson averaged rates of 20, 40, and 60 Hz, a number of differences in synaptic transmission were observed. Accordingly, current-clamp, dynamic-clamp, and loose-patch recordings revealed a number of failures at the postsynaptic cell, although the initial onset of evoked activity was still transmitted with higher fidelity. The conclusion of these observations is that *in vivo* auditory synapses are in a tonic state of reduced EPSCs as a consequence of spontaneous spiking.

In the second part the conditioned state of calyx of Held synapse is closer investigated by modeling the short-term dynamics with a biophysically motivated vesicle release model. The mechanisms regulating short-term plasticity can be demonstrated in physiological studies as well as computer models aimed at testing the functional role of them. In the case of the calyx of Held synapse, considerable progress has

been made in understanding the dynamics of transmission both on a physiological and modeling level. Nevertheless, little is known about the processing of complex, long lasting stimulation patterns mimicking the input typically present in the intact brain. Furthermore, calyx of Held synapses are chronically active *emphin vivo* due to spontaneous activity in the auditory brainstem. Here we test synaptic responses to complex stimulation protocols mimicking periods of low and high activity, as well as protocols derived from natural sound clips. Additionally, all stimuli were embedded in chronic background activity attempting to imitate the naturally occurring spontaneous activity. We measured synaptic responses to these stimulus trains and then used the data to test how well several vesicle-release models could capture the dynamics observed physiologically. Already the most basic model variant produced very good results with correlation coefficients between the experimental data and the model prediction of more than 90%. None of the more complex model variants, which incorporated additional physiological effects, could improve this prediction accuracy significantly. The conclusion of these results is that the functional state of chronically active calyces differs from the functional state of silent calyces, and that this chronically active functional state can be described in simpler terms.

Finally the third part focuses on the transition phase between completely rested synapses and synapses conditioned with simulated spontaneous activity. Modeling the transition phase at the beginning of the conditioning period reveals significant changes in the model parameters thus suggesting changes in the underlying biophysical parameters including the vesicle pool size and the release probability. Recovery experiments after switching off the spontaneous activity confirm the reduced pool size and show a very slow recovery on a time scale of minutes. This slow recovery is accompanied by a reduction in the frequency of miniature EPSCs, a measure for the concentration of calcium ions in the presynaptic terminal. The observed changes again confirm the finding that synapses under the influence of ongoing activity show different properties than completely rested synapses.

Overall the results of this study show that spontaneous activity has significant influences on the synaptic dynamics of cells in the MNTB. The point of view that the calyx of Held is not just a relay station transforming excitatory input into inhibitory output is further strengthened, and this has consequences for the encoding of signals throughout the auditory pathway.

# Zusammenfassung

Diese Arbeit beschäftigt sich mit der Rolle des medialen Nucleus des Trapezkörpers (MNTB) während der Schallverarbeitung. Im experimentellen Teil werden *in vitro* Versuche an akuten Hirnschnitten von mongolischen Wüstenrennmäusen durchgeführt. Parallel dazu erklärt ein theoretischer Ansatz die experimentellen Resultate unter Zuhilfenahme eines mathematischen Modells, welches die Vesikelausschüttung beschreibt.

Eine der herausragenden Eigenschaften auditorischer Neuronen *in vivo* ist die Spontanaktivität, die sogar auftritt, wenn jegliche sensorische Stimuli fehlen. Entladungen, die von Schall verursacht werden, sind daher in dieses zufällige Hintergrundfeuern eingebettet. Die Heldsche Calyxsynapse wird *in vitro* als schnelles Relais angesehen, dass zuverlässig auf hohe Stimulationsfrequenzen (bis zu 800 Hz) antworten kann. In Hirnschnitten ist Spontanaktivität aufgrund der Präparationsmethode allerdings nicht vorhanden. Diese Studie beschäftigt sich mit der Frage, wie anhaltende Aktivität die synaptische Übertragung beeinflusst. Die Antwort gliedert sich in drei Teile.

Im ersten Teil wird eine phenomologische Beschreibung des Einflusses von Spontanaktivität auf die synaptische Übertragung gegeben. Hierzu wurden spontane Feuerraten *in vivo* ermittelt und als zufällige Stimulationsmuster *in vitro* verwendet. Nach einer zweiminütigen Konditionierungsphase mit poissonverteilten Feuerraten von 20, 40 und 60 Hz konnten mehrere Unterschiede in der synaptischen Übertragung festgestellt werden. Dazu passend zeigten current-clamp, dynamic-clamp und loose-patch Aufnahmen mehrere Ausfälle der postsynaptischen Zelle, obwohl der Beginn der evozierten Aktivität noch mit hoher Genauigkeit übertragen wurde. Diese Beobachtungen führen zu dem Schluss, dass sich auditorische Synapsen *in vivo* als Folge der Spontanaktivität in einem andauernden Zustand reduzierter EPSCs befinden.

Im zweiten Teil wird der konditionierte Zustand der Heldschen Calyxsynapse durch Modellierung der Kurzzeitdynamik mit einem biophysikalisch motivierten Modell der Vesikelausschüttung genauer beschrieben. Die Mechanismen, die die Kurzzeitdynamik

regulieren, können anhand von physiologischen Studien oder Computermodellen veranschaulicht werden, die dazu ausgelegt sind, die funktionelle Aufgabe dieser Dynamik zu testen. Im Fall der Calyxsynapse wurden schon viele Ergebnisse sowohl in physiologischen Experimenten als auch in Computermodellen erzielt. Nichts desto trotz ist wenig über die Verarbeitung von lang laufenden Stimulationsmustern, die die im intakten Gehirn typischen Eingangssignale nachahmen, bekannt. Darüber hinaus sind Heldsche Calyxsynapsen *in vivo* aufgrund der Spontanaktivität des auditorischen Hirnstamms chronisch aktiv. In diesem Teil werden die Antworten von Synapsen auf komplexe Stimulationsprotokolle getestet, die Perioden hoher und niedriger Aktivität nachahmen und auf Protokolle, die von natürlichen Geräuschen abgeleitet wurden. Zusätzlich wurden alle Stimulationen in chronische Hintergrundaktivität eingebettet, um die natürlich vorkommende Spontanaktivität zu imitieren. Die synaptischen Antworten wurden gemessen und dazu benutzt, verschiedene Modelle der Vesikelausschüttung auf ihre Fähigkeit zu testen, die physiologisch beobachtete Dynamik vorherzusagen. Schon die einfachste Modellvariante erzeugte sehr gute Resultate mit Korrelationskoeffizienten zwischen den experimentellen Daten und der Modellvorhersage von über 90%. Keine der komplexeren Varianten, die zusätzliche physiologische Effekte berücksichtigten, konnte die Genauigkeit der Vorhersage signifikant steigern. Das Fazit dieser Ergebnisse besteht darin, dass der funktionelle Zustand der chronisch aktiven Calyx sich vom funktionellen Zustand nicht aktiver Calyces unterscheidet und dass dieser Zustand chronischer Aktivität einfacher beschrieben werden kann.

Der dritte Teil der Arbeit beschäftigt sich mit der Übergangsphase zwischen vollständig ausgeruhten Synapsen und Synapsen, die mit simulierter Spontanaktivität konditioniert wurden. Die Modellierung der Übergangsphase am Anfang der Konditionierung lässt signifikante Änderungen der Modellparameter erkennen. Dies legt nahe, dass sich auch die zugrunde liegenden biophysikalischen Parameter wie die Anzahl der Vesikel und die Freisetzungswahrscheinlichkeit ändern. Experimente über die Erholungsphase nach Beendigung der Spontanaktivität bestätigen die reduzierte Vesikelanzahl und zeigen eine sehr langsame Erholungsphase mit einer Dauer im Bereich von Minuten. Diese langsame Erholung wird von einer Abnahme der Frequenz von Miniatur EPSCs begleitet, welche ein Maß für die Konzentration von Kalziumionen im präsynaptischen Terminal darstellen. Diese gemessenen Unterschiede bestätigen die Erkenntnis, dass sich Synapsen unter dem Einfluss von andauernder Aktivität anders verhalten als vollständig ausgeruhte Synapsen.



Insgesamt zeigen die Resultate dieser Studie, dass Spontanaktivität signifikante Einflüsse auf die synaptische Dynamik von Zellen des MNTB hat. Der Standpunkt, dass die Heldsche Calyx mehr als ein Relais zum Umschalten von Exzitation in Inhibition ist, wird weiter gestärkt. Dies birgt Konsequenzen für die Signalverarbeitung in der gesamten auditorischen Verarbeitungskette.



# 1 Introduction

The medial nucleus of the trapezoid body (MNTB) is probably one of the best studied nuclei in the mammalian brain. The system is studied so well because the synapses found in this nucleus, the so-called calyces of Held, are extraordinarily big compared to almost all other synapses. Therefore, they are accessible to direct patch-clamp recordings, a big experimental advantage and the main reason why they have become one of the model systems for studying synaptic transmission. Being a model system attracts a lot of attention, but as expected most people doing research on this nucleus want to understand how synapses work in general, they are not particularly interested in the function of this special synapse. Therefore, the job of this synapse and of the whole nucleus in the surrounding processing chain is surprisingly little investigated.

The main reason why the MNTB has not drawn the attention of systematic network studies might be that there seems to be a very easy explanation of the functionality of this nucleus. This would of course make further investigations needless. So, what is this simple functionality? The MNTB is a nucleus in the auditory brainstem and has one dominating input, the calyx of Held synapse. This input is excitatory and the output of the MNTB is inhibitory. The simple view of the MNTB functionality is that the nucleus generates one output spike for every incoming spike, thereby working as a sign-inverting relay. In terms of information processing this corresponds to a multiplication with  $-1$ , one of the easiest manipulations possible. How would more complex transformations look like? A cell with only one synapse (this is an idealized view, but will be valid for most parts of this work) does not have many possibilities to alter the information of the incoming spike train. In the case of the calyx of Held it can basically do two things: It can decrease the spike count by leaving out certain spikes in its response or it can dynamically change the delay between incoming and outgoing spike, thereby altering the inter spike intervals.

These possibilities still sound fairly easy, but as a closer look at the different stages between input and output reveals a picture that is a little bit more complicated. The

process between arrival of a spike at the nucleus and generation of the response can be divided into two parts, the generation of a synaptic current at the calyx of Held and the answer of the principal cell to this synaptic input. The input to the MNTB is a precisely timed stream of action potentials. Each one of these action potentials is converted in the synapse to a certain amount of released neurotransmitter molecules. These are generating a synaptic current which is depolarizing the principal cell and thereby possibly leading to an action potential, the output of the MNTB. So the ‘digital’ input (action potentials do not have a meaningful amplitude) is converted to an ‘analog’ signal (the synaptic strength) and then transferred back to a ‘digital’ output (the outgoing action potential).

To understand the function of the MNTB, three aspects are important. First, the role of the MNTB in sound processing. Where is it located in the processing chain and in which tasks is it involved? Second, how do the inputs to the MNTB look like and what specializations does the nucleus show? Third, which rules govern the temporal dynamics of the synaptic transmission? The following sections will summarize the current state of knowledge about these three fields.

## 1.1 The auditory brainstem

The MNTB is the second processing stage after the mechanical vibrations of sound have been transferred to electrical signals in the hair cells of the cochlea (Evans, 1992). The hair cells send projections to the cochlear nucleus (CN). This nucleus shows a big variety of many different cells projecting to different nuclei (Cant and Benson, 2003). The globular bushy cells in the anteroventral part of the CN send axons to the MNTB (Smith et al., 1991). These axons terminate in giant glutamatergic synapses, the so called calyx of Held synapses. They are highly specialized for fast and reliable transmission and due to their big size one of the best studied synapses in the whole mammalian brain. The output of the MNTB is glycinergic and it is the main source of inhibition in the auditory brainstem. The MNTB projects exclusively to ipsilateral nuclei. The main targets are the lateral superior olive (LSO) and the medial superior olive (MSO) (Sanes and Siverls, 1991; Smith et al., 1998). Additional projections to higher nuclei like the nuclei of the lateral lemniscus and the inferior colliculus as well as projections to the MNTB itself and back to the CN have been reported (Spangler et al., 1985; Sommer et al., 1993; Riemann and Reuss, 1998).

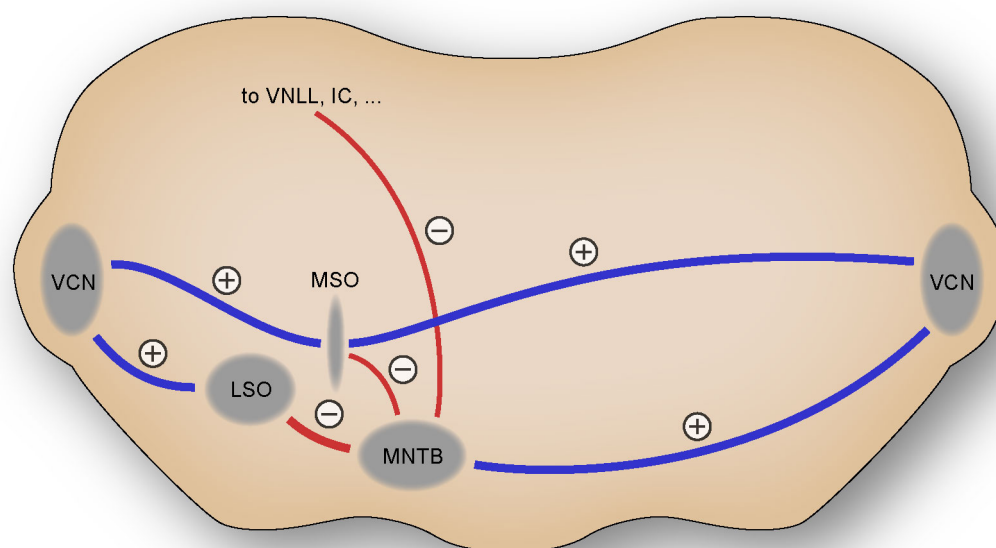


**Figure 1.1:** A schematic drawing of the auditory brainstem. Depicted are the most important pathways in which the MNTB is involved. Excitatory (glutamatergic) projections are drawn in blue, inhibitory (glycinergic) connections in red.

This work uses Mongolian gerbils (*Meriones unguiculatus*) as experimental animals. In contrast to other rodents, gerbils hear quite well in the low frequency regime ( $< 2000$  Hz). The lowest detection thresholds are around 5000 Hz, but they can perceive sounds with frequencies as low as several 10 Hz. This is very similar to the hearing curve of humans (Ryan, 1976) and makes gerbils a popular model system for auditory processing. The MNTB receives input from the whole perceivable frequency range. As already mentioned the main projections of the MNTB are to the MSO and the LSO. These nuclei are the first processing stages, where binaural information converges. The main function of these two nuclei is thought to be the processing of information about the location of a sound source in the horizontal plane (Tollin, 2003; Grothe, 2000). There are two strategies to determine the azimuthal origin of a sound, namely interaural intensity differences (IID) and interaural time differences (ITD).

IIDs are caused by the shielding effect of the head which dampens sounds that have to travel through the head to reach the opposing contralateral ear. This effect works well for high frequencies with wave lengths significantly smaller than the head

diameter. IIDs are supposedly mainly processed in the LSO. This nucleus receives excitatory input from the ipsilateral side and inhibitory input from the contralateral side. Simply spoken it compares the firing rates of the two inputs and answers with a firing rate corresponding to the relation between excitation and inhibition. The determination of a firing rate requires integration over time. As a consequence of this rate code, no precise timing of the individual inputs is necessary. The inhibitory input to the LSO originates from the MNTB. The important feature of the MNTB output for this task is a well defined firing rate, not precise timing. Well defined in this regard means a firing rate which is mainly depending on the sound source location (high firing rates for ipsilateral origin and low rates for contralateral origin).

Of course, this is not the only function of the MNTB. It also sends projections to the MSO and is therefore involved in the processing of ITDs. In contrast to IIDs, the ITD processing depends on very precise timing of the inputs. In the MSO the arrival times of a specific sound at the two ears are compared. Idealized a sound generates similar spike trains in the cochlea of both ears with a time delay between the two patterns that corresponds to the time delay caused by the different traveling times from origin to ear. Cells in the MSO receive these two spike trains as excitatory input and fire with a rate which is mainly depending on the time delay between the inputs, thereby coding for the timing difference. Additionally to the two excitatory inputs the cells also receive a notable amount of inhibitory input, mainly originating from the MNTB. This input is thought to be responsible for the fine tuning of the ITD-rate function (Brand et al., 2002; Grothe, 2003; McAlpine and Grothe, 2003). According to this theory the timing of the inhibitory signal would need to be comparably precise to the excitatory signals. For the MNTB this means, that the precision of its input has to be conserved.

Generally spoken, for the sound source analysis of high frequency input precise timing is not so much necessary, as the information is conveyed using a rate code rather than a time code. In the low frequency regime instead, precise timing is crucial, as the information processing depends on the comparison of arrival times of different inputs. This description is a little bit simplified, it does for example not account for low frequency processing in the LSO (Tollin and Yin, 2005) or envelope ITD processing of sounds with high frequency carrier waves (Joris and Yin, 1995). But for the investigation of the MNTB functionality the two presented processing strategies are sufficient. As the MNTB is involved in high as well as low frequency processing, the

input output relation should exhibit precise time delays and at the same time produce well defined firing rates. This does not mean that the time delay should be as constant as possible and the firing rate should be highly conserved (this would correspond to the simple relay idea). It only means that the random fluctuations in time delay and firing rate should be as small as possible. How the firing rate and the time delay are altered in the MNTB is subject to this study.

## 1.2 The calyx of Held

Cells of the MNTB are highly specialized. Their main input is a giant glutamatergic synapse, the calyx of Held. Besides this input, they also receive a significant amount of inhibitory input (Banks and Smith, 1992; Awatramani et al., 2004), as well as conventional excitatory input (Forsythe and Barnes-Davies, 1993; Hamann et al., 2003). Unfortunately, no solid data about the origin of the conventional input to the MNTB is available. It is therefore hardly possible to draw conclusions about their function. For this reason the additional inputs will in large parts of this work not be considered.

In contrast to this, a lot of information is known about the calyceal input. As already apparent from figure 1.2 the calyx differs from other synapses in many ways, first of all its size. Several electron-microscopy studies (Lenn and Reese, 1966; Nakajima, 1971; Sätzler et al., 2002; Taschenberger et al., 2002) as well as many electrophysiological studies (Sakaba et al., 2002; Neher and Sakaba, 2003) have been conducted to characterize the quantal parameters of the calyx of Held. A summary of the specializations of the calyx of Held can be found here (Schneppenburger and Forsythe, 2006). One of the most important features in the context of this study is the very large vesicle pool size. It enables the synapses to generate big excitatory postsynaptic currents (EPSC) even under high frequency stimulation and allows to a certain degree faithful transmission of the incoming signal. Electron-microscopy studies have shown the presence of  $\sim 550$  active zones containing on average two docked vesicles (Sätzler et al., 2002). Electrophysiological studies using EPSC fluctuation analysis support these results (Meyer et al., 2001). The other important feature besides a faithful transmission is the synaptic delay. Especially in the context of ITD processing precise timing is very crucial and a constant delay might be favorable. Moreover, the detour over the MNTB to invert excitation to inhibition introduces an additional synaptic transmission into the pathway. To allow the inhibition to shape the ITD rate function, the signals should arrive si-

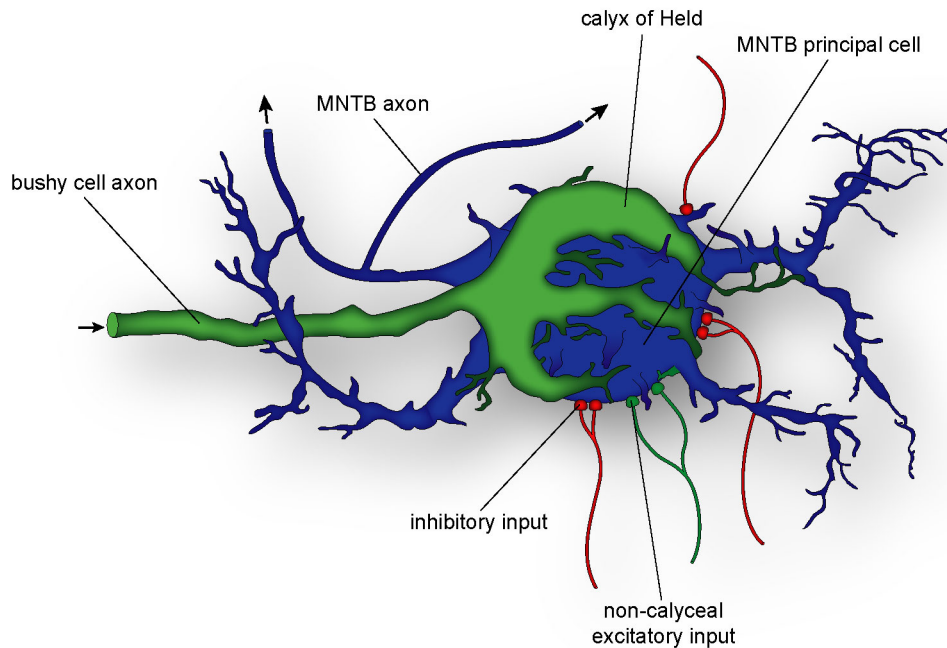


**Figure 1.2:** An artist's rendering of a MNTB neuron, modified from microscope pictures (Morest, 1968). The calyx of Held is shown in green. It has a finger-like structure which is grasping the blue principal cell. This structure guarantees a big contact area while at the same time leaving enough space to quickly remove neurotransmitter from the synaptic cleft. Additionally, several glycinergic inhibitory inputs and non-calyceal excitatory inputs are drawn in red and green, respectively.

multaneously at the binaural nuclei (Brand et al., 2002). Therefore, this extra synapse has to be tuned for fast transmission with a minimal delay. Indeed the presynaptic action potential is very fast with a half-width of  $\sim 0.2$  ms (Borst and Sakmann, 1998; Kushmerick et al., 2006; Taschenberger and von Gersdorff, 2000). The synaptic delay between the peak of the presynaptic inward current deflection and the onset of an EPSC in the postsynaptic cell is  $\sim 0.5$  ms (Fedchyshyn and Wang, 2007).

### 1.3 Short-term plasticity

Information processing at the calyx of Held means the transformation of a stream of 'digital' events carrying no amplitude information (action potentials) into 'analog' signals with amplitude (synaptic release of a certain amount of vesicles). The size of



the amplitudes is determined by the arrival times of the preceding action potentials. It is changing on different time scales. On long time scales (minutes up to hours) effects like a permanent increase of synaptic strength called long term potentiation (LTP) or a decrease called long term depression (LTD) can be induced (Chang et al., 2003; Kotak and Sanes, 2000). These effects are often related to up and down regulation of second messenger cascades (Trussell, 2002). On short time scales (milliseconds to seconds) the synaptic strength is governed by completely different factors. It depends on the number of vesicles available for release, on their  $\text{Ca}^{2+}$  sensitivity, and on the properties of the  $\text{Ca}^{2+}$  influx in answer to arriving action potentials. These three parameters determine how many vesicles are released for a single synaptic event. But the synaptic strength not only depends on the amount of released vesicles, it also depends on the state of the postsynaptic receptors. In the following paragraphs, three presynaptic mechanisms, namely vesicle pool depletion,  $\text{Ca}^{2+}$ -channel inactivation, and accumulation of  $\text{Ca}^{2+}$  in the presynaptic terminal will be introduced. To complete the picture also a postsynaptic mechanism, namely receptor desensitization will be mentioned.

Short-term depression and facilitation are phenomenological terms and simply refer to a decrease or increase in EPSC amplitude in answer to repeated stimulations. The underlying mechanisms can be of pre- as well as postsynaptic nature. In gerbils used in this study (aged P14 - P19) short-term depression is the dominating factor. EPSCs show a strong decrease in amplitude during stimulation with high-frequency pulse trains. This decrease follows an exponential time course. Two possible reasons for this depression have been proposed:  $\text{Ca}^{2+}$ -channel inactivation or vesicle depletion. For low frequency stimulation (2 Hz - 30 Hz) in young rats (P7 - P10),  $\text{Ca}^{2+}$ -channel inactivation is suggested to be the major cause of EPSC depression (Xu and Wu, 2005). A decrease in  $\text{Ca}^{2+}$  influx causes fewer vesicles to fuse with the presynaptic membrane even if enough readily releasable vesicles are present. This leads to a decreased amount of released neurotransmitters and smaller EPSCs. For higher frequencies depletion of the vesicle pool becomes the dominating cause for short-term depression as the vesicle recycling rate gets significantly smaller than the vesicle consumption. For calyx of Held synapses the release probability in animals aged P8 - P10 is above 0.2 (Schneggenburger et al., 1999). This means that for every event more than a fifth of the vesicles in the readily releasable pool is released. The recycling process shows a double exponential recovery of the pool with a fast time constant of  $\sim 200$  ms and a

slow time constant of several seconds (Wang and Kaczmarek, 1998; Sakaba and Neher, 2001a). According to these values already a stimulation with a 10 Hz train leads to a serious amount of depression as the inter spike interval of 100 ms is only half as long as the fast characteristic time constant of recovery.

Phenomenologically, facilitation at the calyx is only visible at decreased extracellular  $\text{Ca}^{2+}$  concentrations. Lower extracellular  $\text{Ca}^{2+}$  levels lead to less  $\text{Ca}^{2+}$  influx into the terminal and thus to a lower release rate. This reduces the amount of depression, thereby unmasking the effect of facilitation. Facilitation is generally thought to be caused by an elevation in intracellular  $\text{Ca}^{2+}$  remaining from the preceding stimuli (Zucker and Regehr, 2002; Dittman et al., 2000; Borst and Sakmann, 1998; Cuttle et al., 1998). This theory is supported by the fact that  $\text{Ca}^{2+}$  chelators can attenuate both residual  $\text{Ca}^{2+}$  and facilitation (Zucker and Regehr, 2002). Due to the overwhelming effect of vesicle pool depletion  $\text{Ca}^{2+}$  accumulation only plays a minor role in the short-term dynamics of the calyx of Held.

Another effect influencing short-term dynamics of synaptic transmission is the post-synaptic  $\alpha$ -Amino-3-hydroxy-5-methyl-4-isoxazolepropionic acid (AMPA) receptor desensitization (Wang and Kaczmarek, 1998; Zhang and Trussell, 1994). Experiments with cyclothiazide, an agent that prevents AMPA receptor desensitization showed that high stimulation frequencies (200 Hz) can lead to changes in the depression time course of developing calyces (Joshi et al., 2004). However, it is not present anymore at ages of P16 to P18 (Renden et al., 2005). As the gerbils of this study are P14 and older, the effect of receptor desensitization should be negligible. This leaves vesicle pool depletion and the recovery time course of the vesicle pool as the two dominant factors of short-term dynamics at the calyx of Held.

## 1.4 Objective of this work

Though the MNTB has drawn a lot of attention in the *in vitro* community, the link between *in vitro* experiments and the role of the MNTB in the network of the auditory brainstem is hardly investigated. As already mentioned, this is probably mainly due to the fact, that the MNTB was for a long time regarded as a simple switch for the inversion of excitation to inhibition. But as recent *in vivo* studies revealed that the necessary one to one transmission is not true (Kopp-Scheinpflug et al., 2003; Guinan and Li, 1990), the view of the MNTB as a simple relay station cannot be maintained

---

anymore. This of course raises the question about the additional functionality of the MNTB. This study is a first step to gain a coherent picture about the role of the MNTB in auditory processing. It focuses on the synaptic transmission at the calyx of Held, though also a few statements about the functionality of the nucleus as a whole will be made. The synaptic transmission is studied *in vitro*, but with a strong focus on natural experimental conditions. This means physiological solutions and temperature, but also naturalistic input patterns. With this approach, the gap between *in vitro* and *in vivo* experiments can be bridged and the functionality of the calyx of Held synapse can be related to the auditory network.



## 2 Materials and Methods

### 2.1 In vivo recordings

Auditory responses from 36 single neurons were recorded in 16 Mongolian gerbils (*Meriones unguiculatus*) of both sexes, aged between 21 days and 60 days. We found no systematic differences in aurality, firing frequency, threshold, characteristic frequency, or other response parameters of neurons, which depended on the age of the animal (data not shown), and thus the data from all 36 neurons were pooled. In our sample there was also no covariation between spontaneous activity and auditory threshold or between spontaneous activity and a neuron's characteristic frequency (regression analysis, data not shown). Data were collected simultaneously for this study and a different project involving MNTB response properties (data not shown). All experiments complied with institutional guidelines and were approved by the appropriate government authorities (Reg. Oberbayern AZ 55.2-1-54-2531-57-05).

#### 2.1.1 Surgical procedures

Before surgery, animals were anaesthetized by an initial intraperitoneal injection (0.5 ml / 100 g body weight) of ketamine (20%) and xylacine (2% both in physiological NaCl). During surgery and recordings, a dose of 0.05 ml of the same mixture was applied subcutaneously in scheduled intervals that were based on the animal's body weight. Constant body temperature was maintained using a thermostatically controlled heating blanket.

Skin and tissue covering the upper part of the skull were removed, and a small metal rod was mounted to the frontal part of the skull using UV-sensitive dental-restorative material (Charisma, Heraeus Kulzer, Germany). Custom made ear-phone holders were attached to the gerbil head, allowing for the safe insertion of ear-phones or probe tube microphones into the ear canal. The animal was then transferred to a sound attenuated chamber and mounted in a custom-made stereotaxic instrument ([Schuller](#)

et al., 1986). The animal's position in the recording chamber was standardized in reference to stereotaxic landmarks on the skull (Loskota et al., 1974). For electrode penetrations to the MNTB, a small hole of approximately 1 mm<sup>2</sup> was cut into the skull lateral to the lambdoid suture. Micromanipulators were used to position the recording electrode according to landmarks on the brain surface and a reference point, which was used for all penetrations. The meninges overlying the cortex were removed and saline was applied to the opening to prevent dehydration of the brain.

Typical recording sessions lasted 10 - 14 h. After successful recordings, the animal was sacrificed by injecting an overdose of chloral hydrate (Sigma, Germany). The last electrode position was then marked with a current induced lesion (20  $\mu$ A for 80 - 120 s). The head was fixated in 4% paraformaldehyde and prepared for anatomical processing. Transverse sections were cut and Nissl-stained to verify the recording sites. An example of an anatomical verification is shown in figure 2.1 C. The lesion site can be clearly seen in the center of the left MNTB.

### 2.1.2 Recordings of neural activity

Single-unit responses were recorded extracellularly using 10 M $\Omega$  glass electrodes filled with 1M NaCl. The recording electrode was advanced under remote control, using a piezodrive (Inchworm controller 8200, EXFO Burleigh Products Group Inc, USA). Extracellular action potentials were recorded via an electrometer (npi electronics, Germany or Electro 705, WPI, Germany), a 50/60 Hz noise eliminator (Humbug, Quest Scientific, Canada), a band-pass filter (VBF/3, Kemo, Italy) and an amplifier (Toellner 7607, Germany), and subsequently fed into the computer via an A/D-converter (RP2-1, Tucker-Davis Technologies, USA). Clear isolation of action potentials from a single neuron (signal to noise ratio > 5) was achieved by visual inspection on a spike-triggered oscilloscope and by offline spike cluster analysis (Brainware, Tucker-Davis Technologies, USA). Two examples of recorded single cell spikewaveforms are shown in figure 2.1 A and B. The unit in figure 2.1 A is an example of a neuron with a low spontaneous rate (10 Hz), while figure 2.1 B shows an example of a neuron with a very high spontaneous rate (107 Hz). Both units were recorded from the same animal; the histological verification of the recording site is shown in figure 2.1 C.

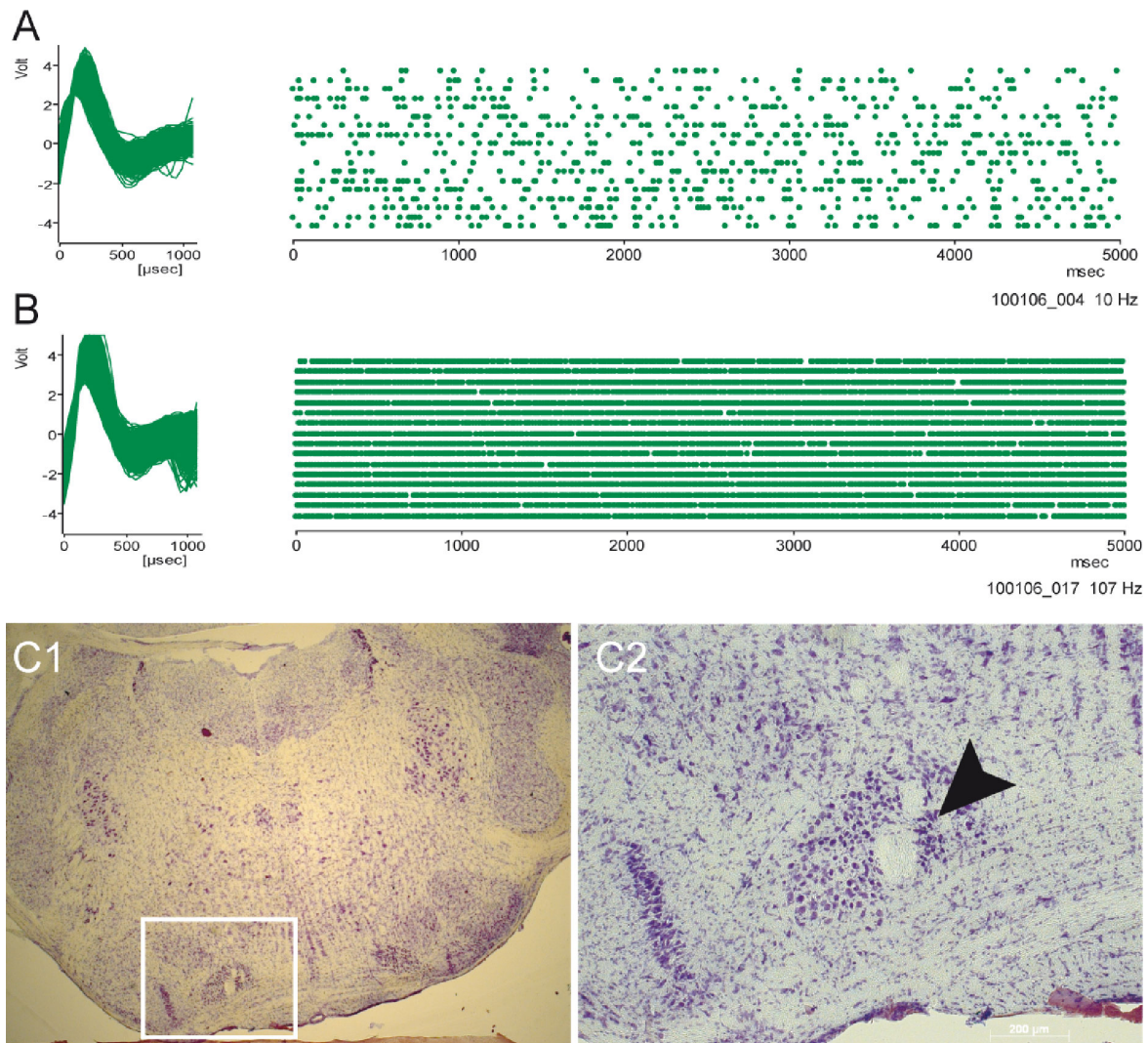


**Figure 2.1:** A and B: Spike waveforms and raster displays of two single MNTB neurons of our data sample. The overlay of the spike waveforms indicates well isolated single units. The raster plots show the spontaneous firing rates of the two neurons, which were 10 Hz and 107 Hz, respectively. Both units were recorded in the same animal. C1 and C2: Anatomical reconstruction of the recordings site in the same animal. C1 represents an overview of the brainstem (coronal section) while C2 is a magnification of the recording site. The black arrow marks the electrical lesion produced with the recording electrode, which is in the center of the MNTB.

### 2.1.3 Stimulus presentation and recording protocols

Stimuli were generated at a 50 kHz sampling rate using TDT System III (Tucker-Davis Technologies, USA). Digitally generated stimuli were converted to analog signals (DA3-2 / RP2-1, Tucker-Davis Technologies, USA), attenuated (PA5, Tucker-Davis Technologies, USA) and delivered to earphones (MDR-EX70LP, Sony, Germany).

The standard stimulus was a 200 ms toneburst with a rise-fall-time of 5 ms, presented at a repetition rate of 2 Hz. Stimulus presentation was randomized. To search for acoustically evoked responses, noise stimuli were delivered binaurally. When an auditory neuron was encountered, we first determined its best frequency (BF) and absolute threshold audiovisually to set stimulus parameters subsequently controlled by the computer. The frequency that elicited responses at the lowest sound intensity was defined as BF, the lowest sound intensity evoking a noticeable response at BF as threshold. These properties were confirmed by offline analysis of the frequency versus level response areas. Monaural pure tones to each ear and binaural pure tones without interaural intensity or time differences were presented to define the aurality of the neuron. MNTB neurons responded only to stimulation of the contralateral ear with a tonic/primary like firing pattern and were not affected by stimulation of the ipsilateral ear.

Spontaneous activity of a neuron was determined by recording action potentials in several 5 s long intervals without sound stimulation, and averaging the measured firing rate. All quantifications of *in vivo* data are based on offline analysis with the software packages Brainware (Tucker-Davis Technologies, USA), Matlab 6.5 (The Mathworks, Inc., USA), and IGOR 5 (Wavemetrics, USA).

## 2.2 In vitro recordings

Coronal slices of brainstem were prepared from Mongolian gerbils (*Meriones unguiculatus*) aged 14 to 19 days old. Data from these different ages were pooled, since no age-dependent variation in synaptic amplitudes, degree of depression, response to conditioning, or firing probability was observed (data not shown).



### 2.2.1 Slice preparation

Animals were briefly anesthetized by isoflurane inhalation (Isofluran Curamed, Curamed Pharma, Germany) and decapitated. The brainstem was dissected out under ice-cold dissection ringer (125 mM NaCl, 2.5 mM KCl, 1 mM MgCl<sub>2</sub>, 0.1 mM CaCl<sub>2</sub>, 25 mM glucose, 1.25 mM NaH<sub>2</sub>PO<sub>4</sub>, 25 mM NaHCO<sub>3</sub>, 0.4 mM ascorbic acid, 3 mM myo-inositol, 2 mM pyruvic acid; all chemicals from Sigma, Germany). Sections of 200 - 250  $\mu$ m were cut with a vibratome (VT1000S, Leica, Germany). Slices were transferred to an incubation chamber containing extracellular solution (ECS) (125 mM NaCl, 2.5 mM KCl, 1 mM MgCl<sub>2</sub>, 2 mM CaCl<sub>2</sub>, 25 mM glucose, 1.25 mM NaH<sub>2</sub>PO<sub>4</sub>, 25 mM NaHCO<sub>3</sub>, 0.4 mM ascorbic acid, 3 mM myo-inositol, 2 mM pyruvic acid; all chemicals from Sigma, Germany) and bubbled with 5% CO<sub>2</sub> - 95% O<sub>2</sub>. Slices were incubated for 1 hour at 37<sup>0</sup> C, after which the chamber was brought to room temperature. Recordings were obtained within 4 - 5 hours of slicing.

### 2.2.2 Whole-cell recordings

All recordings were performed at 36<sup>0</sup> - 37<sup>0</sup> C. After incubation, slices were transferred to a recording chamber and continuously superfused with ECS at 3 - 4 ml/min through a gravity-fed perfusion system. MNTB neurons were viewed through a Zeiss Axioskop 2 FS microscope equipped with DIC optics and a 40x water-immersion objective (Zeiss, Germany). Whole cell recordings were made with an EPC 10 double amplifier (HEKA Instruments, Germany). Signals were filtered at 5 - 10 kHz and subsequently digitized at 20 - 100 kHz using Patchmaster Version 2.02 software (HEKA Instruments, Germany). Uncompensated series resistance was between 5.5 M $\Omega$  and 15 M $\Omega$  and was compensated to values between 2.1 and 5.8 M $\Omega$  with a lag time of 10  $\mu$ s. Potential changes in series resistance were monitored throughout the recordings and data collection was discontinued whenever series resistance changed by more than 2 M $\Omega$ . All voltages are corrected for a -12 mV junction potential.

Patch pipettes were pulled from 1.2 mm borosilicate glass (WPI, Germany) or 1.5 mm borosilicate glass (Harvard Instruments, United Kingdom) using a Sutter P-97 electrode puller (Sutter Instruments, USA) or a DMZ Universal Puller (Zeitz Instruments, Germany). Pipettes were filled with potassium gluconate based internal solution for current clamp recordings (120 mM K-Gluconate, 4 mM MgCl<sub>2</sub>, 10 mM HEPES, 5 mM EGTA, 10 mM trisphosphocreatine, 4 mM Na<sub>2</sub>-ATP, 0.3 mM tris-

GTP, 0.5 mM CaCl<sub>2</sub>, all chemicals from Sigma, Germany) or cesium methanesulfonate based solution for voltage clamp recordings (125 mM CsMeSO<sub>3</sub>, 4.5 mM MgCl<sub>2</sub>, 9 mM HEPES, 5 mM EGTA, 14 mM tris-phosphocreatine, 4 mM Na<sub>2</sub>-ATP, 0.3 mM tris-GTP, 1.5 mM CaCl<sub>2</sub>, all chemicals from Sigma).

During all recordings, 500 nM strychnine hydrochloride (Sigma, Germany) and 20 μM SR95531 were added to the bath to block glycinergic and GABA<sub>A</sub>-ergic inhibition, respectively. During voltage clamp recordings, 5 mM QX-314 (Alomone Labs, Israel) was added to the pipette fill to eliminate sodium currents.

### 2.2.3 Stimulation of synaptic inputs

Synaptic currents were elicited either by midline stimulation of the calyceal input fiber bundle with a 5 MΩ bipolar stimulation electrode (matrix electrodes with 270 μm distance, Frederic Haer Company, USA). Stimuli were 100 μs long square pulses of 10 to 40 V delivered with a STG 2004 computer controlled 4-channel stimulator (Multi-channel Systems, Germany) and a stimulation isolation unit (Iso-flex, AMPI, Israel). The stimulator permitted completely independent uploading and operation of the four channels allowing the seamless integration and thus, true embedding of simulated auditory signals (i.e. high-frequency bursts) in the simulated spontaneous activity. Spontaneous activity was simulated by using 20 Hz, 40 Hz, and 60 Hz Poisson distributed stimulus trains (figure 3.3 A - C). Sound evoked activity was simulated by short trains consisting of 20 stimuli at 100 Hz, 300 Hz, or 600 Hz.

### 2.2.4 Conductance clamp experiments

Excitatory conductances were simulated with a SM-1 amplifier (Cambridge Conductance, Cambridge, United Kingdom). The 10 – 90% rise of the current output in response to a voltage change for this amplifier is 290 ns. Reversal potentials were set to 0 mV for the excitatory postsynaptic conductances (EPSCs). The conductance waveforms used were previously recorded as EPSCs in voltage clamp mode. After extrapolating the artifacts, EPSCs were normalized. All conductance values correspond to peak conductances. In experiments in which background leak was added, a constant step command was fed from the computer into the conductance clamp amplifier via a separate channel, and the reversal potential for this channel was set to -60 mV. The separately calculated output of both channels was added together and fed to the

HEKA amplifier.

### 2.2.5 Miniature EPSC analysis

For the detection of miniature EPSC a routine developed by Holger Taschenberger was used. This routine is based on a template detection algorithm described earlier (Clements and Bekkers, 1997). In short the routine uses an artificial mini template and compares this template with the trace which is analyzed. To find similarities a cross correlation between the template and the normalized and offset corrected trace is calculated. In this study a successful mini detection was defined by a peak in the correlation trace bigger than five times the standard deviation of the correlation trace.

## 2.3 Vesicle release model

To assess the short term dynamics of synaptic currents, a vesicle release model was implemented and fitted to the experimental data. The underlying assumptions of the model were a single and homogeneous pool of synaptic vesicles with a constant release probability  $P_R$  and a single exponential recovery time course with a decay time  $\tau$ . The dynamically changing current amplitudes were described by the following equation:

$$\frac{dI}{dt} = - \sum_n P_R \cdot I \cdot \delta(t - t_n) + \frac{I_0 - I}{\tau}$$

with  $I$  representing the amount of neurotransmitter available from all readily releasable vesicles in the presynaptic terminal;  $t_n$  indicating the time points of synaptic events;  $I_0$  being the amount of neurotransmitter in case of a fully recovered functional vesicle pool. The first term represents the synaptic depression while the second term represents the recovery from depression. This differential equation can be solved to calculate the current corresponding to the amount of vesicles available at the synaptic event  $n$  based on values calculated for event  $n - 1$  as follows:

$$I_n = I_0 - (I_0 - I_{n-1}(1 - P_R)) \cdot \exp\left(\frac{-(t_n - t_{n-1})}{\tau}\right)$$

The synaptic current  $i_n$  is a fraction of the available vesicles and is calculated with the equation  $i_n = P_R \cdot I_n$ . This value was compared to the experimentally measured

EPSC amplitudes. The model has three free parameters, namely  $P_R$ ,  $\tau$ , and  $I_0$ . To calculate the optimal parameter set the squared error

$$\frac{1}{N} \sum_{n=1}^N \Delta i_n^2 = \frac{1}{N} \sum_{n=1}^N (i_n(\text{experiment}) - i_n(\text{model}))^2$$

was minimized using the downhill simplex method (Nelder and Mead, 1965).

### 2.3.1 Model variants

To account for additional influences on short term dynamics of synaptic currents, three variants of the vesicle release model were implemented. In the first variant, the single exponential recovery was replaced by a double exponential time course (Wang and Kaczmarek, 1998):

$$\frac{dI}{dt} = - \sum_n P_R \cdot I \cdot \delta(t - t_n) + \frac{I_0^{fast} - I}{\tau_{fast}} + \frac{I_0^{slow} - I}{\tau_{slow}}$$

For the second extension synaptic facilitation was included (Varela et al., 1997). The release probability was raised for every synaptic event by the factor  $F \cdot (1 - P_R)$  to restrict the release probability to values smaller than 1. In between events it decayed with the characteristic time constant  $\tau_R$  back to its minimum value  $P_R^{min}$ .

$$\frac{dI}{dt} = - \sum_n P_R \cdot I \cdot \delta(t - t_n) + \frac{I_0 - I}{\tau}$$

$$\frac{dP_R}{dt} = \sum_n F \cdot (1 - P_R) - \frac{P_R^{min} - P_R}{\tau}$$

In the third variant, an additional factor  $R(t)$  representing receptor desensitization was included (Graham et al., 2004):

$$i_n = P_R \cdot I_n \cdot R(t)$$

The time course of this factor was described by the following equation:

$$\frac{dR}{dt} = \sum_n D \cdot \frac{I_n}{I_0} - \frac{1 - R}{\tau_D}$$

The factor  $D$  defines the percentage of receptors which desensitize for each synaptic event,  $\tau_D$  describes the exponential recovery from this desensitized state.

Since the model variants affect distinct parts of the basic model, the improvements can also be combined. For all three variants and their combinations, the additional free parameters were included into the parameter optimization and the squared error was minimized similar to the simple model.

### 2.3.2 Model predictions

For stimulation patterns with regular inter pulse intervals the model can also be used to calculate predictions for the steady state amplitude  $I^*$  in dependence of the stimulation frequency  $f$  and the characteristic time constant  $\tau_A$  that describes the exponential time course from any amplitude to this steady state. To calculate these two values, the iterative formula for  $I_n$  is rewritten as

$$I_n = a + b \cdot I_{n-1}$$

with  $a$  and  $b$  representing the more complex terms from the original equation describing the basic model:

$$a = I_0 - I_0 \cdot \exp\left(\frac{-(t_n - t_{n-1})}{\tau}\right)$$

$$b = (1 - P_R) \cdot \exp\left(\frac{-(t_n - t_{n-1})}{\tau}\right)$$

The steady state amplitude can be calculated by equating the current at event  $n$  and event  $n - 1$ .

$$I^* = \frac{a}{1 - b} = I_0 - \frac{I_0 \cdot P_R}{\exp(1/f \cdot \tau) - 1 + P_R}$$

The inter pulse interval  $t_n - t_{n-1}$  has been replaced with the inverse of the stimulation frequency  $1/f$ . Multiplying  $I^*$  with the release probability  $P_R$  gives an estimate for the steady state EPSC which can be compared to experimental values.

To calculate the time constant  $\tau_A$  the deviation from the steady state  $J_n$  is defined as follows:

$$J_n := I_n - I^*$$

Now the resulting iterative equation  $J_n = b \cdot J_{n-1}$  can be rewritten in a non-iterative way:

$$J_n = b^n \cdot J_0$$

By replacing  $n$  with  $t/\Delta t$  and  $J$  with  $I$  one can obtain an explicit solution of this equation:

$$I(t) = I^* + \exp\left(\frac{\ln b}{\Delta t} \cdot t\right) \cdot J_0$$

The characteristic time constant can now be extracted from the exponent and results in

$$\tau_A = -\frac{\Delta t}{\ln b} = -\frac{\Delta t}{\ln(1 - P_R) - \Delta t/\tau} = \frac{1}{1/\tau - f \cdot \ln(1 - P_R)}$$

## 2.4 Statistical analysis

Data were analyzed in IGOR 5 (Wavemetrics, USA), MS Excel 2003 (Microsoft, USA), and Matlab 6.5 (The Mathworks Inc., USA). Unless otherwise noted, all errors are reported as the standard error of the mean. Statistical significance was tested with a student's t-test, unless otherwise noted. Significant differences are marked with a single asterisk for p values smaller than 0.05, with a double asterisk for p values smaller than 0.01, and with a triple asterisk for p values smaller than 0.001.

# 3 Synaptic Transmission at the Calyx of Held Under *In Vivo* Like Activity Levels

## 3.1 Introduction

The calyx of Held is a large synaptic terminal innervating principal neurons of the medial nucleus of the trapezoid body (MNTB) (Forsythe, 1994; Held, 1893; Kuwabara et al., 1991; Smith et al., 1991). MNTB neurons sign-invert calyceal excitation into glycinergic inhibition to various nuclei in the auditory brainstem (Banks and Smith, 1992; Bledsoe et al., 1990; Moore and Caspary, 1983; Spangler et al., 1985; Thompson and Schofield, 2000). *In vitro*, the signal derived from the calyx generates large EPSCs with a short synaptic delay (Barnes-Davies and Forsythe, 1995; Borst and Sakmann, 1996; Futai et al., 2001; Taschenberger et al., 2002; Taschenberger and von Gersdorff, 2000). Speed and fidelity of synaptic transmission are considered very reliable up to several hundred Hertz in mature animals (Futai et al., 2001; Joshi et al., 2004; Leão and Gersdorff, 2002; Schneggenburger et al., 2002; Taschenberger et al., 2002; Taschenberger and von Gersdorff, 2000; von Gersdorff and Borst, 2002; Wu and Kelly, 1993), leading to a view of the calyx of Held as a very reliable relay synapse.

All the *in vitro* work described above was performed in brain slices. Inherently, auditory brain slice preparations differ from intact brains in various parameters, including spontaneous activity. *In vivo*, neurons of the auditory brainstem fire spontaneously at frequencies that vary from  $> 1$  Hz up to 100 Hz or more, a property which results mainly from the dynamics of the transduction channels in the cochlear hair cells (Geisler et al., 1985; Hudspeth, 1997; Hudspeth, 1989; Kiang, 1965; Liberman, 1978; Roberts et al., 1988), resulting in spontaneous firing of the auditory nerve (Geisler et al., 1985; Liberman, 1978). Spontaneous firing can also be observed in many brainstem

nuclei including the cochlear nucleus (Brownell, 1975; Goldberg and Brownell, 1973; Joris et al., 1994; Schwarz and Puil, 1997; Spirou et al., 1990; Spirou et al., 2005) and MNTB (Kadner et al., 2006; Kopp-Scheinpflug et al., 2003; Smith et al., 1998; Sommer et al., 1993).

In an intact brain, MNTB neurons fire spontaneously at levels, which might be suitable to chronically induce some forms of short-term plasticity, such as synaptic depression or facilitation (Schneeggenburger et al., 2002; von Gersdorff and Borst, 2002). Sound stimuli, i.e. streams of high-frequency activity embedded in this spontaneous firing (Klyachko and Stevens, 2006) would then be processed by the synapse on the background of chronic depression or facilitation (figure 3.1 A). Due to the nature of the brain slice preparation, spontaneous activity and its potential effects on short-term plasticity might be lost in standard *in vitro* recordings (figure 3.1 B). If that were the case, properties of synaptic transmission in the calyx of Held under *in vivo* conditions might be different from those commonly observed *in vitro*.

This study investigates synaptic transmission in the calyx of Held under *in vivo* like spontaneous activity levels. We measured the rates and statistical properties of spontaneous firing in the MNTB of Mongolian gerbils (*Meriones unguiculatus*) *in vivo*. Subsequently, we stimulated calyceal inputs in gerbil MNTB brain slices at physiological temperature for prolonged periods of time with stimuli that mimicked the spontaneous activity as closely as possible. We assessed changes in synaptic transmission resulting from this long-term stimulation, such as synaptic currents, the degree of depression, recovery from depression, as finally the spiking properties of ‘spontaneously active’ neurons (figure 3.1 C).

## 3.2 Results

### 3.2.1 *In vivo* spontaneous firing rates of MNTB cells

The first goal was to determine the spontaneous firing rates of MNTB neurons in the intact brain of Mongolian gerbils (*Meriones unguiculatus*). Neural activity was recorded *in vivo* from single cells in the MNTB with standard extracellular recording techniques. When a neuron was encountered and isolated, its basic response features such as aurality, auditory threshold, and frequency tuning were assessed. Among the 36 neurons from which activity was recorded, thresholds for sound stimulation ranged from 0 to 60 dB SPL (mean = 32 dB  $\pm$  2.8 dB SPL), and characteristic frequencies were



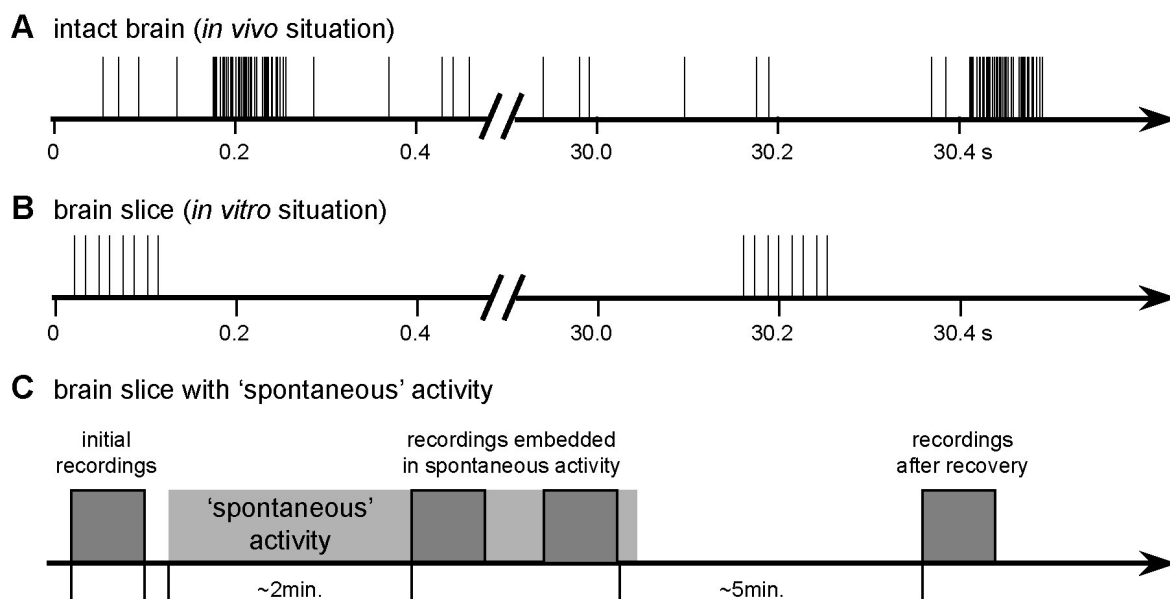


**Figure 3.1:** A: Illustration of *in vivo* activity in the MNTB. In the intact brain, MNTB neurons are chronically spontaneously active. Responses to sound stimuli, indicated by high-frequency bursts, are embedded in the background activity. B: In a typical slice preparation, the background activity is not present, such that trains of high-frequency stimuli used to imitate responses to sound are embedded in periods of complete silence. C: Our experimental approach attempted to bring the spontaneous activity back into slice preparations. Responses to simulated sound stimuli were tested to obtain a baseline of synaptic properties, then spontaneous activity was simulated for several minutes, then the same 'sound stimuli' were tested again while they were embedded in background activity. At the end of data collection, the cell was allowed to recover and the same set of simulated sound stimuli was tested again to assess the level of recovery.

between 486 Hz and 16.8 kHz. Consistent with known input patterns to the MNTB, all neurons could be excited when sound was presented to the ear contralateral to the recording site. None of the neurons showed any effects of ipsilateral stimulation. After a neuron's basic response properties to auditory stimulation were assessed, its spontaneous firing rate in the absence of sound stimulation was measured over at least 50 s and average discharge rates were calculated and defined as the neuron's spontaneous firing rate. Among the 36 neurons, spontaneous firing rates ranged from 0.15 Hz to 110 Hz (figure 3.2 A). The mean spontaneous rate was  $24.9 \pm 5.5$  Hz. Short clips of spike trains are shown in figure 3.2 B. The spontaneous rates of these neurons were 16, 40, and 69 Hz, respectively. An analysis of the interspike intervals (ISI) revealed that the spikes are near- Poisson-distributed with the exception that

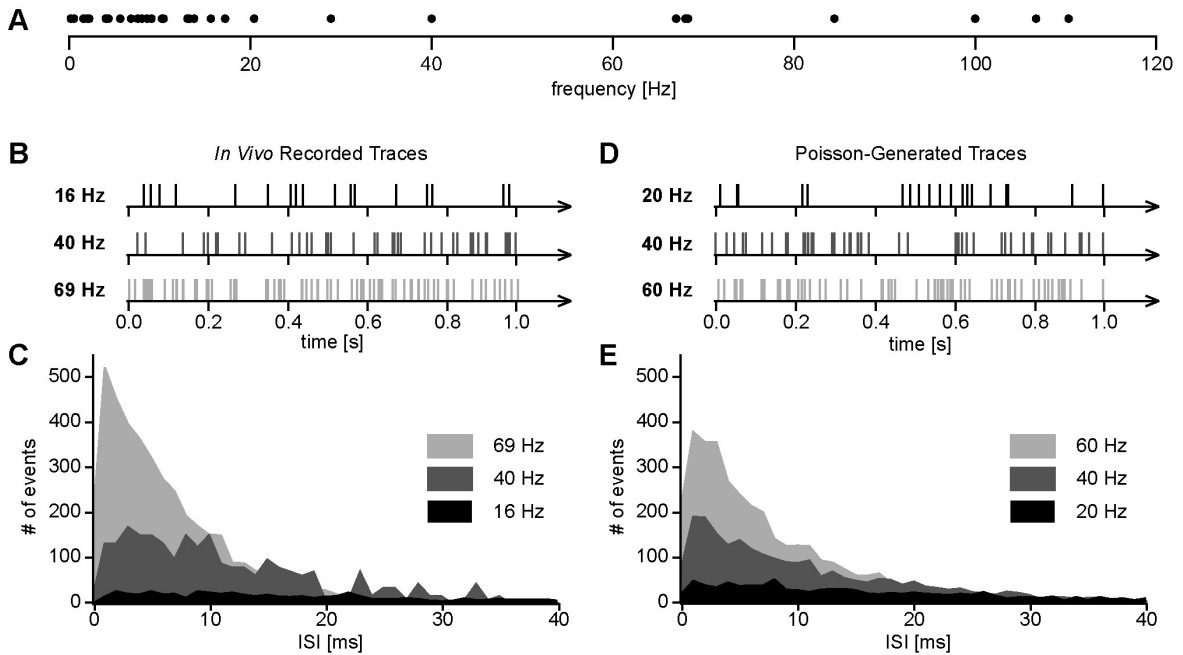


**Figure 3.2:** A: Distribution of spontaneous firing rates measured among our sample of 36 neurons. Each dot represents the average spontaneous firing rate of one neuron. The mean spontaneous firing rate among the 36 neurons was  $24.9 \pm 5.5$  Hz. B and C: *In vivo* recordings of spontaneous activity from three MNTB neurons, clips of original trace (B), interspike interval (ISI) distribution (C). While the spontaneous firing rates differed between the neurons and were 16 Hz, 40 Hz, and 69 Hz, the ISI distribution was near-Poisson-distributed in each case. D and E: Based on the results from B and C, three stimulation protocols of simulating spontaneous activity in brain slices at 20 Hz, 40 Hz, and 60 Hz were created. ISI distribution was designed to be near-Poisson.

very short inter-spike intervals ( $< 1$  ms) are underrepresented (three ISI histograms in figure 3.2 C).

### 3.2.2 Introducing spontaneous rates into slice preparations of the MNTB

Based on these *in vivo* data, three representative frequencies of spontaneous rates were chosen for stimulation of the *in vitro* brain slice preparations, namely 20 Hz, 40 Hz, and 60 Hz (figure 3.2 D). The distribution of the spike events in each one of these trains was chosen to be near-Poisson distributed to imitate the *in vivo* spontaneous activity as closely as possible (figure 3.2 E). MNTB calyceal input fibers were stimulated with these spike trains for prolonged periods of time and voltage clamp recordings were

performed from MNTB principal neurons. Calyceal inputs were stimulated for at least 2 minutes with the protocols described above. During two minutes of conditioning, 7200 Poisson-distributed stimuli were presented in case of the 60 Hz train, 4800 stimuli in the case of the 40 Hz train, and 2400 stimuli in the case of the 20 Hz conditioning train.

### 3.2.3 Effects of ‘spontaneous’ firing on excitatory synaptic currents in the calyx of Held

At the beginning of each experiment, a synapse was completely recovered, i.e. no stimuli had been given to the input fibers for at least several minutes. During the two-minute conditioning period with Poisson-distributed activity, EPSCs depressed substantially with at least two exponential components. The three graphs in figures 3.3 A-C show EPSC amplitudes of three different neurons in response to 2 minute conditioning stimuli at 20 Hz (figure 3.3 A), 40 Hz (figure 3.3 B), and 60 Hz (figure 3.3 C). Each dot in the graphs represents the amplitude of one EPSC, and the solid lines represent double-exponential fits. The initial EPSC amplitudes in the three examples were between about 5 and 9 nA, and are fairly typical values for rested calyx of Held / MNTB recordings in animals of this age group (Taschenberger and von Gersdorff, 2000; von Gersdorff and Borst, 2002). We term this value the ‘initial amplitude’ or ‘ $A_0$ ’. The synaptic current then depressed substantially during the first few events of the stimulus train (inserts in figures 3.3 A-C, initial steep declines of amplitudes), then declined much slower (later shallow decline of amplitudes), and then stabilized during the second half of the 2 minute train to values between about 2 and 3 nA. We were interested in these steady state values measured during the second half of the conditioning period, because we hypothesize that these values represent the state of the rested synapse *in vivo*. The reason is that a calyx of Held in the functioning brain of a gerbil presumably would fire spontaneously at frequencies similar to the conditioning frequencies used in this experiment and thus, synaptic currents, even in the absence of any sound input, would be chronically depressed to values similar to the ones measured during the steady state period of the conditioning phase. Therefore, we term these steady state current values the ‘in-vivo initial amplitude’, in short ‘*in vivo*  $A_0$ ’. Figure 3.3 D compares values of rested  $A_0$  values to *in vivo*  $A_0$  values for our sample of neurons. On average, during 20 Hz of spontaneous activity, the *in vivo*  $A_0$  was 46% of the rested  $A_0$ . When the fiber bundle was stimulated with 40 Hz or 60 Hz, the *in vivo*  $A_0$  values

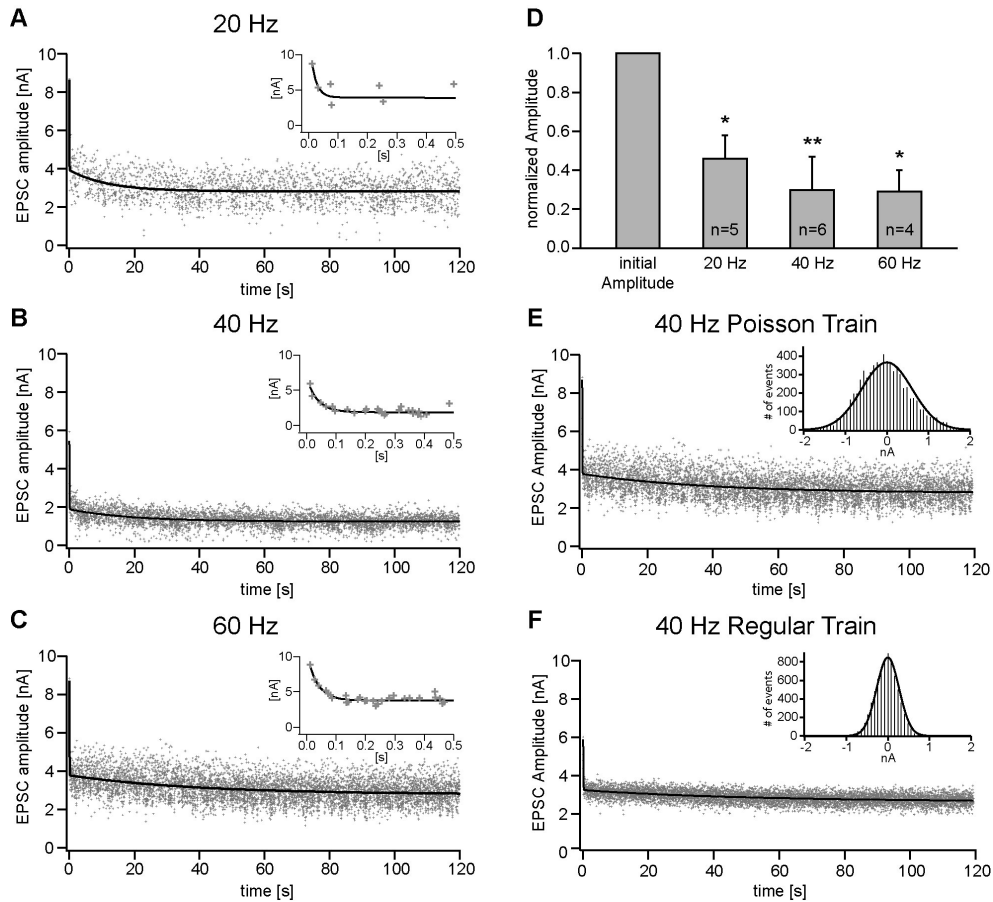


**Figure 3.3:** A-C: EPSC amplitudes of three representative neurons that were stimulated with 20 Hz, 40 Hz, and 60 Hz ‘spontaneous’ activity, respectively. Graphs show the changes of EPSC amplitudes during the two minute conditioning period. Each dot represents the amplitude of one EPSC. Inserts: Magnification of events during the first 0.5 s of conditioning. The solid lines represent double-exponential fits with the following time constants: 20 Hz:  $\tau_{fast} = 18.3$  ms,  $\tau_{slow} = 11.7$  s; 40 Hz:  $\tau_{fast} = 36.5$  ms,  $\tau_{slow} = 19.1$  s; 60 Hz:  $\tau_{fast} = 35.6$  ms,  $\tau_{slow} = 39.3$  s. D: Comparison of initial EPSC amplitudes, termed ‘rested  $A_0$  values’, and EPSC amplitudes after the two minute conditioning protocol, for our sample of neurons. For the 20 Hz conditioning protocol, the *in vivo*  $A_0$  value was 46% of the rested  $A_0$ , for the 40 Hz conditioning it was 30%, and for the 60 Hz conditioning it was 29%. An asterisk next to a bar indicates a significantly different mean compared to the control (unconditioned) situation (student’s t-test). The average initial, rested  $A_0$  values of EPSC amplitudes for the three groups were: 20 Hz group:  $7.17 \pm 0.82$  nA; 40 Hz group:  $6.76 \pm 0.74$  nA; 60 Hz group:  $6.41 \pm 0.66$  nA; these values were not significantly different from each other (ANOVA). E and F: Comparison of EPSC variability for one neuron in response to a Poisson-distributed 40 Hz stimulus train (A) and a regular 40 Hz stimulus train (B). In both cases, synaptic current amplitudes converge to the same value, although the variability in response to the Poisson distributed stimuli are about twice the variability in response to regularly spaced stimuli of the same frequency.

were 30% and 29% of the rested  $A_0$  values, respectively. These values suggest that typical synaptic amplitudes in the calyx of Held might be much smaller *in vivo* than observed in standard *in vitro* experiments.

To assess the effects of the Poisson distribution, 5 neurons were tested with trains composed of Poisson distributed stimuli vs. trains with regularly spaced stimuli of identical frequencies. The type of stimulus train did not affect the time course of synaptic depression, or the value of the observed *in vivo*  $A_0$  (figure 3.3 E and F). The difference of  $A_0$  values within each pair were not statistically different (t-test,  $p = 0.74$ ). However, the variability of synaptic currents was much larger in the case of Poisson-distributed stimuli compared to evenly spaced stimuli (figure 3.3 E and F, inserts). On average, the standard deviation of synaptic currents was 0.04 when stimuli with regularly spaced intervals were used. Presumably, one physiological basis of this variability is the stochastic nature of vesicle release. In contrast, the standard deviation of current amplitudes is much larger (0.08) when stimuli are poisson-distributed. Most likely, the reason for this larger variability is the additional effect of changing inter-spike intervals, which is added to the variability caused by stochastic release. However, note that the type of stimulus train does not appear to affect the observed *in vivo*  $A_0$ .

### 3.2.4 Effects of simulated tone-bursts on ‘rested’ versus ‘spontaneously’ active synapses

Our next goal was to determine the effects of the ‘spontaneous’ activity on the processing of high-frequency trains by the calyx of Held synapse. The high-frequency trains attempt to simulate simple sound-evoked activity, such as short tones. We tested trains of 20 pulses at 100 Hz, 300 Hz and 600 Hz, which simulated tones of 200 ms, 67 ms, and 33 ms duration, respectively. Effects of each stimulus train were tested before the conditioning period, i.e. on the rested synapse, and then after the conditioning period while the simulated tone activity was embedded in the ‘spontaneous’ activity, and a third time at least five minutes after the ‘spontaneous’ stimulation was stopped. Figure 3.4 A shows an EPSC train recorded in response to a 300 Hz / 20 pulse stimulus train from a rested neuron. The synaptic current measured in response to the first event was about 6.9 nA. Subsequently, the synaptic current depressed substantially during the stimulus train, such that the current measured in response to event 20 was depressed to 1.6 nA, i.e. the current at event 20 was only 23% of the initial current.

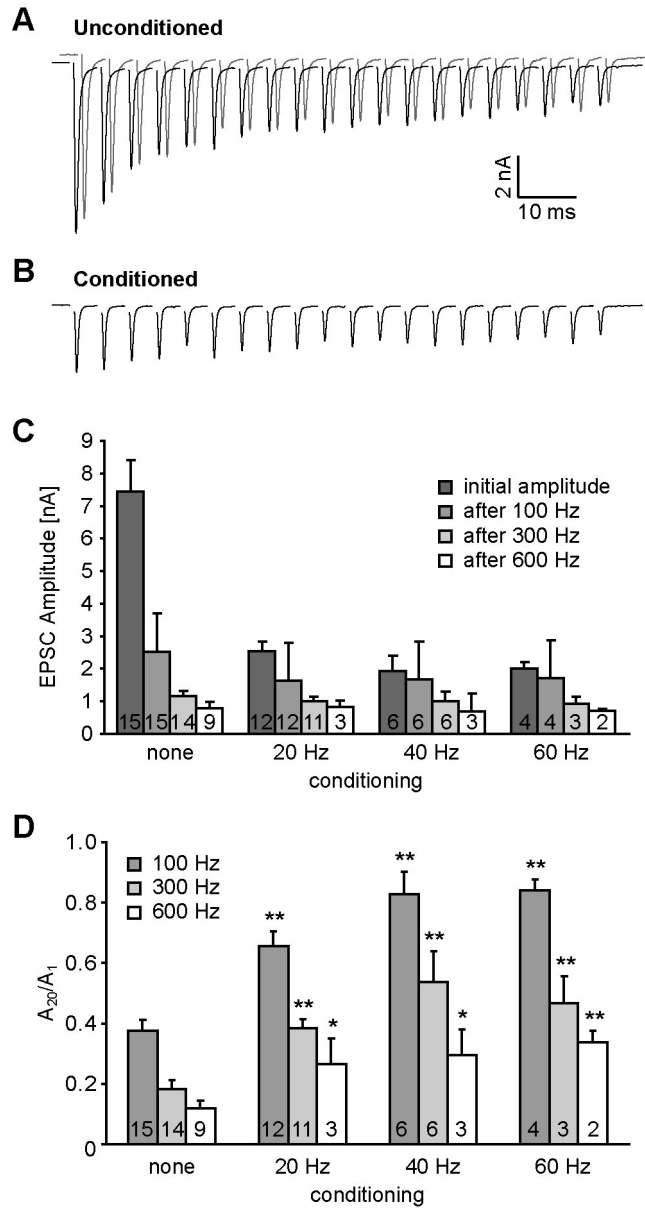


**Figure 3.4:** A–B: Responses of one neuron to the same 300 Hz / 20 pulse stimulus train before conditioning with spontaneous activity (A, black line), while the 300 Hz train was embedded in 60 Hz spontaneous activity (B), and about 5 minutes after the ‘spontaneous’ activity was ended (A, gray line). C: Absolute EPSC amplitudes with various conditioning and test frequencies. Trains of 100, 300, and 600 Hz were tested with 20 stimuli in the trains in each case. Dark bars labeled ‘initial amplitude’ refer to the EPSC amplitude of the first event of a train (similar for 100-, 300-, and 600-Hz stimulus trains), whereas the bars labeled ‘after 100/300/600 Hz’ refer to the amplitude of the 20<sup>th</sup> event in the train of the respective frequency. Numbers in the bars indicate sample size. D: Ratios of synaptic current amplitudes in response to the last stimulus over the current of the synaptic response to the first stimulus of the 20 pulse trains. Trains of 100 Hz, 300 Hz, and 600 Hz were tested with 20 stimuli in the trains in each case. Low ratios indicate substantial relative depression during the 20 pulse stimulus trains, while high ratios in graph indicate low relative synaptic depression. Numbers in the bars indicate sample size. An asterisk next to a bar indicates a significantly different mean compared to the control (unconditioned) condition, which is shown by the same color bar in the group ‘none’ (student’s t-test).

After the synapse had been conditioned with ‘spontaneous’ activity of 60 Hz, the synaptic current in response to event 1 of the same 300 Hz train was about 2.1 nA and thus, substantially lower than in the rested synapse (figure 3.4 B, first event). More interestingly, the relative depression induced by the 300 Hz train was substantially less than it was under control conditions, such that the synaptic current at event 20 was still about 1.1 nA. Therefore, in the preconditioned synapse, the current was depressed to only 54% of the value of the first event in the train, suggesting that the degree of relative synaptic depression under *in vivo* conditions might be substantially smaller than measured by *in vitro* recordings from rested synapses.

After the cell was allowed to recover for 5 minutes, i.e. received no stimulation, the synaptic amplitudes and depression ratios recovered to pre-conditioning values (figure 3.4 A, gray trace), suggesting that the observed effects shown in figure 3.4 B are reversible and specific, and cannot be attributed to synaptic rundown or other damaging effects of the intense stimulation protocol.

Figure 3.4 D shows the amount of relative synaptic depression induced by the various 20-pulse trains. The bars represent the ratio of the 20<sup>th</sup> over the 1<sup>st</sup> postsynaptic current amplitude of the train, i.e. small values indicate that at event 20 only a small portion of the initial synaptic current was measured and therefore, synaptic depression caused by the train was substantial. High values indicate that the high-frequency trains induced a much smaller amount of relative depression, since the current measured at event 20 of the train was more similar to the initial current.

Overall, the 100 Hz trains induced the lowest amount of synaptic depression (dark gray bars), the 600 Hz trains the highest amount (white bars). More interestingly, the same high frequency train induced a much smaller amount of relative depression when the synapse was previously conditioned with spontaneous activity. For example, in the unconditioned synapse, a 100 Hz / 20 pulse train depressed the synaptic current on average to 38% of the initial value. However, when the synapse was conditioned with 60 Hz of ‘spontaneous’ activity, the decrease in amplitude during the train was much smaller such that the amplitude in response to event 20 was 84%, i.e. more than twice as high as in unconditioned synapses. In all cases the high-frequency trains induced a much smaller amount of relative synaptic depression when the synapses were previously conditioned with ‘spontaneous’ activity.

### 3.2.5 Recovery of firing is very fast under *in vivo* conditions

Our next goal was to determine the recovery from synaptic depression in ‘spontaneously’ active synapses. Recovery from depression is a critical property, especially in highly active auditory brainstem synapses, since the speed of recovery determines how well the neuron can respond to acoustic events that occur shortly after the first event. We first measured the recovery of firing patterns of MNTB neurons *in vivo* (figure 3.5 A). Two identical tone bursts of 200 ms duration were presented to single MNTB units with a variable pause between them. The first tone burst elicited a certain firing rate and firing pattern in the neuron. When the second, identical tone burst was presented after only a very short pause, it elicited a lower response rate in the neuron, which was most apparent during the onset portion of the response (figure 3.5 A, top panel). As the pause between the two tones was increased, neural responses to the second tone recovered progressively and at some point resembled the responses measured to the first tone (figure 3.5 A, lower panels). The *in vivo* recovery time course of six MNTB neurons is plotted in figure 3.5 B. Among these six neurons, the average *in vivo* recovery time constant was  $82 \pm 23$  ms, suggesting that recovery of neural responses in the MNTB to acoustic stimuli *in vivo* is typically very short.

This finding raises a dilemma, since recovery from synaptic depression has been measured in the calyx of Held *in vitro*, with very different results. In these experiments, the presynaptic vesicle pool was depleted, either with a depleting high-frequency stimulus, or by voltage clamping the presynaptic terminal to a positive potential. Following this pool depletion, test stimuli were given at distinct time intervals to assess



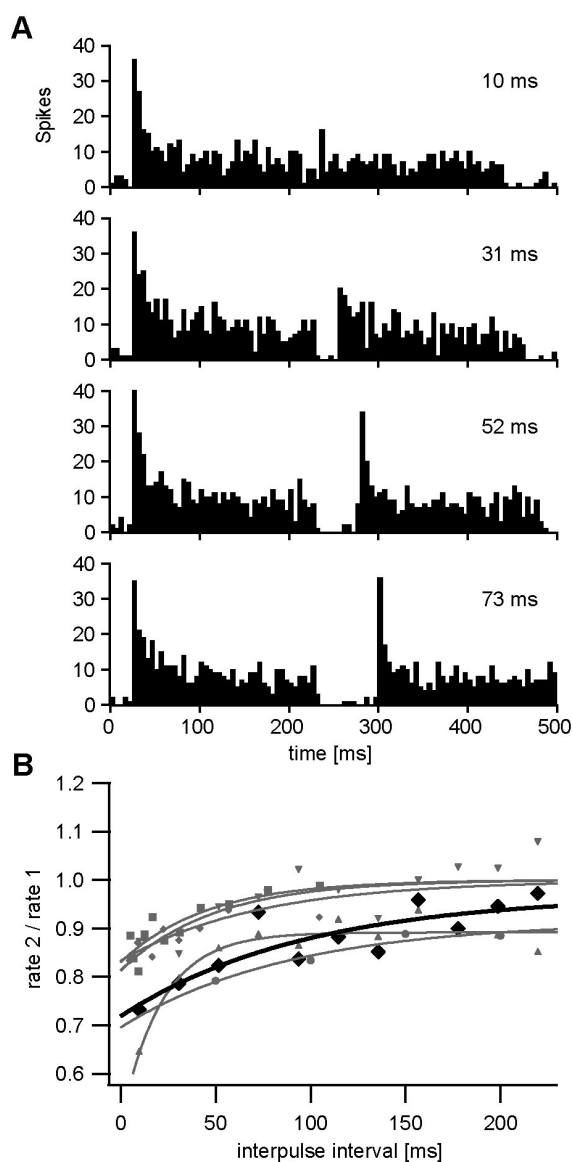


**Figure 3.5:** A: Peri stimulus time histograms (PSTHs) of a single MNTB neuron's *in vivo* responses to two identical BF tone bursts of 200 ms duration with varying inter-stimulus intervals. As the inter-stimulus interval was increased, the neuron's responses to the second tone recovered back to a point where the responses to the second tone were comparable to the neuron's firing pattern in response to the first tone. Tones were presented at 1200 Hz and 30 dB above threshold. The firing frequencies in response to the first tone were about 260 Hz for the onset response only (= first 15 ms) and about 80 Hz for the sustained part of the response. For the second tone, the onset response varied between 90 Hz (10 ms inter stimulus interval) and 260 Hz (73 ms inter stimulus interval) while the sustained part varied between 52 Hz (10 ms inter stimulus interval) and 72 Hz (73 ms inter stimulus interval). B: Time constants of *in vivo* recovery of firing of six single MNTB units. The neuron presented in A is indicated by the bold black line.

the degree of recovery of vesicle release. These experiments typically found recovery time constants at the order of seconds, not milliseconds (von Gersdorff et al., 1997; Borst and Theunissen, 1999) however, also double exponential time courses have been observed (Wang and Kaczmarek, 1998).

The *in vivo* data and the *in vitro* data are not directly comparable due to additional recoveries at the level of the hair cells, auditory nerve, and cochlear nucleus, as well potential effects of inhibition. However, the *in vivo* recovery shown in figure 3.5 B has to present an upper limit for the vesicular recovery at the level of the calyx of Held, since the calyx of Held is one element of the network tested with the *in vivo* experiment. In other words, recovery from synaptic depression at the calyx of Held might be equivalent or shorter, but could never be longer than the values measured *in vivo*. Therefore, the *in vivo* data postulate that recovery from synaptic depression at the calyx of Held should occur with time constants of no longer than about 80 ms.

### 3.2.6 Recovery from depression is very fast in spontaneously active synapses

To test this postulation, we measured recovery from depression *in vitro*. Recovery time constants were determined initially in unconditioned neurons by depleting the vesicle pool with a high-frequency train, then allowing the synapse to recover for a specified amount of time, and finally measuring the relative amplitude of a test EPSC. An example of a neuron in which the time course of recovery was determined with this method is shown in figure 3.6 A and B. Figure 3.6 A shows data points on a magnified time axis, following a recovery time course that was best described with an exponential that had a time constant of 72 ms. The average fast time constant of our sample of neurons was  $87 \pm 16$  ms. However, the fast time constant did only account for about half of the recovery. Complete recovery to the rested  $A_0$  value could best be described with double exponential fits (figure 3.6 B). The slow time constant of the same neuron shown in figure 3.6 A was 1.84 s (figure 3.6 B), while the average slow time constant of our sample of neurons was  $1.59 \pm 0.17$  s. In each case tested, the two time constants together could account for the complete amplitude of the rested  $A_0$  value.

Due to the nature of the experimental protocol, recovery from depression could not be measured in conditioned synapses with the same method as above, since the required time intervals (up to several seconds) would be far longer than the amount

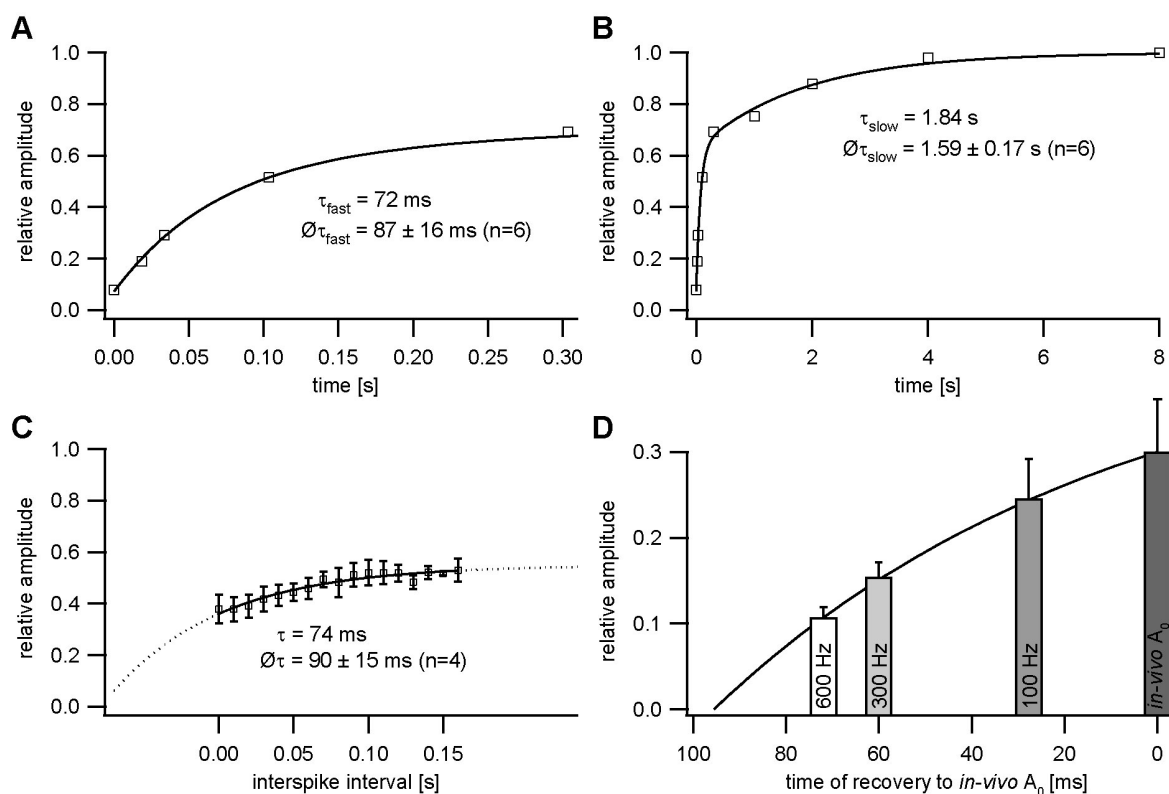


**Figure 3.6:** A and B: Recovery from depression in unconditioned synapses. The recovery could be best described with double exponential fits that had fast time constants of  $87 \pm 16 \text{ ms}$  and slow time constants of  $1.59 \pm 0.17 \text{ s}$ . C: Recovery from depression in conditioned synapses. Only the fast component was measured here and was found to be very similar to the fast component of unconditioned synapses. D: Recovery from depression in active synapses happens within milliseconds. The *in vivo*  $A_0$  point is indicated at time = 0. Typical values for synaptic currents after a 100 Hz, 300 Hz, and 600 Hz / 20 pulse stimulus train are marked in the graphs. Time elapsed between those values and the *in vivo*  $A_0$  point indicate the time it would take for the synapse to recover *in vivo* from one of the mentioned 20 pulse stimulus trains.

of time that a neuron is un-active during ‘spontaneous’ activity. Therefore, the time course of recovery in conditioned neurons was measured by fitting an exponential to the time course of EPSC amplitude recovery as a function of the preceding inter pulse interval. The various inter-pulse intervals, which inherently occur during a Poisson-distribution of spikes yield a suitable range of time periods to measure the fast recovery time constant. When this was done, we found fast time constants very similar to those found in unconditioned synapses. Figure 3.6 C shows an example of a cell in which recovery from depression was measured with the described method. For events where

the test stimulus followed shortly after a previous stimulus, the EPSC amplitude of the test EPSC was small. As the time interval before the test stimulus increased, the amplitude of the EPSC progressively increased, presumably due to recovery from depression. For this neuron, the time constant of recovery from depression was 74 ms. The average recovery time constant for our sample of neurons was  $90 \pm 15$  ms. As for the unconditioned synapses, the relative contribution of the fast time constant to overall recovery was accounted for about half of the rested  $A_0$  amplitude. Therefore, we assume that the (missing) slow component of recovery in conditioned synapses might be similar to that of unconditioned synapses, although we were unable to measure this parameter for the reason described above.

The fast recovery time constants of both unconditioned and conditioned synapses are very similar to the recovery time constants measured *in vivo* shown in figure 3.5 , suggesting that recovery from activity in the calyx of Held occurs at a similar time course as the recovery of other components of the circuit. While we also found a slow component of recovery which was in a similar range as described previously by other groups, our *in vivo* data suggest that the short time constant might be the dominant one for *in vivo* recovery.

This point is further illustrated in figure 3.6 D. The general idea of this figure is that recovery *in vivo* does not proceed up to the point of a completely full pool, i.e. the rested  $A_0$  seen in silenced synapses in brain slices. Rather, *in vivo*, recovery of the calyx progresses up to the *in vivo*  $A_0$ , i.e. the value of synaptic current that is typically available to a spontaneously active and thus chronically depressed synapse for the processing of high-frequency sound stimuli. The graph in figure 3.6 D plots a typical exponential time course of recovery with a time constant of 90 ms, as determined above. The typical '*in vivo*  $A_0$ ' point of a synapse, which is spontaneously active at 60 Hz without acoustic input, is marked at time 0 (value = 29% of the rested  $A_0$ , see figure 3.3 D). When the synapse now processes a tone burst of 20 pulses at 100 Hz, 300 Hz, or 600 Hz, the synaptic amplitude depresses even further, typically to the points indicated by the respective bars (values taken from graphs in figure 3.4 D). At the end of the tone burst, the synapse recovers back to the *in vivo*  $A_0$  value, which, depending on the frequency of the tone burst, takes between 25 and 74 ms. In other words, a spontaneously active synapse might only need 25 to 74 ms to recover from a high-frequency sound input, because the synapse is chronically depressed by the spontaneous activity and thus recovers only partially back to the steady state

level. As soon as the synapse is recovered back to the *in vivo*  $A_0$  value, it should be completely recovered for *in vivo* purposes.

### 3.2.7 Reduced synaptic reliability in active calyces

The data presented so far suggest that synaptic currents produced by the calyx of Held under simulated *in vivo* conditions are considerably smaller than typically measured *in vitro* in rested or silent brain slices. The very large synaptic currents produced by rested calyces in older animals are known to bring postsynaptic neurons well above threshold for firing and thus allow for secure synaptic transmission (Taschenberger and von Gersdorff, 2000). In the light of the synaptic currents seen under the simulated *in vivo* conditions, which were presented above, we next asked the question if these reduced currents are still suitable for failsafe synaptic transmission.

This question was addressed with three different techniques. First, current-clamp data were obtained from MNTB neurons, while the calyceal fiber bundle was stimulated, with stimulation protocols equivalent to those used for the voltage clamp experiments shown above. Figure 3.7 A shows the firing pattern of a representative neuron in response to a 300 Hz / 20 pulse stimulus train. Consistent with previous reports, the neuron responded faithfully to the 300 Hz train, i.e. it fired one action potential in response to each synaptic event, when the slice was rested. However, after the neuron was conditioned with 60 Hz of ‘spontaneous’ activity as described above, the same 300 Hz stimulus train elicited a substantial number of synaptic failures in this neuron (figure 3.7 B). For those events where the neuron failed to fire an action potential, a small excitatory postsynaptic potential (EPSP) could be observed in the voltage trace, suggesting that the calyx of Held fired an action potential and produced a synaptic current in response to the stimulus. However, the synaptic current appears to have been sub-threshold. The probability of a failure to occur increased with the number of the event in the 20 pulse train. Events early in the train were less likely to fail than events in the latter part of the stimulus train.

Among our sample of neurons tested with this method, we observed some variability in the number of failures, as well as other response characteristics. For example, some neurons showed fewer failures, while others showed higher number. Also, in some neurons stimulation of the fiber pathway with 300 Hz resulted in a small plateau from which action potentials to the stimuli were fired (figure 3.7 A), while the plateau was absent in other neurons. Also, we observed some variation in the height of the action

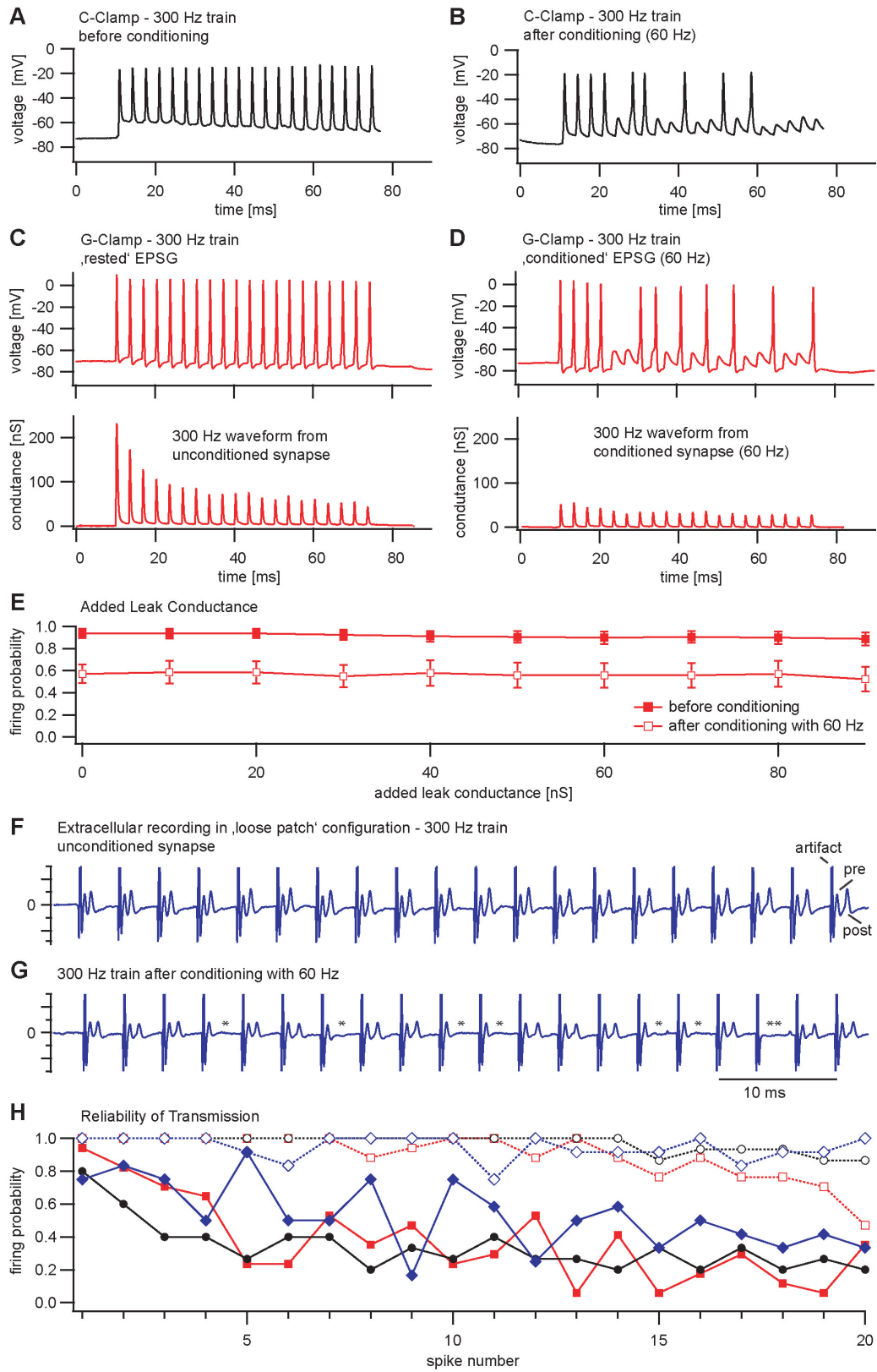


**Figure 3.7:** Reliability of synaptic transmission in spontaneously active synapses. A: Current-clamp recording of a MNTB neuron while the calyceal input fibers were stimulated with a 300 Hz / 20 pulse train. The neuron responded to each stimulation with one action potential. B: After the slice was conditioned with 60 Hz of spontaneous activity, a number of failures could be observed during the same 300 Hz train. For each failure, an EPSP can be observed in the place of the missing action potential, suggesting that the failure was postsynaptic. C, top panel: Responses of a MNTB neuron when a 300 Hz conductance waveform was used to simulate currents of a rested synapse. The neuron responded to each event with one action potential, similar as observed when the calyceal fibers were stimulated. The conductance waveform is shown in the lower panel. Peak conductance was 232 nS. D, top panel: Responses of a MNTB neuron when a 300 Hz conductance waveform was used to simulate currents of a synapse that was conditioned with 60 Hz of spontaneous activity. The neuron failed to respond to a number of events. The corresponding conductance waveform is shown in the lower panel. Peak conductance was 56 nS. E: Various levels of background leak were added to the EPSP waveforms under conductance clamp conditions, effectively reducing the input resistance of the neurons to values that are closer to input resistances observed in neurons under *in vivo* conditions. F and G: Example of a loose-patch recording of a MNTB neuron while calyceal input fibers were stimulated. In loose patch recordings, no gigaseal is formed and no break-in into the cell is performed. Since the recording is effectively extracellular, the internal environment of the postsynaptic cell is undisturbed. Even under these conditions, MNTB neurons exhibited a substantial number of failures in response to a 300 Hz train, when the slice was conditioned with 60 Hz of spontaneous activity. Artifact = stimulation artifact; pre = prepotential = presynaptic action potential; post = postsynaptic action potential. Postsynaptic failures are indicated by a single asterisk. For one event, neither a prepotential nor a postpotential could be observed (double asterisk), suggesting an axonal failure for that event. H: Firing probability as a function of the number of the event in the 20-pulse train. The black graphs with circular symbols represent data from 5 neurons tested with current clamp as described in A and B. The red graphs with squared symbols represent data from 7 neurons tested under conductance-clamp conditions, as described in C and D. The blue graphs with diamond symbols represent data from 6 neurons tested with extracellular, loose-patch recordings. For all experimental methods, few failures could be observed under conditions that correspond to a rested synapse, and occurred towards the end of the 20 pulse train (open symbols). However, for situations that correspond to a spontaneously active synapse, the same 300 Hz trains elicited a substantial number of failures. (closed symbols)

potential. Differences in channel complement, or best frequency to which the neuron was tuned might account for this variability.

For our sample of neurons, the probability of a postsynaptic spike was tested as a function of the position of the event in the train. In the unconditioned synapse, the firing probability was almost 100% throughout the 300 Hz stimulus train; very few failures occurred towards the end of the stimulus train (figure 3.7 H, black line and open circles,  $n = 5$ ). However, when synapses were conditioned with 60 Hz of spontaneous activity, the number of failures during the 300 Hz train increased (figure 3.7 H, black line and closed circles,  $n = 5$ ). In most cases, postsynaptic neurons still answered reliably during the initial events of the train; but the reliability dropped sharply afterwards.

The reliability of synaptic transmission was also tested with conductance clamp recordings. The advantage of conductance clamp was twofold: First this method does not rely on the presynaptic axons and the calyx to follow the intense stimulation protocol. Therefore, synaptic failures due to axonal failures can be ruled out more reliably than with the technique presented above. Second, conductance clamp offers the possibility of combining simulated synaptic currents with added background leaks to reduce the neuron's input resistance (see below). In our recordings, EPSC waveforms derived from 300 Hz EPSC trains were used to simulate calyceal synaptic currents in response to a 300 Hz stimulus train. Two waveforms were used in these experiments, a 300 Hz / 20 pulse EPSC waveform that simulated synaptic currents of a rested calyx (figure 3.7 C, lower panel), and an EPSC waveform that simulated the response of a calyx to the same stimulus train embedded in spontaneous activity (figure 3.7 D, lower panel). Both waveforms were previously recorded as EPSC waveforms from a MNTB neuron under voltage clamp conditions, while electrically stimulating the input fibers to the calyx. The waveforms were chosen to reflect the observation that peak EPSC currents are larger in rested than in conditioned synapses (figure 3.3 D), and that synaptic depression within a high-frequency train is reduced in active synapses (figure 3.4 A and B). Conductance clamp recordings with these two waveforms were performed on 7 MNTB neurons. The neurons fired action potentials reliably when excitatory synaptic currents typical for a rested calyx were injected (figure 3.7 C, top panel). In the rare case that failures could be observed, they occurred towards the end of the train (figure 3.7 H, red line and open squares,  $n = 7$ ). However, when currents typical for a spontaneously active synapse were used, failures in the neuron's



response to the 300 Hz / 20 pulse EPSP train could be observed (figure 3.7 D, top panel). These failures tended to occur more frequently towards the end of the EPSP waveform, but could sometimes also be observed early in the train (figure 3.7 H, red line and closed squares,  $n = 7$ ).

Interestingly, the firing probabilities and frequencies for conditioned synapses shown in figure 3.7 E closely match those observed *in vivo*. For both the current and the conductance clamp experiments, the firing probability of the first few events in the train was 0.7 to 1.0. For a train frequency of 300 Hz, this corresponds to a firing frequency of about 200 to 300 Hz. The onset portion of the *in vivo* spike trains shown in figure 3.5 A had a firing frequency of about 260 Hz (considered is the response to first tone of the pair only). The average firing frequency of the neuron in response to the latter part of the 200 ms tone was about 80 Hz. This corresponds well to the *in vitro* data shown in figure 3.7 E, where the firing probability of the neuron to the latter portion of the train is about 1/3, i.e. about 100 Hz.

A number of studies have observed that a neuron's input resistance is substantially higher in brain slices than in the intact brain (Bernander et al., 1991; Pare et al., 1998, e.g. ). The main reason for this observation is that neurons in the intact brain receive a large number and variety of synaptic inputs. When these inputs are activated at different points in time, postsynaptic receptors open and thus decrease the neuron's input resistance. In brain slices, many of these inputs are silent and/or cut, with the result that the neuron's input resistance increases. It is unknown, if and how much the input resistance of an MNTB neuron differs in brain slices compared to the intact brain, since the projection pattern to MNTB neurons is much simpler than in the case of e.g. cortical neurons. However, prominent glycinergic inhibition to MNTB has been described *in vitro* (Awatramani et al., 2004). These inputs, when activated, will decrease the input resistance of postsynaptic neurons. An artificially high input resistance in neurons of MNTB brain slices would facilitate the neuron's responses to synaptic events. In other words, it would require less synaptic current to bring a neuron to the firing threshold than it would take under *in vivo* conditions. In this case, the synaptic failures shown in figures 3.7 A-E would be an underestimate of the true *in vivo* failure rates. We attempted to address this issue by adding a background leak to MNTB neurons during the presentation of the EPSP waveforms. The background leak had a constant amplitude of 10 to 90 nS with a reversal potential of -60 mV and effectively reduced the input resistance of the postsynaptic neuron up to 5-fold.

Figure 3.7 E shows the overall firing probability of six MNTB neurons, when EPSC waveforms of 300 Hz trains plus various amounts of background leak were tested. As expected, the firing probability decreased with increasing background leak, however, the effect was minor.

The last approach to test the reliability of synaptic transmission was with a ‘loose-patch’ extracellular approach. For these experiments, an MNTB neuron in a brain slice was only loosely patched without obtaining a gigaseal, and no break-in into the neuron was performed, such that the recordings were effectively extracellular. In some recordings, action potentials of both the calyx of Held (termed ‘prepotential’), as well as the postsynaptic principal neuron could be observed. An example is shown in figure 3.7 F and G. In this recording, stimulation of the calyceal input fibers produced three peaks in response to each event. The first one was the stimulation artifact (labeled ‘artifact’), followed by the prepotential (labeled ‘pre’), and then followed by the postsynaptic action potential (labeled ‘post’). The advantage of this method is that the interior environment of the postsynaptic cell is left undisturbed. For whole cell recordings, a common concern is that the perfusion of the neuron with artificial intracellular fluid might change the firing properties of the neuron, which would result in inaccurate measurements of failure rates. However, even when the postsynaptic neuron was left intact, transmission failures could be observed in the calyx of Held / MNTB synapse when the slice was driven at *in vivo* type activity levels. Figure 3.7 F shows a loose-patch recording of a rested brain slice. Consistent with the data shown above, the synapse was very fail-safe when a 300 Hz / 20 pulse train was tested, i.e. each prepotential was followed by a postsynaptic action potential (figure 3.7 F). However, when the slice was conditioned with 60 Hz spontaneous activity, a substantial amount of failures could be observed in response to the same 300 Hz test train (figure 3.7 G). Postsynaptic failures are indicated by a single asterisks. In one case, neither a prepotential nor a postpotential could be observed (marked by a double asterisk), suggesting that for this event the failure must have occurred in the calyceal input fiber. The red lines in figure 3.7 E show the average reliability of transmission measured with this technique (red line and closed squares: unconditioned synapses,  $n = 6$ ; red line and open squares: conditioned synapses,  $n = 6$ ).

Furthermore, the latency of synaptic transmission was increased, when synapses were spontaneously active (figure 3.7 B and G). In this cell, the synaptic latency increased by 0.19 ms when the synapse was conditioned. For all 11 neurons from

which spike-latency data was available, the average latency increase was  $0.4 \pm 0.13$  ms. This discrepancy matches well with the discrepancy between published values for *in vitro* synaptic latency (Taschenberger et al., 2002; von Gersdorff and Borst, 2002) vs *in vivo* latency (Guinan and Li, 1990; Kopp-Scheinflug et al., 2003) at the calyx of Held. These data suggest that highly active calyces have a longer latency than previously reported *in vitro*, but also that our conditioning protocol might be suited to transform calyces into a functional state which closer resembles the functional state of an active calyx of Held.

In summary, the data presented in figure 3.7 suggest that the calyx of Held / MNTB synapse shows a substantial amount of synaptic failures, after cells were stimulated for several minutes with Poisson-distributed activity. One possible interpretation of these results is that *in vivo*, the MNTB might not be the simple and reliable relay that is commonly observed under standard *in vitro* conditions.

### 3.3 Discussion

The main question addressed in this study is the question of how synaptic transmission in the calyx of Held synapse changes when synapses are stimulated for prolonged periods of time with Poisson-distributed activity, which, we hypothesize, imitates naturally occurring spontaneous activity. There are four main findings. First, the introduction of ‘spontaneous’ activity into *in vitro* preparations of the calyx of Held considerably depresses synaptic currents, even at relatively low spontaneous frequencies of 20 Hz. Second, in these ‘spontaneously active’ synapses, the degree of additional depression induced by high-frequency trains (i.e., simulated sound inputs) is reduced considerably. Third, recovery from synaptic depression is very fast. Data from corresponding *in vivo* extracellular recordings also show fast recovery of firing and are consistent with these *in vitro* findings. Fourth, in chronically active synapses with reduced synaptic currents, the reliability of transmission is reduced during high-frequency bursts of afferent input.

#### 3.3.1 Background firing in MNTB neurons

Spontaneous activity in the lower auditory system is a widespread phenomenon. It is assumed that this activity is explained by the probabilistic behavior of the transduction channels of the inner hair cells and the resulting chronic transmitter release at the

hair cell synapse. The spontaneous activity is still present at the level of the cochlear nucleus (Brownell, 1975; Goldberg and Brownell, 1973; Joris et al., 1994; Schwarz and Puil, 1997; Spirou et al., 1990; Spirou et al., 2005) and most auditory brain stem nuclei, such as MSO in bats (Grothe, 1994), MNTB in cats (Smith et al., 1998), MNTB in gerbils (Kopp-Scheinpflug et al., 2003), and MNTB in rats (Sommer et al., 1993). Consistent with our data presented here, studies of spontaneous activity in the lower auditory system typically report a large variability of rates among neurons, even within the same species or the same nucleus. One possible explanation for this large variability is that different neurons receive inputs from different classes of auditory nerve fibers with low, medium, or high spontaneous rates (Liberman, 1978), which would give rise to auditory brain stem neurons with very diverse spontaneous firing rates.

For the experiments presented here, three frequencies of Poisson-distributed activity were chosen for stimulation of brain slices: 20, 40, and 60 Hz. Although the mean spontaneous firing rate in our sample of neurons was 24.9 Hz and thus closer to the lowest of these frequencies, the three frequencies chosen for stimulation successfully cover the spectrum of observed *in vivo* spontaneous rates (see figure 3.2 A) see also former work (Kopp-Scheinpflug et al., 2003). However, because of the nature of the brain slice preparation, the original *in vivo* spontaneous firing rate of a given neuron is unknown. Therefore it is possible or even likely that an originally low spontaneously active neuron was stimulated with a high-frequency stimulus train and vice versa. However, all neurons in our *in vitro* sample responded stereotypically and in a very similar fashion to our various stimulus protocols and no responses were observed that could be explained by the use of an inappropriate background stimulation rate.

Measurements of spontaneous activity presented in this study were performed under anesthesia. As with almost every type of anesthesia, the ketamine–xylazine mixture used in this study might have depressed the neurons' spontaneous activity to a certain degree (Destexhe et al., 2003). Therefore the actual spontaneous firing rates in MNTB neurons of behaving gerbils might be higher than those shown in this study. On the other hand, the values for spontaneous activity determined here match closely with findings of other studies using various species and various types of anesthesia or, in some cases, no anesthesia at all (Irvine, 1992; Kiang, 1965; Ryan and Miller, 1978). We therefore conclude that the values presented here are representative or, at worst, a conservative lower limit of the true effects induced by spontaneous activity.

We also note that double-walled sound-attenuated rooms by themselves create the biologically unnatural situation of complete absence of sound. Natural auditory environments always contain a certain level of background noise, which contributes to the background activity of auditory neurons. Therefore, the effects of chronic activity on synaptic transmission in behaving animals might be even larger, but are not likely to be smaller than presented here.

### 3.3.2 Prolonged spontaneous spiking changes properties of synaptic transmission

Our data show that prolonged stimulation even at a frequency of 20 Hz decreases synaptic currents to less than half of the original value, whereas stimulation with frequencies of 60 Hz reduces currents to about one third. It might be surprising to find that such low frequencies cause such a high degree of depression because all brain slices were prepared from animals well past the onset of hearing and recordings were performed at physiological temperature.  $\alpha$ -Amino-3-hydroxy-5-methyl-4-isoxazolepropionic acid (AMPA) receptor desensitization as well as N-methyl-D-aspartate (NMDA) currents, although playing a substantial role in preparations from young animals (Neher and Sakaba, 2001; Sakaba and Neher, 2001b), play only a very minor role in animals past the age of hearing onset (Futai et al., 2001; Renden et al., 2005; Taschenberger et al., 2005). Under these conditions, MNTB neurons can follow stimulation frequencies of  $\geq 600$  Hz for at least short periods (Futai et al., 2001; Taschenberger and von Gersdorff, 2000; Wu and Kelly, 1993). The depression we observed in response to long-term stimulation progressed with at least two time constants: an initial, fast time constant, which can be seen during the first few stimulus pulses, and a much slower time constant. The mechanisms for the slow time constant are unclear, but are likely to be multiple and will be studied in the future. When the processing of high-frequency trains was tested in rested versus spontaneously active synapses, the observed relative degree of synaptic depression caused by the high-frequency train was much larger in the rested than in the active synapse. This might have important functional implications at the calyx of Held, which sustains high levels of activity.

Our findings also suggest that recovery from synaptic depression is very fast under biologically relevant activity levels. These time constants of about 90 ms are an order of magnitude shorter than previously reported values for rested synapses, which are in

the range of several seconds (von Gersdorff et al., 1997, 4.2 s), but see also work (Ishikawa and Takahashi, 2001; Schneggenburger et al., 2002; Wang and Kaczmarek, 1998; Wu and Borst, 1999). Age, temperature, and species differences might account for some of this discrepancy. However, there is strong evidence suggesting that calcium accumulation in the presynaptic terminal through high-frequency firing may play a role in speeding up the recovery from depression (Wang and Kaczmarek, 1998). It appears that this faster recovery plays a dominant role in active synapses.

### 3.3.3 Reliability of synaptic transmission

*In vitro* studies of the calyx of Held in animals past hearing onset have reported very reliable synaptic transmission and a number of cellular specializations to increase synaptic reliability. Our data are consistent with the view that ‘rested’ calyces produce large synaptic currents and have a high transmission reliability. However, we show that in chronically active synapses, the synaptic currents are much smaller. Our current-clamp, conductance-clamp, and extracellular action potential recordings all suggest that spontaneously active synapses may show synaptic failures during periods of high-frequency activity. Therefore, the calyx of Held may not always show the reliable 1:1 transmission postulated from *in vitro* experiments in rested synapses. This finding is consistent with previous *in vivo* results from the MNTB. Among the *in vivo* studies performed in the MNTB only those where both presynaptic and postsynaptic activity have been recorded simultaneously can address the question of transmission failures at the calyx of Held synapse. To our knowledge, two studies report simultaneous pre- and postsynaptic recordings at the MNTB and both agree on the occurrence of postsynaptic failures (Guinan and Li, 1990; Kopp-Scheinflug et al., 2003) *in vivo*. However, the two studies differ in the number of failures observed. Guinan and Li found failures mainly with prolonged high-frequency stimulation of the afferent fiber bundle and only occasionally with sound stimulation, whereas Kopp-Scheinflug et al. found a substantial number of failures with sound stimulation. Species differences might account for some of this discrepancy, but note that these recordings were performed with intact synaptic inhibition and under anesthesia. Because MNTB neurons are known to receive a substantial amount of glycinergic inhibition (Awatramani et al., 2004), it is possible that some of these failures are the result of spike suppression by inhibition and that some of the difference observed in the two studies arises from differential recruitment of synaptic

inhibition. Nevertheless, the presence of synaptic inhibition alone also questions the interpretation of the calyx of Held as a fail-safe ‘relay’ synapse. This view has been formed by previous *in vitro* studies performed in slices from animals past hearing onset, where EPSCs well above action potential threshold have been measured even in response to stimulus frequencies of several hundred Hertz. However, these stimulus trains typically consisted of no more than 20 – 50 stimuli, with considerable recovery time of several seconds between trials. Our experimental setup avoided these periods of silence because they do not occur under *in vivo* conditions. Presumably the lack of prolonged periods of recovery keeps calyces in a chronic state of synaptic depression and causes transmission to fail during periods of embedded high-frequency activity.

In conclusion, the aim of this study was to perform a first description of the effects of prolonged ‘spontaneous activity’ on synaptic transmission at the calyx of Held synapse. We conclude from our data that synaptic transmission in the calyx of Held differs in a number of significant ways when synapses are stimulated with a Poisson-distributed stimulus train for prolonged periods of time. Future studies will determine the specific contribution of multiple modulators, receptors, or channel types in the calyx of Held synapse to the ‘rested’ or the ‘spontaneously active’ synaptic state.





# 4 Modeling Short-Term Synaptic Plasticity at the Calyx of Held Using *In Vivo* Like Stimulation Patterns

## 4.1 Introduction

The short term dynamics of synaptic transmission under various activity levels have been modeled in a number of synapses (Markram and Tsodyks, 1996; Abbott et al., 1997; Tsodyks et al., 1998; Gundlfinger et al., 2007), among them the calyx of Held in the auditory brainstem. Basic features of most of these models are the vesicle release from a readily releasable vesicle pool as well as a pool size-dependent vesicle recovery (Weis et al., 1999). Beyond these basic features, additional effects have been incorporated, for example calcium dependent facilitation (Varela et al., 1997) or postsynaptic receptor desensitization (Graham et al., 2004). These physiological effects of short term plasticity have been demonstrated to shape synaptic transmission at the calyx of Held, thus the inclusion of them into the modeling process are supposed to yield more accurate models with higher predictive power.

Models of vesicle release dynamics are typically based on data recorded from *in vitro* brain slice preparations. In the case of the calyx of Held, these preparations lack the chronic background spontaneous activity that calyces experience in the intact brain (Irvine, 1992; Kadner et al., 2006; Kopp-Scheinflug et al., 2003; Sommer et al., 1993; Smith et al., 1998). This spontaneous activity is a common feature of some brain areas and one of the hallmarks of neurons in the auditory brainstem. On average, it evokes firing rates of about 25 Hz at the calyx of Held in gerbils. As shown in chapter 3, calyces in brain slice preparations lacking this chronic activity differ in a

number of physiological properties of synaptic transmission, such as baseline synaptic amplitudes, depression during high-frequency stimulation, recovery from depression, or transmission fidelity.

The focus of the present study was to find a model variant, which essentially captures transmission at the calyx of Held during typical *in vivo* activity levels. Rather than including all known parameters of short term plasticity into the model, our approach was to evaluate different models incorporating different physiological effects, and to test how well each one of these variants could predict neural responses to the complex stimulation patterns used in the study. To imitate naturally occurring activity as closely as possible, all presented stimuli were embedded in chronic background activity resembling the spontaneous activity present in the intact brain. The embedded test stimuli incorporated a large amount of statistical complexity, and in some cases were derived from auditory responses to sound clips. Different variations of the basic model were used to predict the synaptic currents produced by a given calyx of Held to these stimuli, and these predictions were compared to the neuron's actual responses as determined through voltage-clamp recordings from gerbil brain slice preparations.

## 4.2 Results

The central goal of this study was to model the short term dynamics of synaptic strength at the calyx of Held synapse in response to highly complex stimulation patterns. We furthermore wanted to investigate synaptic dynamics under conditions mimicking the *in vivo* situation of chronically active synapses as closely as possible. Therefore, we embedded our various stimulation protocols in spontaneous background activity mimicking the naturally occurring spontaneous firing of cells in the auditory brainstem. As shown in chapter 3, this activity causes several changes in the synaptic dynamics, mainly a significant decrease in synaptic strength and a decrease of synaptic depression in response to high frequency stimulation. For the present study, we used a Poisson-distributed pulse train with a mean frequency of 20 Hz to simulate spontaneous background activity. Neurons were initially stimulated with this background activity for at least two minutes to 'condition' the synapses. During this conditioning period, the synapses reached a new steady state with significantly lower synaptic currents (chapter 3). We term this condition the '*in vivo* like rested state' of the synapse, since we assume that *in vivo*, calyces of Held are in this state in the absence of any

sound stimulation but in the presence of spontaneous activity. All other stimulations used in the present study were embedded in this background activity, and the change between stimulus and background was gapless, guaranteeing a true embedding of the recorded stimulus. This experimental design attempts to imitate the *in vivo* situation, where periods of sound stimulation are embedded in the naturally occurring spontaneous activity. The mean initial synaptic strength of all cells measured as the EPSC in voltage-clamp experiments was  $12.2 \pm 1.2$  nA ( $n = 16$ ). During the two minutes of conditioning with the 20 Hz Poisson train this value dropped to  $4.1 \pm 0.6$  nA, corresponding to a decrease to 34% of the initial amplitude.

### 4.2.1 Poisson distributed test trains

The first set of test stimuli consisted of Poisson-distributed trains with varying mean frequencies. The stimulus consisted of 34 segments and had alternating periods of low and high activity levels as depicted in figure 4.1 A. Each one of these 34 periods had a given mean frequency, which was applied for a brief time period and then changed at the beginning of the next segment of the stimulus train. The distribution of single events within these periods was Poisson, with the exception that inter pulse intervals smaller than 1 ms were not used. The low activity periods had mean frequencies ranging from 5 to 50 Hz, whereas the high activity periods had mean frequencies between 100 and 350 Hz. The entire stimulus was 30 s long and consisted of 1201 stimulations.

We had two motivations to choose this particular type of stimulation. First, this stimulation protocol is highly complex and is made of many very different sequences of inter pulse intervals. Therefore, it is possible to obtain a lot of information about synaptic dynamics with this stimulus. Second, it covers the full range of frequencies experienced by MNTB cells in an intact brain. A normal Poisson train with a fixed mean frequency could, for example, not account for longer periods of low activity reflecting silence and at the same time mimic sound input which would result in high activity. Therefore, a pattern with varying mean frequencies reflects naturally occurring auditory activity closer.

For each neuron, experiments were started by conditioning the synapse to background activity for at least 2 minutes with the 20 Hz Poisson stimulus described above. Next, the Poisson test train with varying mean frequencies described here was played to calyces, embedded into the 20 Hz background activity and repeated

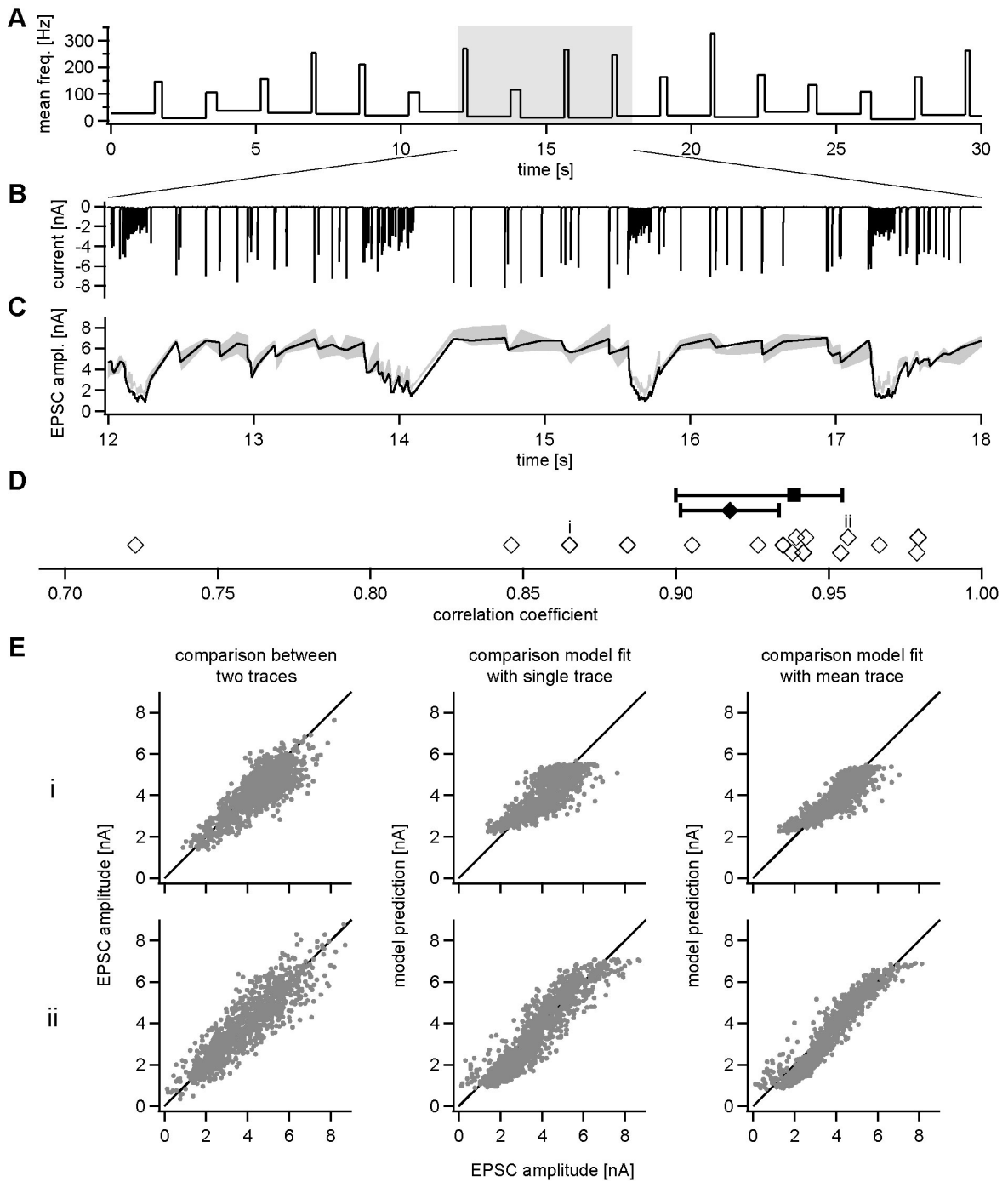


**Figure 4.1:** A: Time course of the first stimulation protocol. The graph represents the mean frequencies of the pulse trains. The single events in each period are Poisson-distributed. The low frequency segments have durations of 2 s each, the high frequency segments consist of 50 stimulation events each. B: Clip of a voltage-clamp trace of an EPSC train recorded from a neuron that was stimulated with the train described in A. The trace represents one single recording. In this and all other figures showing data traces, stimulation artifacts were blanked for clarity. C: EPSC amplitudes extracted from the data trace shown above. Presented are data from four repetitions of the same stimulus. The gray area indicates the maximum and minimum amplitude recorded among the four repetitions. The black line represents the predicted EPSC amplitudes to the same stimulus train calculated by the basic vesicle release model. D: distribution of correlation coefficients. The open diamonds show the correlation coefficients between the mean over four recordings and the corresponding model predictions for each one of the 16 neurons. The closed diamond represents the mean correlation coefficient over all 16 neurons with its standard error; the closed square is the median with the interpolated 0.25 and 0.75 percentile. E: Scatter plots comparing EPSC amplitudes of the same two neurons (i and ii) under various conditions. The left column shows the correlation between two single recordings of the same stimulus from the same cell, the scatter indicates the variation between the two trials. The center column shows the correlation between data from a single trial (i.e. a single trace) and the corresponding model fit. The x-axis plots the EPSC amplitudes recorded in voltage-clamp, the y-axis plots the amplitude computed by the model. The two scatter plots in the right column plot the comparison between the mean over four traces and the corresponding model prediction.

four times wherever possible. An example of a single voltage-clamp trace of recorded EPSCs is shown in figure 4.1 B. EPSC amplitudes were extracted and the mean amplitudes were calculated from the four repetitions. The gray area in figure 4.1 C indicates the maximum and minimum EPSC measured over the four repetitions.

Next, the EPSC amplitudes were modeled using the basic variant of our prediction model. The black line in figure 4.1 C corresponds to the model prediction. The EPSC amplitudes predicted by the model were fit against the mean amplitudes calculated from the four repetitions. For most events, the prediction falls inside the gray area depicted in figure 4.1 C, indicating that the model prediction was in the range of the naturally occurring amplitude variations. To quantify the quality of our predictions, we calculated the correlation coefficient between the predicted and corresponding measured amplitudes. Figure 4.1 D shows the correlation coefficients of all 16 neurons that were tested in this way. The majority of cells show a correlation coefficient of more than 0.9, indicating a very high fit quality. The mean correlation coefficient over the 16 cells was  $0.918 \pm 0.017$ , the median was 0.94.

For two example cells (indicated by ‘i’ and ‘ii’ in figure 4.1 D) the quality of fits is further illustrated with a set of correlation plots, shown in figure 4.1 E. The two plots on the left show a comparison between two consecutive recordings of the same stimulation pattern for each one of the two neurons. For a perfect match, i.e. perfect repeatability, all points would fall on the black diagonal line. The deviations from this line demonstrate the degree of variability between individual trials. For each neuron in our sample, we compared the EPSC amplitudes from the four individual stimulus repetitions to each other (6 comparisons per neuron) and calculated the average correlation coefficient for each neuron ( $0.603 \pm 0.012$  to  $0.961 \pm 0.002$ ,  $n = 16$ ). The average correlation coefficient for all 16 neurons was  $0.880 \pm 0.019$ .

The two center plots in figure 4.1 E show the comparison between single EPSC traces and corresponding model prediction for the two sample neurons. The distribution of points is very similar to the left plot. Among our sample of neurons, the average correlation coefficient obtained by correlating data from each one of the four single traces with the corresponding model prediction was  $0.884 \pm 0.018$  (4 comparisons per neuron, value for individual cells varied between  $0.749 \pm 0.012$  and  $0.955 \pm 0.004$ ,  $n = 16$ ). These values are almost identical to the average correlation coefficient obtained by correlating single traces with each other, suggesting that the accuracy of predictions provided by our model was maximal such that the remaining inaccuracies in the predictions were mainly due to biological noise. The two plots on the right compare the mean EPSCs calculated over four repetitions to the corresponding model predictions. The spread of points is smaller than in the other cases. As stated above, the average correlation coefficient obtained by comparing model predictions to the average EPSC amplitude was  $0.918 \pm 0.017$  and thus higher than in the cases described above. Presumably, by averaging over four repetitions, the biological variability was reduced partially, with the result that the model predictions improved somewhat. The remaining prediction errors might be reduced even further with more repetitions. These data suggest that overall, the predictions obtained with our relatively simple model were quite good, and errors were almost within the range of biological variation. However, note that the graphs in figure 4.1 E reveal a very slight S-shaped distribution of points in both the single trace as well as the average trace fits. This S-shape was seen for most of the recorded cells and indicates a (small) systematic prediction error of the model, with an underestimation of small and very large amplitudes and an overestimation of medium amplitudes.

### 4.2.2 Model variants

Although the simple vesicle release model already provided a very accurate description of synaptic short term dynamics at the chronically active calyx of Held, some systematic deviations remained. This may not be surprising, as a large number of effects of short-term plasticity have been shown to influence synaptic strength. Some of them were incorporated in previous models, for example synaptic facilitation caused by an increase in calcium concentration (Varela et al., 1997), or postsynaptic receptor desensitization (Graham et al., 2004). The single exponential time course for vesicle recovery that we assume in our basic model has long been replaced by a double exponential recovery reflecting two populations of vesicles (Wang and Kaczmarek, 1998; Sakaba and Neher, 2001b).

Therefore, we wanted to investigate next how additional degrees of freedom introduced by new parameters improve the model predictions. We chose three extensions, namely a variant with a double exponential recovery, one with added facilitation, and one which accounts for receptor desensitization (details see chapter 2.3.1). Figure 4.2 A shows a short clip of recorded EPSC amplitudes and corresponding predictions obtained with the different model variants. The experimental data, shown in black, is represented as the average of four repetitions of the same stimulus pattern recorded from a single cell. The predictions obtained with the basic model are shown in gray; the colored traces represent predictions obtained with the three model variants. Generally, the differences between the individual model predictions were rather small. To quantify these differences, we plotted the model predictions of the different variants against the experimentally measured values. Figure 4.2 B shows these correlation graphs for the same cell as shown in figure 4.2 A. A summary of the correlation coefficients between predictions and experimental data of all 16 neurons tested with various models is shown in figure 4.2 C. The data suggest that the model improvements do not yield better predictions, as the correlation coefficients obtained with the various models are almost the same. Also, the shape of the correlation plots does not change in any obvious way. Finally, we tested combinations of model improvements. For example, we tested a combination of receptor desensitization and double exponential recovery, which neither resulted in higher correlation coefficients, nor an elimination of the systematic deviations shown in figure 4.1 E (data not shown).

In all variants of the model, the parameters were not restricted to certain ranges and all parameters were optimized to generate a model output with the smallest pos-

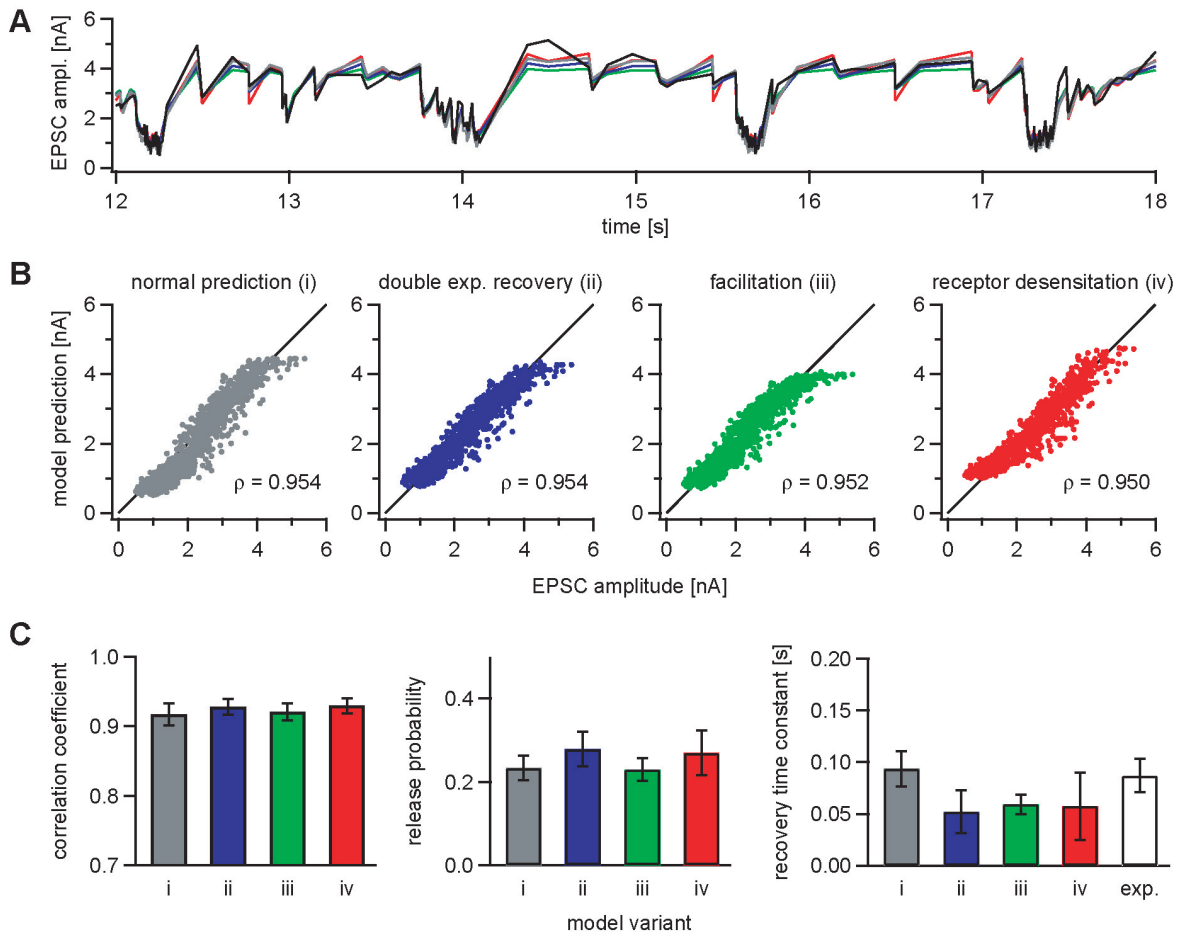


**Figure 4.2:** A: A short clip of data showing the development of EPSC amplitudes over time. The black trace represents the mean amplitude measured over four repetitions. The different model variants are color coded as explained in B. B: Scatter plots comparing predictions computed by the different model variants to actual recorded EPSC amplitudes. The correlation coefficients are noted in the lower right corner of each graph. C: Summary results for all 16 neurons. The first graph shows the average correlation coefficients achieved by each one of the four model variants, the color code is the same as above. The two other bar graphs compare the release probability and the recovery time constant, respectively. For the recovery time constant an independently determined value is added for comparison (white bar).

sible squared error as defined earlier. This strategy yielded parameters, which did not change significantly in the four different scenarios. Summary plots of these parameters, namely correlation coefficient, release probability, and recovery time constant are plotted in figure 4.2 C. In case of the double exponential recovery the fast component of the recovery time course is plotted in figure 4.2 C (right panel). The slow component is



infinitely long in some cases ( $> 10^{10}$  s, 5 of 16 neurons) or has nearly the same value as the fast component ( $\pm 1$  standard deviation, 8 of 16 neurons). In the remaining 3/16 neurons, the slow component assumed independent values. However, in these cases the combination of slow and associated fast component yielded almost identical results as the fast component by itself in the corresponding model variant with single exponential recovery. It appears that in these cases the number of degrees of freedom in the data was smaller than the number of parameters in the fit and therefore, one particular situation could be described by several parameter combinations. All three possibilities lead to the conclusion that the slow component of the recovery was not necessary for an accurate description of the experimental data set. One reason may be that values for the slow component are typically in the range of several seconds (von Gersdorff et al., 1997; Wu and Borst, 1999; Wang and Kaczmarek, 1998), while the largest inter pulse intervals in all our stimulation protocols are in the sub second range. For the model with variable release probability (i.e. the model including synaptic facilitation), the minimal release probability is plotted in figure 4.2 C (center panel). In this model variant, either the parameter increasing the release probability is infinitely small or the recovery time course of the changing release probability is infinitely fast, depending on the seed values used (16 of 16 cells). Again, both possibilities lead to the conclusion that a variable release probability is not important for accurate predictions with our modeling approach. Receptor desensitization is a postsynaptic effect and is therefore not influencing the basic model parameters, but rather altering the output of the basic model. The time courses describing the receptor desensitization for the neurons are either in a range similar to the single exponential recovery from depression and thus cannot be distinguished from it (14 of 16 neurons), or infinitely short (2 of 16 neurons). All the results described above suggest that none of the model extensions yielded useful results, and that the parameter space of the basic model variant could capture the variability in our data set best.

Both release probability and recovery time constant, as determined by our model, are very similar to values that have been obtained from experimental data. The release probability has been measured, for example in the rat MNTB (Schneppenburger et al., 1999; Wu and Borst, 1999), and determined to be around 0.2. The recovery time constant in the gerbil MNTB has been determined in chapter 3 under similar experimental conditions, and is plotted in figure 4.2 C next to the modeling results for comparison. The close agreement of our modeling results with previous experimental

results suggests that the parameters calculated by the model are the computational equivalents to the corresponding physiological phenomena.

### 4.2.3 Stimulation with trains consisting of regularly spaced intervals

One important feature of the firing pattern of auditory brainstem neurons is phase locking. For certain acoustic inputs, especially pure tones of low frequencies, cells fire with high temporal precision and phase lock to certain parts of the sound wave. This is especially true for MNTB neurons, which have a number of cellular specializations for temporal precision (Forsythe et al., 1998; Smith et al., 1998; Taschenberger et al., 2002; Taschenberger and von Gersdorff, 2000; von Gersdorff and Borst, 2002). Phase locking results in a very regular firing pattern not reflected by our Poisson-distributed spike trains. Therefore, we also tested the effects of regular spike trains with varying frequencies. Different frequencies were all tested in a single stimulus, which consisted of various segments with low and high frequencies. Each frequency segment consisted of 20 stimuli and was immediately followed by a segment of 20 stimuli at a different frequency (figure 4.3 A). The different train frequencies were chosen to imitate sound stimuli at various frequencies. Within the train, each switch from a low to a high frequency was matched by a corresponding switch from a high to a low frequency. Note that the frequencies in figure 4.3 A are plotted against stimulus number, not time. Figure 4.3 B shows a short clip of the complete stimulus plotted against time (top panel), and a clip of the corresponding voltage-clamp trace from a sample cell (3B, lower panel). The segments marked by ‘i’ and ‘ii’ are shown at a magnified scale in figures 4.3 C and D (mean over three repetitions). Please note that figure 4.3 C represents a high frequency train (196 Hz) while figure 4.3 D represents a low frequency train (45 Hz) at a different time scale. For comparison, clips of the two trains plotted at the same time scale are shown in the gray inserts of figures 4.3 C and D. To evaluate the data, the 20 EPSC amplitudes of each constant frequency period were extracted and plotted against time (figures 4.3 C and D, lower panels). We then fitted the data points with a single exponential function (solid line in lower panels of figures 4.3 C and D).

Besides mimicking phase-locked acoustic input, trains with regular stimulation patterns allow for the measurement of determine steady state amplitudes and single exponential time courses leading to these steady states. These two values are frequency

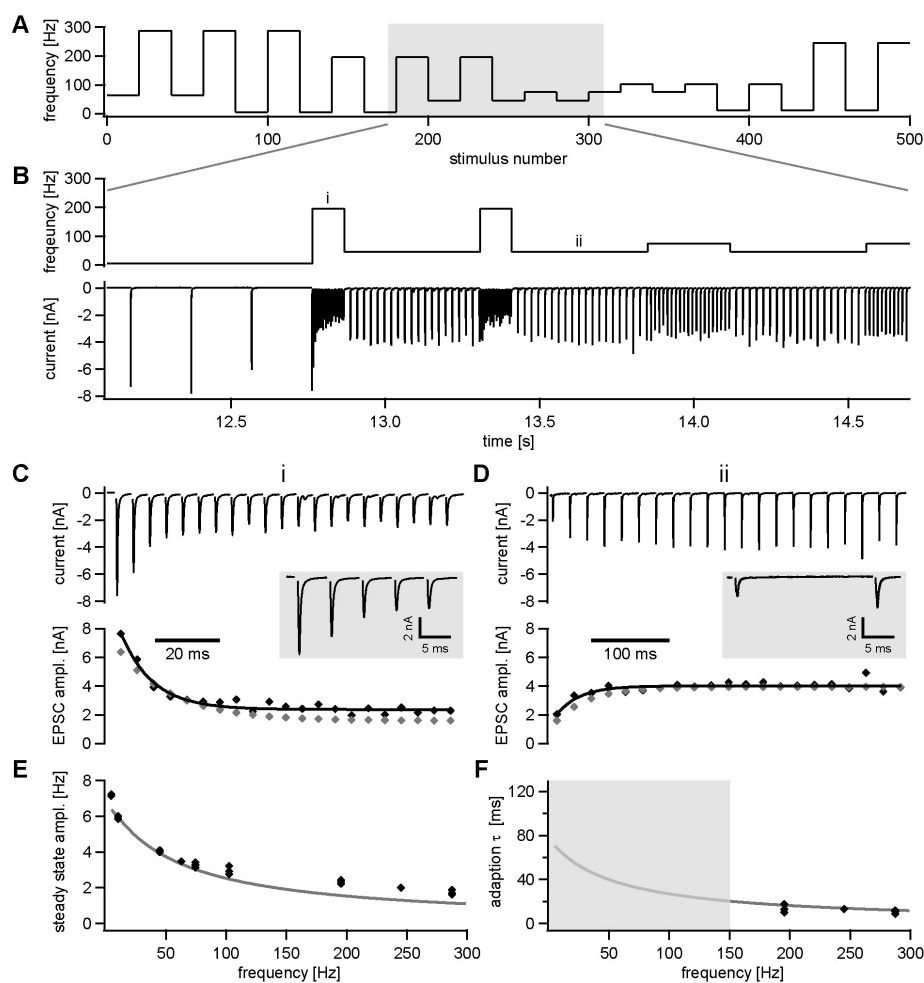


**Figure 4.3:** A: Time course of the second stimulation protocol, plotted against stimulus number, not time. Each period consists of 20 stimulations with constant inter pulse intervals corresponding to the indicated frequency. Frequencies are randomly distributed and range from 5 Hz up to 300 Hz. B: A short clip of the upper trace plotted against time for comparison to the raw data trace below. The raw data is the mean over three repetitions of a voltage-clamp recording. C, D: Detailed views of two sample constant frequency periods. Note that the traces are plotted against different time axes; the gray insets compare the initial parts of the same trains on identical time scales. The graphs below show the extracted EPSCs plotted as black diamonds and the corresponding model predictions plotted as gray diamonds. The black lines represent single exponential fits to the data shown by the black diamonds. E: Summary of the steady state amplitudes for all frequencies. The black diamonds represent the offset of the single exponential fit shown in C and D. The gray line is the model prediction for the steady state amplitude in dependency on the frequency. F: Summary plot of the characteristic time constants of adaptation to the new steady state. As in E, black diamonds represent the time constant of the single exponential fit; the gray line shows the model prediction. The low frequency part has been blanked, see text for further information.

dependent and characteristic for each synapse. In our case, predicting a neuron's response to a train with regularly spaced intervals with the vesicle release model allowed us to not only test the accuracy of the predicted EPSC amplitudes, but also the accuracy of the predicted steady state amplitudes, as well as the dynamics of adjusting to it. We did this by obtaining a data set with Poisson trains as well as a data set with regularly spaced trains from each cell that was tested with this protocol. The Poisson data were used to fit the basic model and calculate the model parameters as described above. Then the obtained parameters were used to calculate predictions for the steady state amplitude as well as for the time course of adaptation to this steady state characterized by the time constant. These two values were then compared to the parameters for the exponential fits of the experimental data. The steady state amplitude corresponds to the offset of the exponential fit and the time constant corresponds to the characteristic time constant of the exponential fit. Figure 4.3 E shows, for the same cell, the comparison for the steady state amplitudes for various frequencies; the gray line corresponds to the model prediction, the black diamonds to the experimentally determined amplitudes. The time constants were plotted in a similar fashion in figure 4.3 F for 150 Hz and above. For lower frequencies, time constants were not determined for the following reason: The experimental approach used exponential fits to determine the time constant, and thus the quality of the fit depended on a reasonable number of data points in the range of one time constant. The predicted time constants were very fast ( $< 50$  ms), therefore the transition to the new steady state happened for low frequencies within just a few events. Because of fluctuations in the measurements of EPSC amplitudes the resulting error in the fitted time course was too large to allow any meaningful statements. To indicate this, time constants are not shown for frequencies below 150 Hz (gray box in figure 4.3 F).

The average differences between model predictions and measured EPSC amplitudes over our sample of 5 neurons are shown in figure 4.4. The absolute differences for the steady state amplitude are plotted in figure 4.4 A; deviations from zero indicate differences between calculated and measured EPSC amplitudes. Since steady state amplitudes depend on the stimulation frequency and are larger for lower stimulation frequencies, absolute differences between measured and calculated amplitudes also tend to be larger for lower frequencies. Therefore, we also calculated the normalized difference (black squares in figure 4.4 B) and compared this difference to the coefficient of variation (CV) of the calculated steady state amplitudes. The CV was calculated as

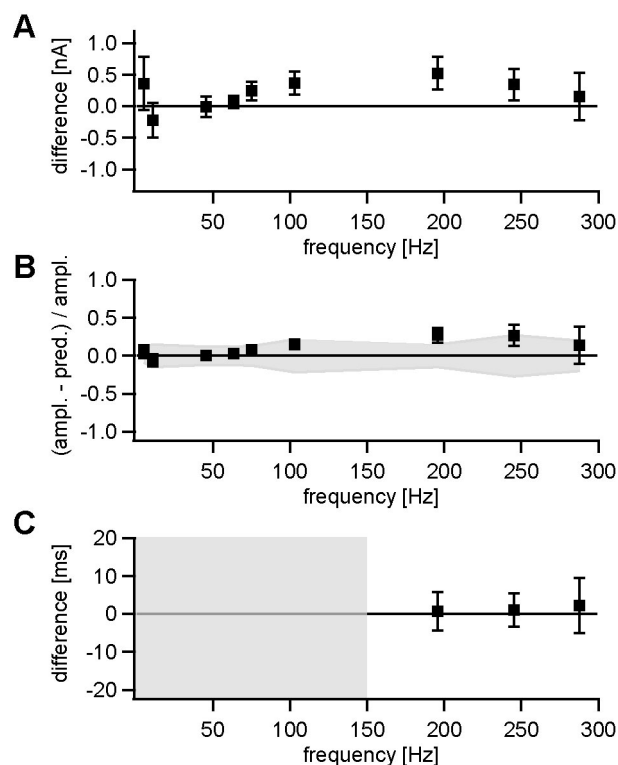


**Figure 4.4:** Summary graphs showing the differences between experimental data and model prediction over 5 cells. A: Difference between the offset of the single exponential fit (i.e. measured steady-state amplitude) and predicted steady state amplitude. B: The same difference as in A, but normalized to the offset of the exponential fit. The area marked in gray indicates the coefficient of variation of the recorded EPSC amplitudes (for details see text). C: Difference between the characteristic time constant of the exponential fit and the model prediction. Low frequencies were blanked, for details see text.

the mean CV of the single cells, averaged over the sample of 5 neurons and is plotted in figure 4.4 B in gray. For all tested frequencies but one (196 Hz), the normalized difference between predicted and measured steady-state amplitude was smaller than one CV. Besides steady-state amplitudes, the model also predicted the neuron's time course for reaching the steady state amplitude. This calculated time constant was compared to the measured time constant in 5 neurons; the differences between the two are plotted in figure 4.4 C. For the considered frequencies the model provided very accurate predictions.

#### 4.2.4 Natural stimuli

Finally, we tested the performance of our model on ‘natural’ input, i.e. with spike trains that represent acoustic stimuli of biological relevance. We obtained these spike trains through *in vivo* recordings from single units in the MNTB of the anesthetized gerbil. The recording procedures were identical to the ones used in chapter 3. The presented stimuli were vocalizations of owl, typical gerbil predators (Lay, 1974). The spectrogram of a 2 s sound sample is depicted in figure 4.5 A.

Using this approach to mimic natural input in a brain slice preparation has two caveats. The first one is the variability of firing patterns between different MNTB cells *in vivo*, mainly caused by the differential tuning between cells. As information about the neuron’s tuning is lost in a slice preparation, it is not possible to stimulate with one spike train associated with the ‘correct’ frequency band. The second caveat arises from the fact that the *in vivo* recordings were conducted in the MNTB and not from globular bushy cells in the CN, which give rise to calyx of Held. Also, we did not perform simultaneous pre- and postsynaptic recordings (Guinan and Li, 1990; Kopp-Scheinflug et al., 2003), and thus, were unable to determine if our single units were calyces or postsynaptic principal neurons. With these caveats in mind, we stimulated calyceal input fibers with spike trains reflecting characteristics of natural sound evoked input. These spike trains have different characteristics than Poisson or regular stimulations and thereby present yet another class of stimulation pattern.

The spectrogram of the sample that we used to stimulate the cells *in vivo* is depicted in figure 4.5 A. The barn owl call has pronounced temporal features with the main energy between 2 and 5 kHz. We chose data recorded from two *in vivo* units to stimulate cells in our slice preparation. The cells had best frequencies of 2500 Hz and 3500 Hz, respectively and showed a clear response to the stimulation. From each of these units we recorded ten repetitions of sound presentation and randomly chose three traces as stimuli for *in vitro* experiments (figure 4.5 B). Thus, a total of six spike trains were used to stimulate each neuron *in vitro*. An example of a voltage-clamp response recorded *in vitro* in response to the trace marked in figure 4.5 B is shown in figure 4.5 C. Similar to the other stimulation protocols, we extracted the EPSC amplitudes and compared them to the model prediction. The model was fitted using data from Poisson stimulations in the same cell, so the comparison between data and model prediction is based on parameters obtained with a different stimulation pattern. This was done to test, if the model could also predict the synaptic strength in response to stimulation

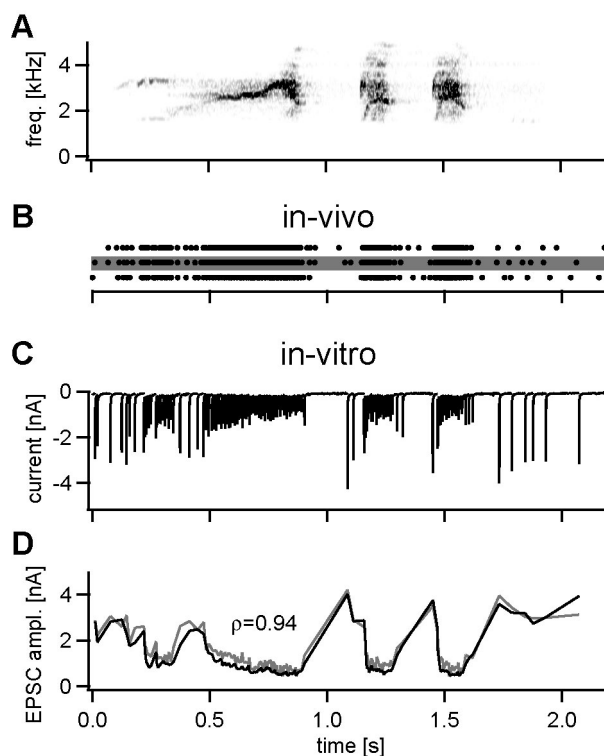


**Figure 4.5:** A: Spectrogram of a presented vocalization recorded from a bran owl (*tyto alba*). B: Raster plot of action potentials recorded during three presentations of the vocalization to a MNTB neuron *in vivo*. All three traces were used to stimulate neurons *in vitro*. C: Voltage-clamp recording from a neuron during stimulation with the firing pattern indicated by the gray bar in B. D: EPSC amplitudes extracted from the data trace. The gray trace indicates the experimental data shown in C, the black trace the corresponding model prediction.

patterns not used for the parameter optimization. Figure 4.5 D shows the comparison for the sample trace from 4.5 C; the corresponding correlation coefficient is 0.94. The mean correlation coefficient over all stimulation patterns recorded in 6 neurons is  $0.88 \pm 0.03$ , suggesting that the predictions were still quite accurate, although not as good as they were for the Poisson trains. One reason for this somewhat lower accuracy may be that the model was not fit against the natural stimulation pattern, but against the Poisson-distributed patterns. Due to the different statistical characteristics of the two patterns, a slight decrease in prediction accuracy was expected. However, please note that the difference in accuracy between predicting the responses to Poisson trains and natural activity was not significant. Therefore, we conclude that the model produced very good predictions for stimulation patterns based on naturally occurring input.

### 4.3 Discussion

The main question this study addresses is how well the response of the calyx of Held synapse to complex trains of continuous activity can be described utilizing vesicle release models. We found that a very basic model including only a constant release probability and a single exponential time course for vesicle replenishment can predict EPSC amplitudes already with very high accuracy. Two key features of the present study are the use of very long lasting and statistically complex stimuli, as well as the embedding of these into chronic ‘spontaneous’ background activity.

Spontaneous activity is one of the hallmarks of auditory brainstem neurons *in vivo*, but for methodological reasons is lost in slice preparations, such that auditory brainstem neurons *in vitro* are typically tested against a background of silence. Previous vesicle release models describing synaptic transmission at the calyx of Held (Weis et al., 1999; Graham et al., 2001; Graham et al., 2004) were based on electrophysiological data recorded from silent *in vitro* preparations (i.e. without the naturally present spontaneous activity), and thus only capture the dynamics of synaptic transmission under these conditions. However, previously we found that synaptic transmission at the calyx of Held in such silent slice preparations differs from transmission under natural activity levels in a number of key parameters such as synaptic amplitude, latency, synaptic depression during trains, recovery from depression, and fidelity of transmission (see chapter 3).

Therefore, the central goals of this study were to model the transmission dynamics of chronically active calyces, compare results obtained with several extensions of the model, and test the performance of the model during complex trains of activity, including activity resulting from sound stimulation with natural and biologically relevant sound clips.

The surprising result is that already the most basic model including only a constant release probability and a single exponential time course for vesicle replenishment performs exceptionally well in predicting EPSC amplitudes. Improving the model by increasing the number of parameters to account for additional biophysical effects such as receptor desensitization, two vesicle pools, or synaptic facilitation on a separate time course does not increase the prediction accuracy. Why does the most basic model, which disregards a number of physiological effects that have clearly been shown to be present in the calyx of Held, perform so well? It is unlikely that the stimulus trains used in the present study were too simplistic to capture the fine details of trans-



mission dynamics. We note that the Poisson-distributed activity, which was used to compute the model parameters, inherently includes a high degree of statistical complexity. Varying the mean frequency of the Poisson-distribution over almost two levels of magnitude introduces additional complexity and ensures that the entire range of activity a MNTB neuron may encounter in the intact brain is covered by the stimulus train. We also tested trains with regular spaced inter spike intervals and stimulus trains derived from sound stimulation with natural sound clips, which increase the amount of statistical complexity even further. Therefore, we assume that any model able to predict responses to the stimuli used in this study correctly should be able to predict responses to any naturally occurring sound situation equally well.

Species, age, and temperature differences may account for some of our findings. Most previous *in vitro* work on the calyx of Held has been performed in preparations from rat or mouse, not gerbil. However, we previously found that synaptic transmission in the calyx of Held of the gerbil is very similar to that of other rodents in basic parameters. Receptor desensitization, while being very prominent in preparations from younger animals, plays a much smaller role in preparations from older animals such as the ones used in this study (Joshi and Wang, 2002; Renden et al., 2005; Taschenberger et al., 2005). This finding may help explain why the model variation with added receptor desensitization did not yield higher correlation coefficients. EPSC amplitudes, or vesicle pools, are known to recover with double-exponential time courses, not single exponential ones as used by our basic model (Wang and Kaczmarek, 1998; Sakaba and Neher, 2001b). However, of the two associated time constants, one is very slow and at the order of seconds. Therefore, ISIs at the order of seconds would be required to measure, or compute, this time constant properly. Due to spontaneous activity in the auditory brainstem, such long periods of silence are uncommon *in vivo*. Since the goal of our study was to capture the dynamics of synaptic transmission under conditions as closely as possible to those in the intact brain, our stimulus trains did not contain any ISIs long enough to properly measure the slow time constant. This might explain why the model variant with the double exponential did not yield higher correlation coefficients than the basic version of the model. It might also explain why the slow time constants were virtually eliminated from the computations during the parameter fitting process, either by assuming infinite values for the time constant, or values that were virtually identical to those of the fast time constant.

We are uncertain why the model variant with added facilitation did not seem to

yield improved predictions over the basic variant. Synaptic facilitation, i.e. an accumulation of calcium in the presynaptic terminal, must certainly be present during chronic stimulation at relatively high frequencies. It is possible that the introduction of chronic background activity into the slice preparations changes the dynamics of synaptic transmission such that the role of the various mechanisms of short-term plasticity are altered in comparison to the state of a rested synapse. Long-term stimulation of a slice preparation with thousands of stimuli might put calyces of Held into a functional state that is much less well understood than the functional state of rested calyces. Thus, it cannot be ruled out that facilitation with an independent time scale, possibly also double exponential recovery, might just not have a significant influence over EPSC dynamics during chronic long term activity. It is also possible that the time courses of these are too similar to the basic features of the model such that the parameter optimization cannot extract them as separate parameters. In this case, the parameters computed by our model would represent a combination of physiological effects. However, the values for release probability and the fast recovery time constant as determined by our model are very similar to values previously reported in the literature, suggesting that they indeed represent these exact physiological parameters rather than an abstract combination of a number of effects. The main conclusion of this study is that a very simple vesicle release model with very few parameters can accurately describe the dynamics of vesicle release at a chronically active synapse. This finding is in contrast to modeling studies performed with data from rested synapses, where the inclusion of additional physiological parameters into the modeling process is required for an acceptable level of predictive power.

# 5 Transition Between Unconditioned and Conditioned State

## 5.1 Introduction

The focus of the two previous chapters was lying on the *in vivo* state of the calyx of Held synapse. In an acute brain slice preparation this *in vivo* state is simulated by ongoing stimulation with a Poisson-distributed activity train. The ongoing activity causes a number of phenomenologically observable changes which were in detail described in chapter 3. To further investigate the properties of the *in vivo* state, the dynamics of the synaptic transmission were modeled with vesicle release models as described in chapter 4. This revealed the surprising fact that synaptic transmission under *in vivo* conditions can be described with a very basic model and that effects like facilitation and receptor desensitization are not necessary to give a satisfactory prediction of the synaptic dynamics.

In slice preparations the completely rested synapse is normally regarded as the steady state. As this synapse is one of a few that can be patch-clamped *in vitro* (Forsythe, 1994; Borst and Sakmann, 1999), it has been characterized extensively in previous studies. A lot of information is known about basic parameters like vesicle release rates (Schneggenburger and Neher, 2000; Sakaba and Neher, 2001b), the recovery time course (Wang and Kaczmarek, 1998; Sakaba and Neher, 2001a) and the vesicle pool size (Sätzler et al., 2002; Schneggenburger et al., 1999; Bollmann et al., 2000). In an intact brain, this rested state is never reached due to continuous firing caused by spontaneous activity of the afferent fibers and therefore the conditioned state in which the cell is constantly firing with a certain frequency is defined as a second steady state, the *in vivo* rested state. The main question addressed in this chapter is how these two

steady states are related to each other. How do the dynamics of synaptic transmission change and on which time scales are these changes occurring?

This chapter investigates both transitions between the two steady states. On one hand the changes at the beginning of the conditioning period and on the other hand the recovery after switching off the conditioning pulse train. The used protocols reveal changes of basic parameters like the vesicle pool size and the release probability. This illustrates further differences between completely silenced synapses and synapses in an *in vivo* state.

## 5.2 Results

### 5.2.1 Beginning of conditioning period

The transition from the completely rested state to the *in vivo* state has already been sparsely described in chapter 3. EPSC amplitudes in answer to stimulation with Poisson-distributed pulse trains were plotted against time and fitted with double exponential functions. In figure 5.1 A an example of a cell stimulated with a 20 Hz train is displayed. The double exponential fit clearly shows a slow tail with a characteristic time constant of 19 s. As it can be seen in figure 5.1 B all 15 cells in which this stimulation protocol was recorded show a double exponential decay with a slow time constant of on average 85 s.

According to the theory of the basic vesicle release model presented in chapter 4 the decrease in amplitude should not show a double exponential decay with a very slow time constant. For stimulations with regular spike trains the calculations for the time course leading from an arbitrary amplitude to the steady state amplitude of a given stimulation frequency predicted a single exponential decay. In the case of Poisson-distributed activity the time course is in theory more complex and cannot be described analytically. Nevertheless, a slow time constant of more than 10 s does not at all comply with the predictions of the vesicle release model as it is far slower than both time constants of the model (stimulation frequency and recovery time constant). Therefore, an additional effect has to be present. One possible explanation for this slow decay might be a change of the model parameters over time. To address this issue, the model was fitted to short intervals of the whole EPSC amplitude trace. The intervals had a length of 10 s and the first interval started 1 s after the beginning of the conditioning period. The first second was eliminated from this analysis to exclude the

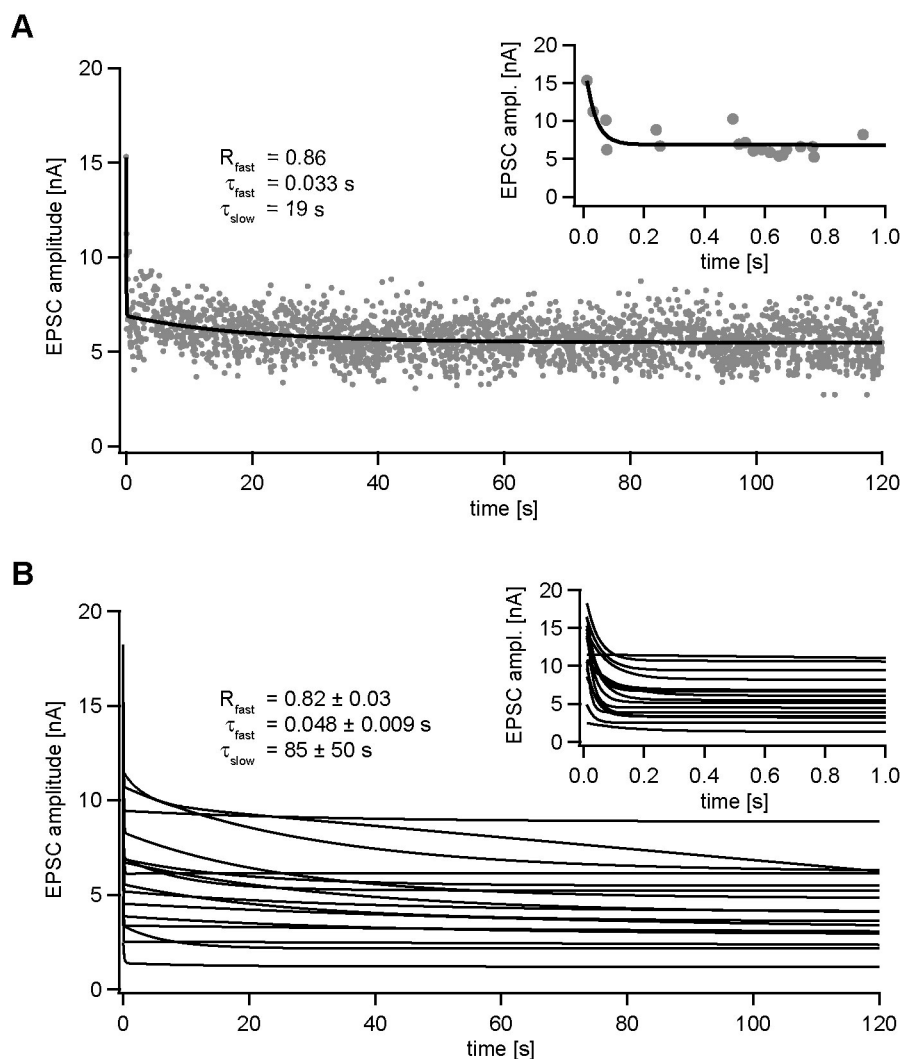


**Figure 5.1:** A: Development of EPSC amplitudes after starting the conditioning. Each gray dot corresponds to a single EPSC. The cell was stimulated with a 20 Hz Poisson-distributed activity train. The black line represents a double exponential fit to the gray dots. The parameters are given in the figure,  $R_{fast}$  is the amplitude fraction of the exponential term with the time constant  $\tau_{fast}$  divided by the sum of the amplitudes of both exponential terms. The inset shows a magnified view of the first second to illustrate the initial step decline. B: Summary plot of 15 cells. All cells were stimulated with the same activity pattern. For clarity only the exponential fits are shown. The parameters and the inset are presented in the same way as in A.

effects of the initial rapid decay phase. The following intervals were shifted by steps with a length of 2 s until the end of the 120 s long conditioning period was reached. The integration time of 10 s was chosen as a compromise between time resolution

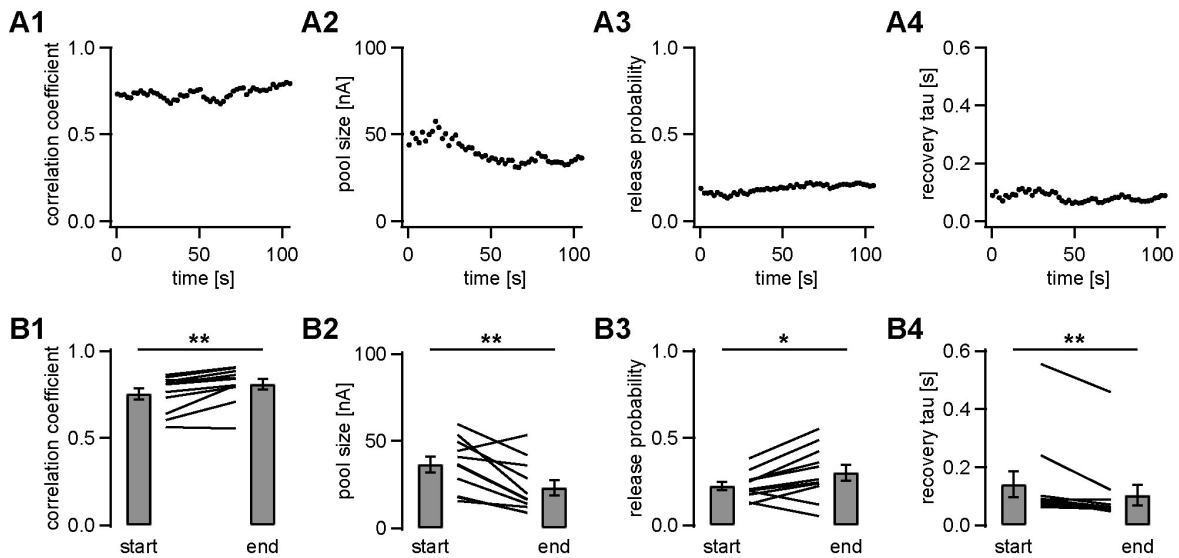


**Figure 5.2:** A: development of model parameters over time. A1 shows the correlation coefficient, A2 - A4 show the three free model parameters. The model was fit to intervals of 10 s and the interval was shifted in steps of 2 s. Responses from the first second were eliminated from this analysis (see text). Each dot corresponds to an independent fit. The time interval of data used for each fit is restricted by the x value of the plotted dot and the x value plus 20 s. B: Comparison of the first and last interval for each of the four considered variables. Significant changes are marked with asterisks.

and signal to noise ratio. This period provides for a stimulation frequency of 20 Hz an average of 200 data points. This is enough input for the model to produce stable parameter sets. On the other side the time interval is still short enough to give a reasonable time resolution.

The graphs in figure 5.2 A show the development of the correlation coefficient and the three free model parameters over time at the beginning of the conditioning protocol. The displayed cell is the same that can be seen in figure 5.1 A. As the minimum time interval that is needed to calculate a stable fit is 10 s, the time resolution of these plots is rather low. Therefore, no function could be fitted to the data points to quantify the time course of the parameter developments. To test the significance of the parameter changes the first and last time intervals were compared for all 15 cells. The results of this evaluation is displayed in figure 5.2 B. The most obvious change is the decrease in vesicle pool size to 0.64 of the value at the beginning of the conditioning. This parameter does not reflect the momentary pool size but the maximal pool size as defined by the model. On the other side this pool size does also not correspond to the

full vesicle pool of a completely recovered synapse. Instead it reflects only the fraction recovered with the fast time constant of the vesicle recovery process. A change in this parameter influences the vesicle recovery time course. In this regard the vesicle pool size is directly related to the changed recovery time constant. Both parameters together define the dynamics of the vesicle pool refilling. Apart from this also the release probability shows a slight increase over time which suggests an accumulation of calcium in the presynaptic terminal.

### 5.2.2 Vesicle pool recovery

The conditioning with spontaneous activity leads to a decrease in EPSC amplitudes beyond the expected fast decay at the beginning of the conditioning pulse train. This is clearly visible in a second slower exponential decay in the fits of the EPSC amplitudes and is also reflected in changes in the model parameters. Nevertheless, the cells completely recover and show similar EPSC amplitudes as before the conditioning after a recovery period of five minutes. This raises the question how the time course of recovery after switching off the ongoing activity looks like.

Recovery experiments normally use a stimulation protocol in which the vesicle pool is depleted and test pulses are recorded at certain time intervals after the depletion to determine the degree of recovery. The vesicle pool can be emptied in two ways, either by depolarizing the presynaptic terminal and thereby causing a calcium influx which is releasing all vesicles (Wu and Borst, 1999) or by stimulating the axon with a high frequency pulse train to release the majority of vesicles from the synapse (Wang and Kaczmarek, 1998). As the first method depends on a direct access to the presynaptic terminal, only the second method was applicable. After depleting the vesicle pool one single test pulse was recorded after a certain time to determine the degree of recovery. This protocol was repeated several times with different time intervals between pool depletion and test pulse to obtain a complete time course of recovery. The repetitions were necessary to avoid errors introduced by recording several test pulses in one sweep as every stimulation is depleting the vesicle pool a little bit and thereby changing the state of recovery. For exact measurements the cells had to be completely recovered between each repetition. This extensive stimulation protocol which involves a lot of repetitions can not be used for conditioned cells as the cells would have to be conditioned a lot of times and would need at least five minutes after each repetition to fully recover. Therefore, a quick variant with only one repetition had to be used

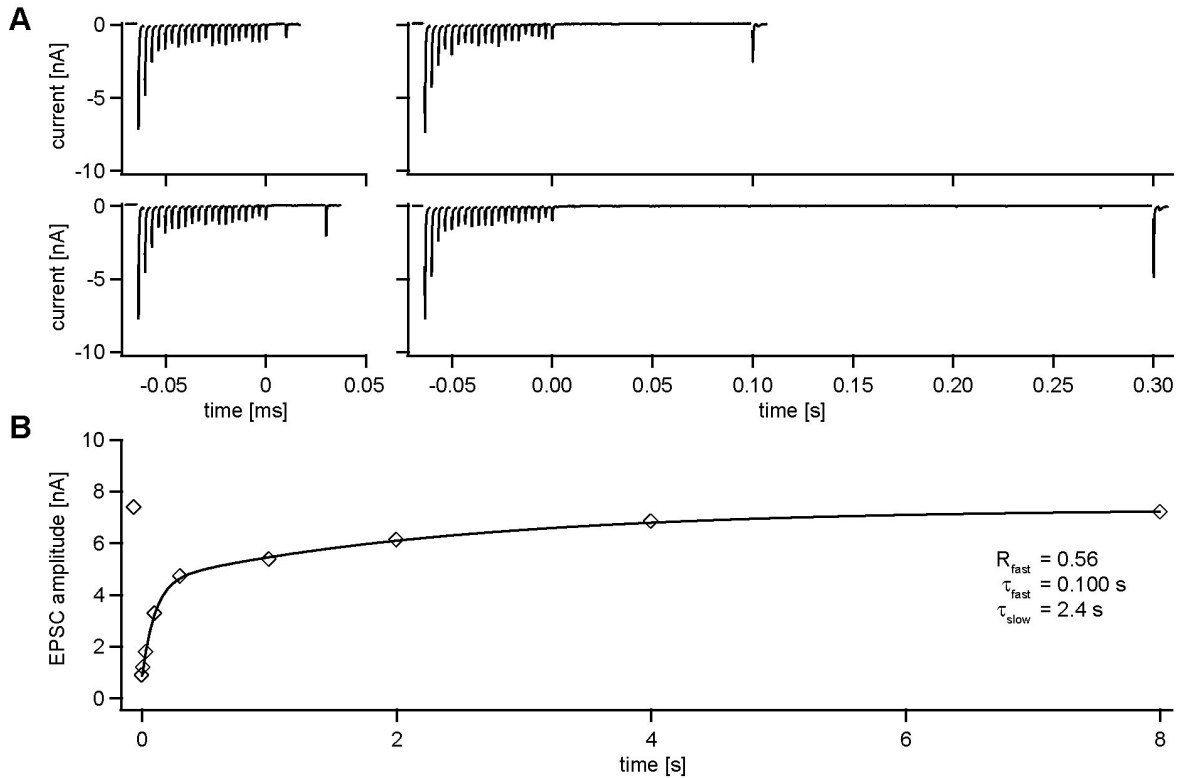


**Figure 5.3:** Vesicle pool recovery. A: EPSC traces illustrating the used protocol. The vesicle pool was depleted with a 300 Hz pulse train of 20 repetitions. Afterwards a single test pulse after different time intervals was recorded. The four traces show the four smallest time intervals. B: Summary of the recorded test pulses. The first diamond corresponds to the mean EPSC amplitude of the first pulse in the 300 Hz sequence. The following diamonds each correspond to the average over three repetitions of a single test interval. The time course was fitted with a double exponential function. Parameters for the shown example are given in the figure. Mean values over 15 cells:  $R_{fast} = 0.57 \pm 0.04$ ,  $\tau_{fast} = 0.098 \pm 0.015$  s,  $\tau_{slow} = 1.73 \pm 0.17$  s.

to investigate recovery from the conditioned state. In this case all probe pulses were recorded in one sweep. As already mentioned this introduces systematic errors and to estimate the influence of these errors classical recovery measurements as described above were recorded for comparison.

Figure 5.3 shows a summary of the classical recovery experiments. To deplete the vesicle pool a 300 Hz pulse train with 20 repetitions was used. After this train, the EPSC amplitudes and therefore the pool size were decreased to  $0.10 \pm 0.02$ . In several sweeps test pulses were recorded after increasing time intervals. Each time interval was repeated three times to calculate stable mean values. Examples of the



first four sweeps can be seen in figure 5.3 A. The amplitudes of the test pulses were plotted against time and fitted with a double exponential function as displayed in figure 5.3 B. The mean values for the two time constants determined from a sample of 15 cells are  $0.098 \pm 0.015$  s and  $1.73 \pm 0.17$  s. The fraction of the fast time constant is  $0.57 \pm 0.04$  s. Compared to earlier studies (Wang and Kaczmarek, 1998) the values for the time constants are smaller. This can be explained by different experimental conditions, namely a higher temperature and older animals.

As a next step the recovery time course of previously conditioned cells was determined. In these cases, another stimulation protocol with only one repetition was used. For a fair comparison this protocol was recorded in conditioned as well as unconditioned cells. The protocol used the same 300 Hz pulse train with 20 repetitions as in the previously described experiments to deplete the vesicle pool. In the unconditioned case, cells were fully recovered before starting the stimulation with the 300 Hz train. In the conditioned case, the 300 Hz train was started directly after switching off the conditioning train. The number of test pulses was reduced to a minimum to keep the error caused by the test pulses as small as possible. Therefore, it was not possible to calculate the characteristic time course very precise and the given values have to be taken with caution.

In figure 5.4 A and B voltage clamp recordings of the two cases are displayed. It is already clearly visible that the EPSC amplitudes in the conditioned case are significantly smaller than in the unconditioned case over the complete recording time. This is confirmed in figure 5.4 B where the extracted EPSC amplitudes of both cases are directly compared to each other. It seems that the EPSC amplitudes of the conditioned cell reached a stable value after the displayed time span of 30 s. This is not the case. They recovered on a very slow time scale and reached the initial amplitudes after a few minutes. After five minutes all cells ( $n = 10$ ) were fully recovered. Due to the small amount of recorded data points and the big fluctuations between single EPSC amplitudes it was not possible to determine the time course of this slow recovery. The amplitude in the conditioned case determined as the offset value of the double exponential fit was decreased to  $0.82 \pm 0.08$  compared to the fully recovered value. The time courses of the two double exponential fits could only be determined with limited accuracy due to the fact that only few test pulses were recorded. They do not show significant changes. The parameters are also comparable to the values calculated in the classical recovery experiments. The systematic error introduced by

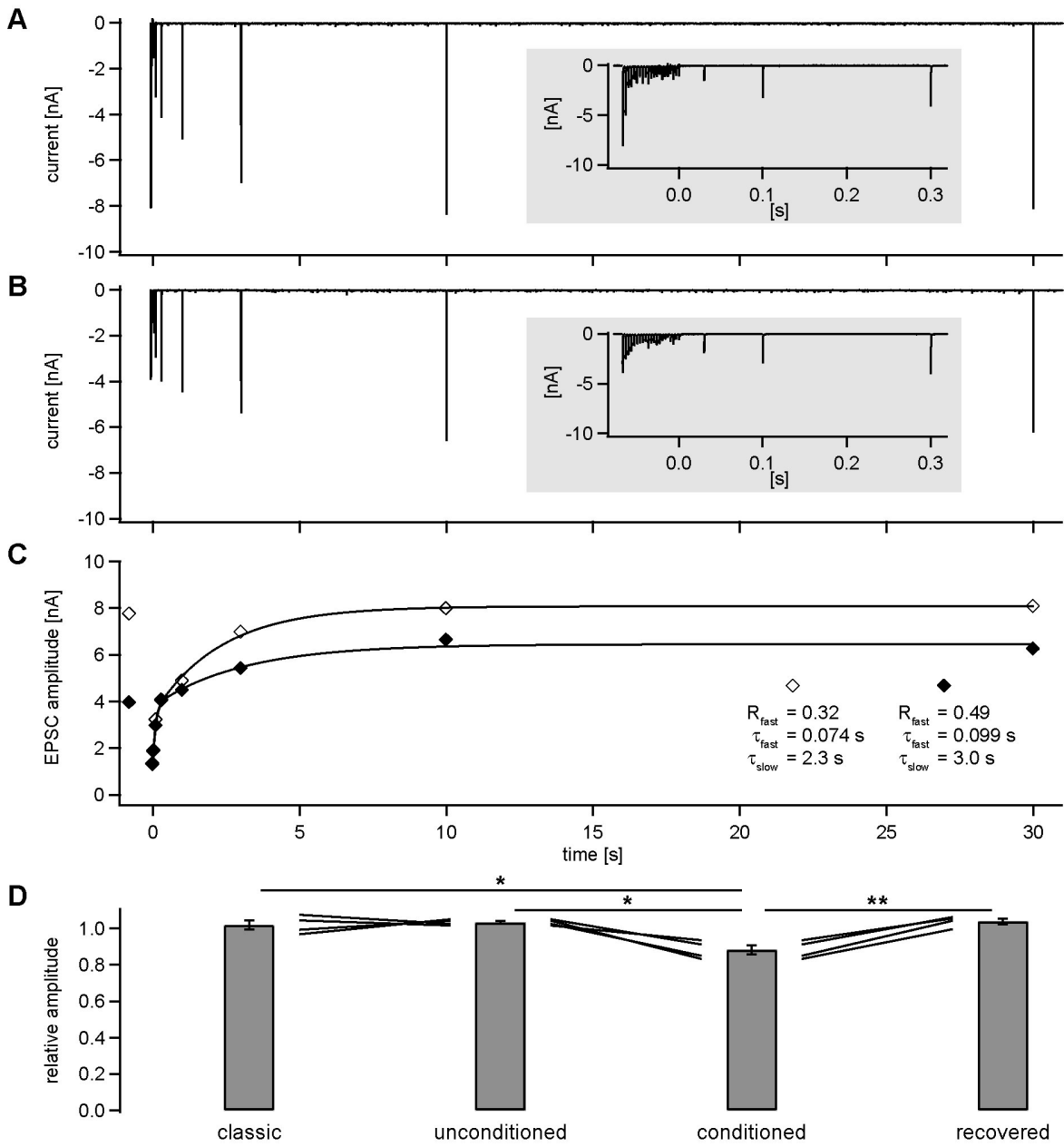


**Figure 5.4:** Comparison of recovery between unconditioned and conditioned state. A: voltage clamp trace illustrating the used stimulation protocol. The pool is depleted with a 300 Hz train of 20 repetitions. Afterwards, probe pulses to test the recovery were recorded in increasing time intervals. The gray inset is a magnification of the first 300 ms. The cell was completely rested before starting the stimulation. B: Corresponding traces in the conditioned case. The cell was conditioned for several minutes before starting the depletion pulse train. C: Comparison of the extracted EPSC amplitudes. Open diamonds correspond to the unconditioned case, closed diamonds to the conditioned case. In the unconditioned case mean values over three repetitions are displayed, for the conditioned case only one repetition was recorded. The first data point of each trace corresponds to the initial amplitudes at the beginning of the 300 Hz pulse train. It was moved back in time along the x-axis for better visibility. Both cases were fitted with a double exponential function. Mean values of the parameters were calculated from 4 cells. Unconditioned case:  $R_{fast} = 0.44 \pm 0.06$ ,  $\tau_{fast} = 0.07 \pm 0.01$  s,  $\tau_{slow} = 2.3 \pm 0.5$  s; conditioned case:  $R_{fast} = 0.49 \pm 0.09$ ,  $\tau_{fast} = 0.12 \pm 0.08$  s,  $\tau_{slow} = 4.6 \pm 1.4$  s. D: Summary of the recovery of EPSC amplitudes in different scenarios. In the 4 cells mentioned above all different protocols could be recorded. Displayed is the relation between the initial amplitude and the offset of the exponential fit function which reflects the amplitude after recovery. The classic case shows the corresponding 4 cells from figure 5.3. The unconditioned and the conditioned case show the relative amplitudes measured with the protocol shown in A – C. The recovered case shows the relative amplitudes after an extensive recovery period of at least five minutes. In the conditioned case amplitudes were significantly reduced compared to all other three cases.

the repeated test pulses does not show an influence on the level of accuracy of these measurements. Figure 5.4 D shows a summary of the long lasting amplitude decrease caused by the conditioning protocol. Only the subset of cells ( $n = 4$ ) in which all measurements could be performed are displayed. They show similar values compared to the whole population. The bars represent relative EPSC amplitudes. They were calculated as the relation between the initial amplitude and the offset of the respective double exponential fits. The classical recovery protocol, the unconditioned recovery protocol recorded in one sweep, and the fully recovered state after five minutes of recovery all show amplitude relations close to one (well within one standard error). The conditioned case shows after a recovery period of 30 s still a significant decrease compared to all other three cases. Nevertheless, it completely recovers, so damage to the cell caused by the extensive stimulation protocol can be excluded. This clearly indicates a change in recovery behavior between unconditioned and conditioned cells.

In summary, the recovery experiments revealed two findings: First, the time course of the vesicle pool recovery does not change significantly due to the ongoing activity

of the conditioning protocol. Second, the conditioned case only recovers partially on a time scale of tens of seconds and recovers completely on a very slow time scale on the order of minutes.

### 5.2.3 Miniature EPSCs

It is known that extensive stimulation leads to an increase in calcium concentration and therefore an increased frequency in the occurrence of miniature EPSCs (Habets and Borst, 2005; Korogod et al., 2005). To investigate if this is also true for the stimulation protocols used in this study miniature EPSCs were extracted from the recovery traces used in section 5.2.2. The test pulses were removed from the trace by cutting out time intervals with a length of 20 ms starting right before the stimulation artifact. The resulting traces were analyzed with a pattern detection algorithm to search for miniature EPSCs.

Figure 5.5 A shows an overlay of all minis detected in the six minutes long recovery trace of one example cell. The black trace displayed on top of the gray single traces corresponds to the mean trace. For further analysis the amplitudes of the minis were calculated by subtracting the baseline from the peak amplitude. For the cell shown in figure 5.5 A the amplitude distribution is plotted in figure 5.5 B and the time interval between successive minis is plotted in figure 5.5 C. The amplitude distribution shows a peak at around 50 pA and a sharp decline towards smaller amplitudes. This is to a certain degree caused by the noise level of the recordings with a standard deviation of 7.1 pA. This leads to fewer detections of minis with small amplitudes. But even if not all minis can be detected, the comparison between beginning and end of the recorded trace is still valid as the noise level and therefore the percentage of undetected minis stays the same over the whole recording time. The mean time interval of 0.100 s between single mini events corresponds to a mean frequency of 10 Hz. The mean mini frequency over all 9 cells in the sample is  $9.6 \pm 1.6$  Hz. The frequency distribution shows a single exponential decay exactly like a Poisson distribution. This means the mini events are not influenced by each other. To describe the time course of the frequency decay after the end of the conditioning period, data from all 9 cells were pooled. The time axis was divided into 5 s bins and the mean mini frequency in each bin was calculated. Mean values over all cells and their standard error for each time bin were calculated and are displayed in figure 5.5 D1. The black discontinuous line corresponds to the mean frequency over time, the gray area surrounding the black

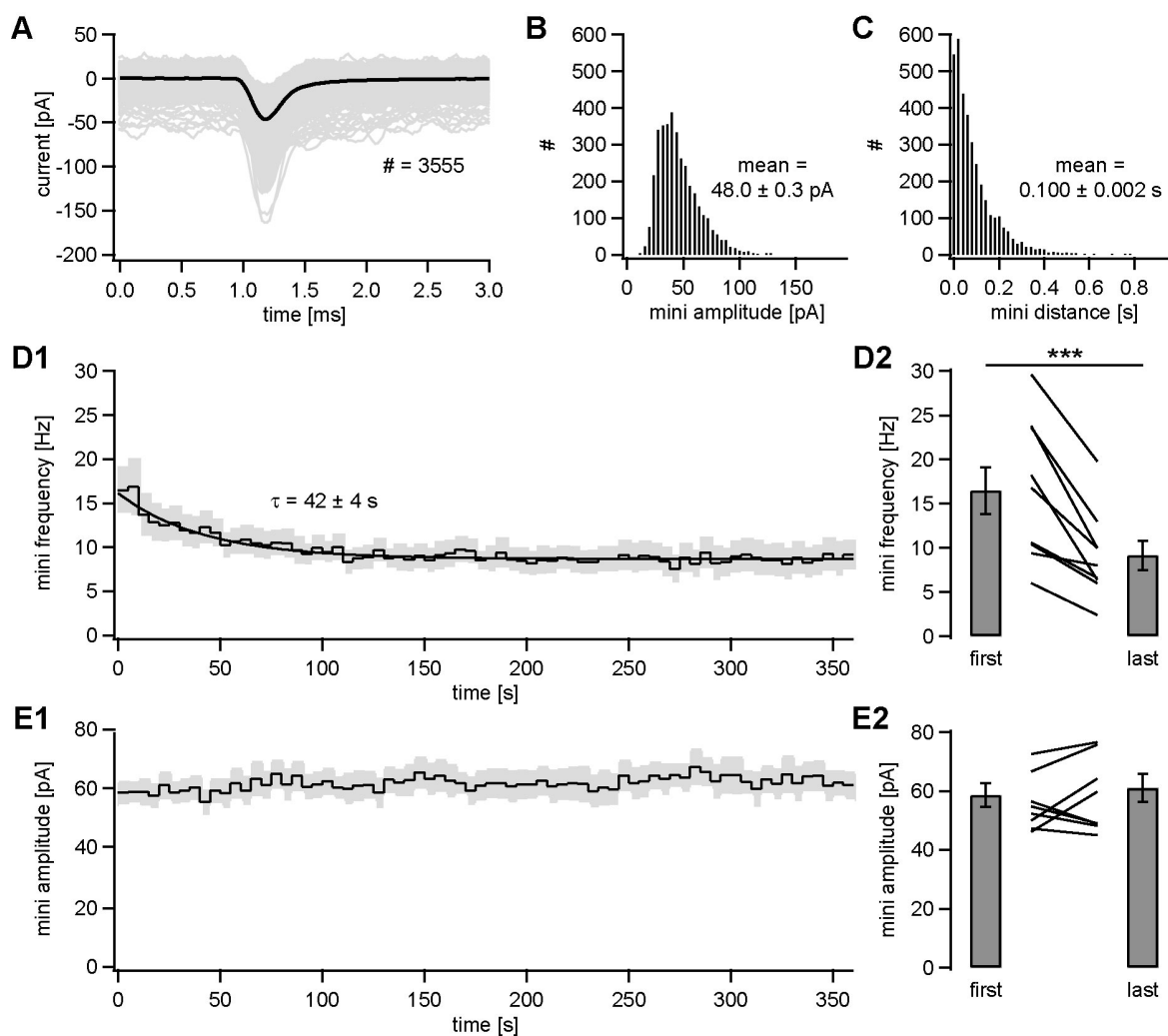


**Figure 5.5:** Development of miniature EPSCs after switching off the simulated spontaneous activity. A: Overlay of all minis recorded in one cell over a period of six minutes after end of the ongoing stimulation. Detected were a total of 3555 minis (average over 9 cells:  $3452 \pm 562$ ). The black trace corresponds to the mean over all minis. B: Histogram of the distribution of mini amplitudes. C: Histogram of the intervals between successive minis. D1: Analysis of the mini frequency development after end of the ongoing stimulation. The data was binned in 5 s intervals and pooled over all 9 cells. The black discontinuous line shows the average frequency in each 5 s interval, the gray area corresponds to the standard error. The black continuous line is a single exponential fit to the data with a characteristic time constant of  $42 \pm 4$  s. D2: comparison of the first and last 5 s interval. The bars show the same data as in D1, the black lines in between represent the single cells. The difference in frequency is highly significant with  $p = 0.0009$ . E: A similar analysis as in D for the amplitudes of the minis. The amplitudes do not change significantly ( $p = 0.40$ ).

line represents the standard error. The mean frequency shows a clearly visible decay over time that can be fit with a single exponential function. The characteristic time constant of the fit is  $42 \pm 4$  s. In figure 5.5 D2 a comparison between the first and the last 5 s bin is shown in detail. The black lines between the bars represent the frequency decay of each of the 9 cells. Every cell shows an obvious decrease and the decrease of the whole population is therefore highly significant. The same analysis as for the frequencies was also done for the mini amplitudes. In this case no change over time could be detected, the amplitudes were not affected by the conditioned protocol. The results are displayed in figure 5.5 E.

### 5.3 Discussion

The main question addressed in this chapter is how the two steady states that have been defined in this study are related to each other. Several changes between these two states such as strongly reduced synaptic amplitudes and a decrease in synaptic depression were observed in the previous chapters. These changes have to happen in a transition phase after switching on the conditioning pulse train and, as the cells do fully recover after the conditioning protocol, have to be reversed after switching off the pulse train.

The basic vesicle release model introduced in chapter 4 describes synaptic dynamics with single exponential functions for the vesicle release as well as the vesicle recovery. This model works very well in the conditioned cell but cannot account for the double exponential decay of synaptic amplitudes at the beginning of the conditioning phase. The time course of the slow component of the decay is on the order of several tens of seconds. This is far slower than the dynamics of the vesicle release model and also slower than any previously described dynamic effect at the calyx of Held. The slow component of the vesicle pool recovery is on the order of a few seconds (see figure 5.3), facilitation (Borst et al., 1995; Barnes-Davies and Forsythe, 1995; Helmchen et al., 1997) and receptor desensitization (Trussell et al., 1993; Zhang and Trussell, 1994), are on the order of milliseconds, calcium channel deactivation is on the order of seconds (Borst et al., 1995; Forsythe et al., 1998).

As the slow decay cannot be explained by known dynamic effects, the influence of this decay on the parameters of the basic model were investigated. The analysis of the dynamics of the free model parameters revealed significant changes in all three

parameters. Though these model parameters are mathematical constructs and do not have a direct correlation to the biophysical processes, their change nevertheless indicates a change of these biophysical processes in the synapse. The increase in release probability can be explained by an increase in the residual calcium concentration inside the presynaptic terminal, an explanation which is supported by the higher mini frequencies seen directly after switching off the conditioning pulse train. The faster recovery time constant predicted by the vesicle release model is not reflected in the recovery experiments. Nevertheless, a change cannot be excluded as the errors of the recovery time constants measured with the used protocol for the recovery experiments are rather big. The decrease in vesicle pool size predicted by the model is reflected by the recovery experiments. The model predicts a decrease to 0.64, the recovery experiments show a decrease in EPSC amplitude to 0.82 of the fully recovered value. The reason for this decrease remains unclear, a decrease in quantal size can be ruled out as the measurements of mini amplitudes clearly demonstrate. Possible explanations could involve a decrease in vesicle pool size due to slow vesicle recycling or postsynaptic effects like some form of long lasting receptor inactivation or desensitization. These results are in contrast to studies about post tetanic potentiation (PTP) (Habets and Borst, 2005; Korogod et al., 2005). The used protocols in these studies are comparable to the conditioning protocol used in this work. But in these studies an increase in EPSC amplitudes after switching off the tetanic stimulation is observed. One of the studies (Korogod et al., 2005) investigates different age groups and observes a trend to less PTP in older animals. As their oldest age group (P12 - P14) is still younger than the animals used in this work (P15 - P19), the effect of PTP might have vanished completely with increasing age and other effects become visible which are causing a decrease in EPSC amplitudes.

As already mentioned the slow component of the decrease in EPSC amplitudes at the beginning of the conditioning is longer than 10 s. Though it was not possible to determine the time course of the parameter changes due to low time resolution, a connection between at least one of these parameters and the decrease in amplitudes is very likely. An increase in release probability as well as a decrease in vesicle pool size would both lead to smaller amplitudes in the conditioned steady state. An increase in the speed of vesicle recovery would instead lead to higher amplitudes. Therefore, a faster vesicle recovery time course makes only sense in combination with a change of at least one of the other parameters.

The recovery experiments showed a very slow recovery process on a time scale beyond 10 s. The exact time course of this recovery could not be determined due to the high fluctuations in the measurements of single EPSC amplitudes. A possible explanation for this very slow increase in amplitude could be the recovery of inactivated  $\text{Ca}^{2+}$ -channels as the time courses are on similar time scales (Forsythe et al., 1998).  $\text{Ca}^{2+}$  has a multitude of effects in the presynaptic terminal and is for example involved in the modulation of the vesicle recycling process (Wu, 2004; Wu et al., 2005). Nevertheless, this explanation is unlikely due to two reasons. First,  $\text{Ca}^{2+}$ -channel inactivation would lead to a decrease in vesicle release probability, a change contrary to the predictions of the model calculations. Second, the time course of another variable, namely the mini frequency was measured and showed a decay with a mean characteristic time constant of 42 s. This decrease most probably corresponds to a decrease of the  $\text{Ca}^{2+}$  concentration in the presynaptic terminal, not an increase as expected for the recovery of inactivated  $\text{Ca}^{2+}$ -channels. Studies about PTP (Habets and Borst, 2005; Korogod et al., 2005) show a similar decrease in mini frequencies after the end of the tetanic stimulation which is closely correlated to a decrease in calcium concentration. The smaller absolute mini frequencies in these studies can be explained by the fact that the recordings were in contrast to this work made at room temperature (Kushmerick et al., 2006). A connection of the very slow recovery of EPSC amplitudes to the decrease in calcium concentration indicated by the drop in mini frequencies might be present but needs further investigation.

In summary, the investigation of the two transitions between the different steady states revealed several phenomenological changes and for some changes also the corresponding time courses. The presented results reinforce the conclusion that the *in vivo* state of the calyx of Held synapse is in many regards different from the completely rested state of synapses in an unconditioned brain slice preparation.



## 6 General Discussion

The main result of this study is the finding that the functionality of cells in the MNTB under *in vivo* like conditions was not described correctly in former *in vitro* studies. There are severe differences between completely rested synapses as they are described in the majority of *in vitro* studies and the permanently active state present in the intact brain. This chapter will address three questions that arise from this result. First: What are the consequences of the described input output relationship on the functionality of the MNTB and how does this affect the role of the MNTB in sound processing? Second: How do the additional inputs to the cells of the MNTB influence the input output relationship? Third: Do the observed differences between *in vitro* and *in vivo* results also apply to other nuclei in the auditory brainstem with similar input characteristics?

### 6.1 The functional role of the MNTB

As mentioned in the introduction the MNTB is involved in different mechanisms of sound source localization, namely IID and ITD processing. The two strategies depend on different characteristics of the incoming signal, therefore the influence of changes in the MNTB output compared to its input should result in different consequences for the two localization mechanisms. The output of the first binaural nuclei, the LSO and the MSO, is very often characterized by their mean firing rate in response to different stimulation patterns. This leads to a relationship between azimuthal position of a sound source and firing rate. Moreover, the two nuclei are often associated with different frequency ranges. According to this view, the LSO processes high frequencies (> 2000 Hz) while the MSO processes low frequencies. This is of course a very simplified picture, but it helps interpreting the role of the MNTB in binaural processing. The following paragraphs will only interpret the MNTB input-output-relationship in context of this very basic view of binaural processing. The central question that will

be addressed is how the transmission behavior of the MNTB in the two scenarios (projection to LSO or MSO) should look like and how the observed results fit to these predictions.

In case of high frequency sound processing in the LSO the firing rate of the different inputs is the crucial criterion. The output rate of the LSO neurons depends on the comparison between excitatory ipsilateral input and inhibitory contralateral input. The inhibitory input comes from the MNTB and is therefore one synapse further away from the initial spike initiation site in the cochlear. This additional synaptic transmission causes an additional delay of approximately 0.5 - 1 ms. For high frequency sounds cells in the auditory brainstem do not fire at a defined phase angle of the sound wave. Their firing probability is distributed evenly over the whole period. This means that no precise matching of the two converging inputs to the LSO is possible. Nevertheless, the excitatory and inhibitory input arrive approximately at the same time at the LSO. The general assumption is that the synaptic delay of the inhibitory input is counterbalanced by a slower transmission velocity on the excitatory side. Independent from the delay of the two inputs the important factor is that the inputs cannot be processed on a cycle by cycle basis as their arrival times are not defined precisely enough. Therefore, only the two overall firing rates are compared and their relation defines the output firing rate. As shown in figure 3.7, the firing rate in the MNTB decreases over time in case of high frequency input. This firing behavior shifts the relation between inhibitory and excitatory input towards the excitatory side for longer stimulations. This poses a problem. According to the easy model (comparing firing rates), this would lead to an imaginary movement of the sound source for longer stimulus durations. *In vivo* and psychophysical experiments do not confirm such a virtual movement. In the proposed scenario, a decrease in firing rate caused in the MNTB seems to be unwanted. The system would have to counteract this decreased firing rate by some kind of 'error correction'. Of course, this would be far away from an optimal coding strategy and is therefore an unlikely scenario. More probably the information processed in the LSO is not coded solely as an overall firing rate, but at least changes in firing rate over time also carry information. What kind of information this is and if it is related to sound source localization cannot be decided with the presented results of this study.

Low frequency processing in the MSO depends on the comparison of arrival times of inputs from the two ears. Cells in the MSO respond maximally only for stimuli

with a specific ITD. According to present ideas (Grothe, 2003; McAlpine and Grothe, 2003), information about the horizontal position of a sound source is coded as firing rate (the higher the rate, the more ipsilateral the sound source). The primary inputs to the MSO are excitatory, but it also receives a notable amount of inhibitory input, most of it originating in the MNTB. This inhibition is thought to shift the maximal response and thereby fine tune the response properties of the cells (Brand et al., 2002). In this scenario the inhibition acts on a cycle by cycle basis and very fast inhibitory postsynaptic potential (IPSP) kinetics and precise timing are crucial. The optimal transfer function of the MNTB would in this regard be a one to one transmission with a constant time delay. A shift in time delay as it has been observed in the MNTB (Fedchyshyn and Wang, 2007) should cause a decrease in firing rate but more important a shift in the peak firing rate of MSO cells to different ITDs. This phenomenon is not observed *in vivo* and is a clear discrepancy between *in vivo* and *in vitro* experiments. Two possible explanations are imaginable. Either the observed increase in time delay is an artifact of the experimental conditions and does not occur *in vivo* or the inhibition does not act on a cycle by cycle basis but in a tonic way. *In vitro* experiments about IPSP kinetics are inconclusive in this point (Magnusson et al., 2005).

It should be noted, that the two described mechanisms for sound localization are highly artificial. The two models determine the horizontal position of a sound source in a way an engineer would do the job. Additionally, the presented sounds are normally simple, for example pure tones or some kind of noise (in the technical sense of the term ‘noise’). The neuronal system instead has been optimized against natural sound sources which normally possess a much more complex structure. The evolutionary optimization favored random changes in the functionality of the system, that lead to an improved detection ability. This process shaped a highly adapted neuronal network, that does not necessarily code information following simple rules. *In vivo* experiments generally show, that the firing behavior of most cells in the auditory brainstem cannot be completely explained by the two introduced mechanisms. Cells tend to follow the rules, but they do not perfectly match them, what would be expected for a completely optimized network. What is the explanation for this? Is the optimization just not finished or do the discrepancies make sense in a more complex view of the system. In case of the MNTB these discrepancies from the simple model are a decrease in firing rate (figure 3.7) and an increase in synaptic delay for high firing rates (Fedchyshyn and Wang, 2007). These two features are contradictory to both presented sound source

detection strategies. A decrease in firing rate is unwanted in case rates are compared to each other (IID processing). An increase in delay is unwanted, if arrival times are compared (ITD processing). In the end both models code information about the sound source with a certain firing rate. In reality, information is most probably not coded as a firing rate, instead all spike times and inter spike intervals carry information. So neither of the two mechanisms fully describes the used coding strategy. The functionality of cells in the MNTB as well as cells in all other brainstem nuclei is governed by complex coding strategies. The nature of these coding strategies is probably defined by the common features of relevant sounds. But how these strategies look like can only to a very limited degree be described by such easy models as they are still common for the lower auditory brainstem. For a complete understanding of the role of the MNTB in sound processing, the presented results suggest, that the two simple models, rate comparison for high frequencies and comparison of arrival times for low frequencies, do not lead to satisfying results.

Apart from the two main projections to LSO and MSO, the MNTB projects as already mentioned also to other nuclei (Spangler et al., 1985; Sommer et al., 1993; Riemann and Reuss, 1998). Unfortunately, the functions of these projections are hardly investigated and therefore only speculative statements about their relevance can be made. Projections to higher nuclei like the lateral lemniscus or the inferior colliculus might shape excitatory input in a way similar to the proposed mechanism in the brainstem (Brand et al., 2002). The general idea of inhibition as a tool for fine tuning response properties might be valid also in higher nuclei. Recurrent projections to the MNTB itself might be involved in side band inhibition. This possibility will be explained in the following section. Finally, the downstream projections to the CN might be involved in processes such as for example adaptation to overall sound intensity levels (Dean et al., 2005). Of course, all these functions are highly speculative, but nevertheless, the multitude of projections might be regarded as a sign for the functional significance of the MNTB in the different information pathways of the auditory brainstem.

## 6.2 Additional input to the MNTB

Cells in the MNTB do not only receive input from the calyx of Held but also from other conventional synapses. It has been shown that they receive a considerable amount of

inhibitory input (Banks and Smith, 1992; Awatramani et al., 2004) as well as non-calyceal excitatory input (Forsythe and Barnes-Davies, 1993; Hamann et al., 2003). What are the functional implications of these additional inputs?

The most obvious result of inhibition is a general decrease in firing probability. Inhibition leads to a lower membrane resistance and therefore more excitatory depolarizing current is needed to cross the threshold for action potential generation. To determine the exact role of inhibition in the MNTB information about the source of the inhibitory inputs would be very helpful. Unfortunately, it is not known where these inputs originate. A likely candidate is the MNTB itself as its projections are glycinergic. In this case the inhibition would act retrograde and could for example be used to sharpen the frequency tuning of the cells. In this scenario a cell with a certain characteristic frequency would receive inhibitory input from neighboring cells with slightly different characteristic frequencies. This leads to a decreased firing probability in answer to frequencies away from the characteristic frequency. The problem with this mechanism is the additional delay introduced by one additional synaptic transmission for inhibitory input. Precise integration of phase locked excitation and inhibition is not possible. The inhibition would not act on the first spike at the onset of an acoustic stimulation.

The non-calyceal excitatory input to the MNTB is characterized by significantly lower amplitudes and slower kinetics compared to calyceal input (Forsythe and Barnes-Davies, 1993). Only very few data about this type of input are available and the functional role remains unclear. As the kinetics are far slower it might act as a kind of tonic excitation and might thereby influence the overall excitability of the cell. But as the source of this excitatory current is also not known a definite statement about the functional significance of this current cannot be made.

## 6.3 Implications for other nuclei

The differences between completely rested and conditioned synapses are caused by simulated spontaneous activity, mimicking the ongoing activity of cells in the MNTB even in the absence of any sounds. As the spontaneous activity is mainly caused by the hair cells in the cochlear, this activity is present throughout the auditory brainstem. It is therefore also affecting other nuclei like the CN, the LSO, or the MSO. The synapses in the MNTB are highly specialized and other nuclei might react differently to ongoing

stimulation. Nevertheless, some of the reported features are most probably also true for other nuclei.

The CN also possesses giant synapses, the so-called endbulbs of Held. Cells in the CN are not innervated by a single giant synapse but by a few, usually three to four (Brawer and Morest, 1975; Ryugo and Sento, 1991). Most other cells in the auditory brainstem possess normal synapses which are far smaller and contain significantly less neurotransmitter vesicles, therefore producing smaller currents. Due to these differences, the transfer of the described effects to other nuclei has to be evaluated individually for the different nuclei.

The CN as the nucleus which is best comparable to the MNTB should show similar effects in the presence of spontaneous activity. It receives input directly from the auditory nerve. Auditory nerve fibers show different rates of spontaneous activities. Often two categories, fibers with low and high spontaneous discharge rates are distinguished (Sachs and Abbas, 1974; Winter et al., 1990). Even the low activity fibers exhibit spontaneous firing rates of several Hz whereas the high activity fibers show firing rates of sometimes more than 100 Hz. These levels of activity are definitely comparable to the spontaneous rates observed in the MNTB (see figure 3.2), probably even a little bit higher as the source of the spontaneous activity is closer to the CN. The most obvious difference between rested and conditioned cells is the strongly reduced amplitude. This is mainly a result of the interplay between release probability and vesicle pool recovery. In the CN of rats (P13 - P16), the release probability has been determined to be around 0.5 (McKay and Oleskevich, 2007), the same is true for the CN of young chicks (P2 - P3). The vesicle pool recovery shows a double exponential time course with characteristic time constants of 35 ms and 1.8 s, respectively (Brenowitz and Trussell, 2001). The recovery time course is quite similar to values measured in this study, the release probability is higher. A higher release probability leads to a more pronounced depression so the decrease in amplitude should be even worse in the CN compared to the MNTB. If this decrease in amplitude leads to a less faithful transmission of action potentials cannot be judged finally as the cells in the CN receive input from multiple giant synapses and might therefore still be more failsafe than the MNTB.

Most other nuclei in the auditory brainstem have conventional synapses. These synapses generate far smaller postsynaptic currents than calyx type synapses. To depolarize cells below action potential threshold, a multitude of simultaneously ac-

tive synapses is necessary. Nevertheless, the main parameters governing the synaptic strength are not expected to be fundamentally different. Some form of synaptic depression is very likely to be present in all spontaneously active nuclei, therefore *in vitro* measurements of postsynaptic currents should be regarded as an overestimation or at least an upper bound of the values expectable in the intact brain for all nuclei in the auditory brainstem.

Overall, it must be stated that this discussion leaves a lot of questions unanswered. Nevertheless, several important conclusions can be drawn. First, the deviations from a one to one transmission behavior in the MNTB lead to conflicts with models describing binaural processing. Therefore, the view of binaural processing in the auditory brainstem has to be refined to account for these deviations. Second, the described effects like strongly reduced synaptic strength might not only be valid for the MNTB, but affect most probably all nuclei in the auditory brainstem that are exposed to spontaneous activity. Therefore, the relationship between *in vitro* and *in vivo* experiments might be different than previously thought.





# Bibliography

Abbott L, Varela J, Sen K, Nelson S (1997) Synaptic depression and cortical gain control. *Science* 275:220–224.

Awatramani G, Turecek R, Trussell L (2004) Inhibitory control at a synaptic relay. *J Neurosci* 24:2643–7.

Banks M, Smith P (1992) Intracellular recordings from neurobiotin-labeled cells in brain slices of the rat medial nucleus of the trapezoid body. *J Neurosci* 12:2819–37.

Barnes-Davies M, Forsythe I (1995) Pre- and postsynaptic glutamate receptors at a giant excitatory synapse in rat auditory brainstem slices. *J Physiol* 488 ( Pt 2):387–406.

Bernander O, Douglas R, Martin K, Koch C (1991) Synaptic background activity influences spatiotemporal integration in single pyramidal cells. *Proc.Natl.Acad.Sci.U.S.A* 88:11569–11573.

Bledsoe S J, Snead C, Helfert R, Prasad V, Wenthold R, Altschuler R (1990) Immunocytochemical and lesion studies support the hypothesis that the projection from the medial nucleus of the trapezoid body to the lateral superior olive is glycinergic. *Brain Res.* 517:189–194.

Bollmann JH, Sakmann B, Borst JG (2000) Calcium sensitivity of glutamate release in a calyx-type terminal. *Science* 289:953–957.

Borst A, Theunissen F (1999) Information theory and neural coding. *Nature Neuroscience* 2:947–957.

Borst JG, Sakmann B (1998) Calcium current during a single action potential in a large presynaptic terminal of the rat brainstem. *J Physiol* 506 ( Pt 1):143–157.

- Borst J, Sakmann B (1996) Calcium influx and transmitter release in a fast cns synapse. *Nature* 383:431–4.
- Borst J, Helmchen F, Sakmann B (1995) Pre- and postsynaptic whole-cell recordings in the medial nucleus of the trapezoid body of the rat. *Journal of Physiology-London* 489:825–840.
- Borst J, Sakmann B (1999) Effect of changes in action potential shape on calcium currents and transmitter release in a calyx-type synapse of the rat auditory brainstem. *Philosophical Transactions of the Royal Society of London Series B-Biological Sciences* 354:347–355.
- Brand A, Behrend O, Marquardt T, McAlpine D, Grothe B (2002) Precise inhibition is essential for microsecond interaural time difference coding. *Nature* 417:543–547.
- Brawer JR, Morest DK (1975) Relations between auditory nerve endings and cell types in the cat's anteroventral cochlear nucleus seen with the golgi method and nomarski optics. *J Comp Neurol* 160:491–506.
- Brenowitz S, Trussell LO (2001) Maturation of synaptic transmission at end-bulb synapses of the cochlear nucleus. *J Neurosci* 21:9487–9498.
- Brownell W (1975) Organization of the cat trapezoid body and the discharge characteristics of its fibers. *Brain Research* 94:413–33.
- Cant NB, Benson CG (2003) Parallel auditory pathways: projection patterns of the different neuronal populations in the dorsal and ventral cochlear nuclei. *Brain Res Bull* 60:457–474.
- Chang EH, Kotak VC, Sanes DH (2003) Long-term depression of synaptic inhibition is expressed postsynaptically in the developing auditory system. *J Neurophysiol* 90:1479–1488.
- Clements J, Bekkers J (1997) Detection of spontaneous synaptic events with an optimally scaled template. *Biophys.J.* 73:220–229.
- Cuttle MF, Tsujimoto T, Forsythe ID, Takahashi T (1998) Facilitation of the presynaptic calcium current at an auditory synapse in rat brainstem. *J Physiol* 512 ( Pt 3):723–729.

Dean I, Harper NS, McAlpine D (2005) Neural population coding of sound level adapts to stimulus statistics. *Nat Neurosci* 8:1684–1689.

Destexhe A, Rudolph M, Pare D (2003) The high-conductance state of neocortical neurons in vivo. *Nat.Rev.Neurosci.* 4:739–751.

Dittman JS, Kreitzer AC, Regehr WG (2000) Interplay between facilitation, depression, and residual calcium at three presynaptic terminals. *J Neurosci* 20:1374–1385.

Evans EF (1992) Auditory processing of complex sounds: an overview. *Philos Trans R Soc Lond B Biol Sci* 336:295–306.

Fedchyshyn MJ, Wang LY (2007) Activity-dependent changes in temporal components of neurotransmission at the juvenile mouse calyx of held synapse. *J Physiol* 581:581–602.

Forsythe ID, Barnes-Davies M (1993) The binaural auditory pathway: excitatory amino acid receptors mediate dual timecourse excitatory postsynaptic currents in the rat medial nucleus of the trapezoid body. *Proc Biol Sci* 251:151–157.

Forsythe I (1994) Direct patch recording from identified presynaptic terminals mediating glutamatergic epscs in the rat CNS, in vitro. *Journal of Physiology* 479:381–7.

Forsythe I, Tsujimoto T, Barnes-Davies M, Cuttle M, Takahashi T (1998) Inactivation of presynaptic calcium current contributes to synaptic depression at a fast central synapse. *Neuron* 20:797–807.

Futai K, Okada M, Matsuyama K, Takahashi T (2001) High-fidelity transmission acquired via a developmental decrease in nmda receptor expression at an auditory synapse. *Journal of Neuroscience* 21:3342–9.

Geisler C, Deng L, Greenberg S (1985) Thresholds for primary auditory fibers using statistically defined criteria. *J.Acoust.Soc.Am.* 77:1102–1109.

Goldberg J, Brownell W (1973) Discharge characteristics of neurons in anteroventral and dorsal cochlear nuclei of cat. *Brain Research* 64:35–54.

Graham B, Wong A, Forsythe I (2001) A computational model of synaptic transmission at the calyx of held. *Neurocomputing* 38:37–42.

- Graham B, Wong A, Forsythe I (2004) A multi-component model of depression at the calyx of held. *Neurocomputing* 58-60:449–454.
- Grothe B (1994) Interaction of excitation and inhibition in processing of pure tone and amplitude-modulated stimuli in the medial superior olive of the mustached bat. *Journal of Neurophysiology* 71:706–21.
- Grothe B (2000) The evolution of temporal processing in the medial superior olive, an auditory brainstem structure. *Progress in Neurobiology* 61:581–610.
- Grothe B (2003) New roles for synaptic inhibition in sound localization. *Nat Rev Neurosci* 4:540–550.
- Guinan J J, Li R (1990) Signal processing in brainstem auditory neurons which receive giant endings (calyces of held) in the medial nucleus of the trapezoid body of the cat. *Hear.Res.* 49:321–334.
- Gundlfinger A, Leibold C, Gebert K, Moisel M, Schmitz D, Kempter R (2007) Differential modulation of short-term synaptic dynamics by long-term potentiation at mouse hippocampal mossy fibre synapses. *J Physiol* .
- Habets R, Borst J (2005) Post-tetanic potentiation in the rat calyx of held synapse. *J.Physiol* 564:173–187.
- Hamann M, Billups B, Forsythe I (2003) Non-calyceal excitatory inputs mediate low fidelity synaptic transmission in rat auditory brainstem slices. *European Journal of Neuroscience* 18:2899–2902.
- Held H (1893) Die centrale gehörleitung. *Archiv für Anatomie und Physiologie - Anatomische Abteilung* Year 1893:201–247.
- Helmchen F, Borst JG, Sakmann B (1997) Calcium dynamics associated with a single action potential in a cns presynaptic terminal. *Biophys J* 72:1458–1471.
- Hudspeth AJ (1989) How the ear's works work. *Nature* 341:397–404.
- Hudspeth A (1997) How hearing happens. *Neuron* 19:947–50.
- Irvine D (1992) Physiology of the auditory brainstem In Popper AN, Fay RR, editors, *Springer Handbook of Auditory Research*, pp. 153–231. Springer, New York.

Ishikawa T, Takahashi T (2001) Mechanisms underlying presynaptic facilitatory effect of cyclothiazide at the calyx of held of juvenile rats. *J Physiol* 533:423–31.

Joris PX, Yin TC (1995) Envelope coding in the lateral superior olive. i. sensitivity to interaural time differences. *J Neurophysiol* 73:1043–1062.

Joris P, Carney L, Smith P, Yin T (1994) Enhancement of neural synchronization in the anteroventral cochlear nucleus. i. responses to tones at the characteristic frequency. *J Neurophysiol* 71:1022–36.

Joshi I, Shokralla S, Titis P, Wang L (2004) The role of ampa receptor gating in the development of high-fidelity neurotransmission at the calyx of held synapse. *J. Neurosci.* 24:183–196.

Joshi I, Wang L (2002) Developmental profiles of glutamate receptors and synaptic transmission at a single synapse in the mouse auditory brainstem. *J. Physiol* 540:861–873.

Kadner A, Kulesza R J, Berrebi A (2006) Neurons in the medial nucleus of the trapezoid body and superior paraolivary nucleus of the rat may play a role in sound duration coding. *J. Neurophysiol.* 95:1499–1508.

Kiang NYS (1965) *Discharge patterns of single fibers in the cat's auditory nerve.* MIT-Press.

Klyachko V, Stevens C (2006) Excitatory and feed-forward inhibitory hippocampal synapses work synergistically as an adaptive filter of natural spike trains. *PLoS. Biol.* 4:e207–.

Kopp-Scheinpflug C, Lippe W, Dorrscheidt G, Rubsamen R (2003) The medial nucleus of the trapezoid body in the gerbil is more than a relay: comparison of pre- and postsynaptic activity. *J Assoc Res Otolaryngol* 4:1–23.

Korogod N, Lou X, Schneggenburger R (2005) Presynaptic  $Ca^{2+}$  requirements and developmental regulation of posttetanic potentiation at the calyx of held. *J. Neurosci.* 25:5127–5137.

Kotak VC, Sanes DH (2000) Long-lasting inhibitory synaptic depression is age- and calcium-dependent. *J Neurosci* 20:5820–5826.

- Kushmerick C, Renden R, von Gersdorff H (2006) Physiological temperatures reduce the rate of vesicle pool depletion and short-term depression via an acceleration of vesicle recruitment. *J. Neurosci.* 26:1366–1377.
- Kuwabara N, DiCaprio R, Zook J (1991) Afferents to the medial nucleus of the trapezoid body and their collateral projections. *J. Comp Neurol.* 314:684–706.
- Lay D (1974) Differential predation on gerbils (*Meriones*) by little owl, *Athenebrahma*. *Journal of Mammalogy* 55:608–614.
- Lenn NJ, Reese TS (1966) The fine structure of nerve endings in the nucleus of the trapezoid body and the ventral cochlear nucleus. *Am J Anat* 118:375–389.
- Leão RM, Gersdorff HV (2002) Noradrenaline increases high-frequency firing at the calyx of held synapse during development by inhibiting glutamate release. *J Neurophysiol* 87:2297–2306.
- Liberman M (1978) Auditory-nerve response from cats raised in a low-noise chamber. *Journal of the Acoustical Society of America* 63:442–55.
- Loskota W, Lomax P, Verity M (1974) *A Stereotaxic Atlas of the Mongolian Gerbil Brain*. Ann Arbor Science Publishers, Inc., Ann Arbor.
- Magnusson AK, Kapfer C, Grothe B, Koch U (2005) Maturation of glycinergic inhibition in the gerbil medial superior olive after hearing onset. *J Physiol* 568:497–512.
- Markram H, Tsodyks M (1996) Redistribution of synaptic efficacy between neocortical pyramidal neurons. *Nature* 382:807–810.
- McAlpine D, Grothe B (2003) Sound localization and delay lines - do mammals fit the model? *Trends in Neurosciences* 26:347–350.
- McKay SM, Oleskevich S (2007) The role of spontaneous activity in development of the endbulb of held synapse. *Hear Res* 230:53–63.
- Meyer A, Neher E, Schneggenburger R (2001) Estimation of quantal size and number of functional active zones at the calyx of held synapse by nonstationary epsc variance analysis. *Journal of Neuroscience* 21:7889–7900.

- Moore M, Caspary D (1983) Strychnine blocks binaural inhibition in lateral superior olivary neurons. *Journal of Neuroscience* 3:237–42.
- Morest DK (1968) The growth of synaptic endings in the mammalian brain: a study of the calyces of the trapezoid body. *Z Anat Entwicklungsgesch* 127:201–220.
- Nakajima Y (1971) Fine structure of the medial nucleus of the trapezoid body of the bat with special reference to two types of synaptic endings. *J Cell Biol* 50:121–134.
- Neher E, Sakaba T (2001) Estimating transmitter release rates from postsynaptic current fluctuations. *Journal of Neuroscience* 21:9638–9654.
- Neher E, Sakaba T (2003) Combining deconvolution and fluctuation analysis to determine quantal parameters and release rates. *Journal of Neuroscience Methods* 130:143–157.
- Nelder J, Mead R (1965) A simplex-method for function minimization. *Computer Journal* 7:308–313.
- Pare D, Shink E, Gaudreau H, Destexhe A, Lang E (1998) Impact of spontaneous synaptic activity on the resting properties of cat neocortical pyramidal neurons in vivo. *J. Neurophysiol.* 79:1450–1460.
- Renden R, Taschenberger H, Puente N, Rusakov D, Duvoisin R, Wang L, Lehre K, von Gersdorff H (2005) Glutamate transporter studies reveal the pruning of metabotropic glutamate receptors and absence of ampa receptor desensitization at mature calyx of held synapses. *J. Neurosci.* 25:8482–8497.
- Riemann R, Reuss S (1998) Projection neurons in the superior olivary complex of the rat auditory brainstem: a double retrograde tracing study. *ORL J Otorhinolaryngol Relat Spec* 60:278–282.
- Roberts W, Howard J, Hudspeth A (1988) Hair cells: transduction, tuning, and transmission in the inner ear. *Annual Review of Cell Biology* 4:63–92.
- Ryan A (1976) Hearing sensitivity of the mongolian gerbil, *Meriones unguiculatus*. *J Acoust Soc Am* 59:1222–1226.
- Ryan A, Miller J (1978) Single unit responses in the inferior colliculus of the awake and performing rhesus monkey. *Exp. Brain Res.* 32:389–407.

- Ryugo DK, Sento S (1991) Synaptic connections of the auditory nerve in cats: relationship between endbulbs of held and spherical bushy cells. *J Comp Neurol* 305:35–48.
- Sachs MB, Abbas PJ (1974) Rate versus level functions for auditory-nerve fibers in cats: tone-burst stimuli. *J Acoust Soc Am* 56:1835–1847.
- Sakaba T, Neher E (2001a) Calmodulin mediates rapid recruitment of fast-releasing synaptic vesicles at a calyx-type synapse. *Neuron* 32:1119–1131.
- Sakaba T, Neher E (2001b) Quantitative relationship between transmitter release and calcium current at the calyx of held synapse. *J Neurosci* 21:462–476.
- Sakaba T, Schneggenburger R, Neher E (2002) Estimation of quantal parameters at the calyx of held synapse. *Neuroscience Research* 44:343–356.
- Sanes DH, Siverls V (1991) Development and specificity of inhibitory terminal arborizations in the central nervous system. *J Neurobiol* 22:837–854.
- Sätzler K, Söhl LF, Bollmann JH, Borst JGG, Frotscher M, Sakmann B, Lübke JHR (2002) Three-dimensional reconstruction of a calyx of held and its postsynaptic principal neuron in the medial nucleus of the trapezoid body. *J Neurosci* 22:10567–10579.
- Schneggenburger R, Forsythe I (2006) The calyx of held. *Cell Tissue Res*. 326:311–337.
- Schneggenburger R, Meyer A, Neher E (1999) Released fraction and total size of a pool of immediately available transmitter quanta at a calyx synapse. *Neuron* 23:399–409.
- Schneggenburger R, Neher E (2000) Intracellular calcium dependence of transmitter release rates at a fast central synapse. *Nature* 406:889–893.
- Schneggenburger R, Sakaba T, Neher E (2002) Vesicle pools and short-term synaptic depression: lessons from a large synapse. *Trends in Neurosciences* 25:206–212.
- Schuller G, Radtke-Schuller S, Betz M (1986) A stereotaxic method for small animals using experimentally determined reference profiles. *Journal of Neuroscience Methods* 18:339–50.



Schwarz D, Puil E (1997) Firing properties of spherical bushy cells in the anteroventral cochlear nucleus of the gerbil. *Hear.Res.* 114:127–138.

Smith P, Joris P, Carney L, Yin T (1991) Projections of physiologically characterized globular bushy cell axons from the cochlear nucleus of the cat. *J Comp Neurol* 304:387–407.

Smith P, Joris P, Yin T (1998) Anatomy and physiology of principal cells of the medial nucleus of the trapezoid body (mntb) of the cat. *Journal of Neurophysiology* 79:3127–42.

Sommer I, Lingenhohl K, Friauf E (1993) Principal cells of the rat medial nucleus of the trapezoid body - an intracellular in-vivo study of their physiology and morphology. *Experimental Brain Research* 95:223–239.

Spangler K, Warr W, Henkel C (1985) The projections of principal cells of the medial nucleus of the trapezoid body in the cat. *J.Comp Neurol.* 238:249–262.

Spirou G, Brownell W, Zidanic M (1990) Recordings from cat trapezoid body and hrp labeling of globular bushy cell axons. *J.Neurophysiol.* 63:1169–1190.

Spirou G, Rager J, Manis P (2005) Convergence of auditory-nerve fiber projections onto globular bushy cells. *Neuroscience* 136:843–863.

Taschenberger H, Leao R, Rowland K, Spirou G, von Gersdorff H (2002) Optimizing synaptic architecture and efficiency for high-frequency transmission. *Neuron* 36:1127–1143.

Taschenberger H, Scheuss V, Neher E (2005) Release kinetics, quantal parameters and their modulation during short-term depression at a developing synapse in the rat CNS. *Journal of Physiology-London* 568:513–537.

Taschenberger H, von Gersdorff H (2000) Fine-tuning an auditory synapse for speed and fidelity: developmental changes in presynaptic waveform, epsc kinetics, and synaptic plasticity. *J Neurosci* 20:9162–73.

Thompson A, Schofield B (2000) Afferent projections of the superior olivary complex. *Microsc.Res.Tech.* 51:330–354.

- Tollin DJ (2003) The lateral superior olive: a functional role in sound source localization. *Neuroscientist* 9:127–143.
- Tollin DJ, Yin TCT (2005) Interaural phase and level difference sensitivity in low-frequency neurons in the lateral superior olive. *J Neurosci* 25:10648–10657.
- Trussell LO, Zhang S, Raman IM (1993) Desensitization of ampa receptors upon multiquantal neurotransmitter release. *Neuron* 10:1185–1196.
- Trussell LO (2002) Modulation of transmitter release at giant synapses of the auditory system. *Curr Opin Neurobiol* 12:400–404.
- Tsodyks M, Pawelzik K, Markram H (1998) Neural networks with dynamic synapses. *Neural Comput.* 10:821–835.
- Varela J, Sen K, Gibson J, Fost J, Abbott L, Nelson S (1997) A quantitative description of short-term plasticity at excitatory synapses in layer 2/3 of rat primary visual cortex. *Journal of Neuroscience* 17:7926–7940.
- von Gersdorff H, Borst J (2002) Short-term plasticity at the calyx of held. *Nat Rev Neurosci* 3:53–64.
- von Gersdorff H, Schneggenburger R, Weis S, Neher E (1997) Presynaptic depression at a calyx synapse: the small contribution of metabotropic glutamate receptors. *Journal of Neuroscience* 17:8137–46.
- Wang L, Kaczmarek L (1998) High-frequency firing helps replenish the readily releasable pool of synaptic vesicles. *Nature* 394:384–8.
- Weis S, Schneggenburger R, Neher E (1999) Properties of a model of  $Ca^{++}$ -dependent vesicle pool dynamics and short term synaptic depression. *Biophysical Journal* 77:2418–2429.
- Winter IM, Robertson D, Yates GK (1990) Diversity of characteristic frequency rate-intensity functions in guinea pig auditory nerve fibres. *Hear Res* 45:191–202.
- Wu L, Borst J (1999) The reduced release probability of releasable vesicles during recovery from short-term synaptic depression. *Neuron* 23:821–832.

Wu LG (2004) Kinetic regulation of vesicle endocytosis at synapses. *Trends Neurosci* 27:548–554.

Wu S, Kelly J (1993) Response of neurons in the lateral superior olive and medial nucleus of the trapezoid body to repetitive stimulation: intracellular and extracellular recordings from mouse brain slice. *Hear Res* 68:189–201.

Wu W, Xu J, Wu XS, Wu LG (2005) Activity-dependent acceleration of endocytosis at a central synapse. *J Neurosci* 25:11676–11683.

Xu J, Wu L (2005) The decrease in the presynaptic calcium current is a major cause of short-term depression at a calyx-type synapse. *Neuron* 46:633–645.

Zhang S, Trussell LO (1994) Voltage clamp analysis of excitatory synaptic transmission in the avian nucleus magnocellularis. *J Physiol* 480 ( Pt 1):123–136.

Zucker RS, Regehr WG (2002) Short-term synaptic plasticity. *Annu Rev Physiol* 64:355–405.



# Contributions to the Manuscript

## Chapter 2

Michael Pecka wrote the description of the *in vivo* procedures.

## Chapter 3

Michael Pecka performed the *in vivo* experiments, Achim Klug and Henrike von Gersdorff wrote parts of the manuscript.



# Curriculum Vitæ

## Joachim Hermann

Address ..... Schleißheimer Str. 61  
80797 München, Germany  
Phone ..... ++4989 / 2180-74316  
E-mail ..... jhermann@lmu.de  
Date of birth ..... 17<sup>th</sup> Mar 77

---

### School Education

Sep 83 – Apr 84      Elementary School in Baldham  
May 84 – Jul 87      Elementary School in Munich  
Sep 87 – Jun 96      Heinrich-Heine-Gymnasium in Munich  
Feb 93 – Apr 93      Three-month stay in New Zealand  
28<sup>th</sup> Jun 96          University entrance diploma

---

### Military Service

Jul 96 – Apr 97      Basic military service in the air force in Mengen and Erding

---

### University Education

Sep 97 – Aug 03      Studies of general physics at the Technical University of Munich  
Aug 02 – Aug 03      Diploma thesis conducted at the chair E22 (Biophysics) on ‘*Electrophoresis of Membrane Associated Proteins*’  
Feb 03 – May 03      Three-month research trip to the University of Stanford  
2<sup>nd</sup> Sep 03            Physics diploma

Nov 03 – Jan 04      Research work at the Technical University of Munich  
Feb 04 – Jan 08      PhD studies in the neurobiology group at the Ludwig–  
Maximilians–Universität in Munich on *‘Information process-  
ing at the calyx of Held under natural conditions’*

---

## Occupational Experience

July 97 – Apr 98      Design of a database frontend for Hypobank on behalf of the  
company Brasse Consult  
Feb 99 – Jun 01      Programming of analysis software for data about fretting in air  
bearings and development of various tools for financial control-  
ling for the company AeroLas

---

## Major Conference Participations

Mar 04                  DPG-Spring Meeting Regensburg:  
*‘Electrophoresis of Membrane Bound Proteins’*  
Feb 06                  ARO 29<sup>th</sup> MidWinter Meeting:  
*‘The Influence of In-Vivo Spontaneous Rates on Short-Term  
Plasticity in the Calyx of Held Synapse’*  
Feb 07                  Cosyne Computational and Systems Neuroscience 2007:  
*‘Processing of Complex Activity Patterns at the Calyx of Held  
Synapse’*  
Mar 07                  31<sup>st</sup> Göttingen Neurobiology Conference:  
*‘Processing of Complex Activity Patterns at the Calyx of Held  
Synapse: A Computation Analysis’*

---

## Publications

Tanaka M, Hermann J, Haase I, Fischer M, Boxer SG (2007) Frictional drag and electrical manipulation of recombinant proteins in polymer-supported membranes. *Langmuir* 23:5638-5644

Hermann J, Pecka M, von Gersdorff H, Grothe B, Klug A (2007) Synaptic transmission at the calyx of Held under in vivo like activity levels. *J Neurophysiol.* 98:807-820



# Danksagung

Jedem, der mir bei dieser Arbeit geholfen hat:

Vielen Dank!



# Ehrenwörtliche Versicherung

Ich versichere hiermit ehrenwörtlich, dass die vorgelegte Dissertation von mir selbstständig und ohne unerlaubte Hilfe angefertigt ist.

München, den 17.01.2008

Joachim Hermann